Free-standing smectic liquid crystal elastomer films

Dissertation

zur Erlangung des akademischen Grades

doctor rerum naturalium
(Dr. rer. nat.)

genehmigt durch die Fakultät für Naturwissenschaften
der Otto-von-Guericke-Universität Magdeburg

von M. Sc. Victor Aksenov

geb. am 22.09.1979 in Blagoweshensk, Russland

Gutachter: Prof. Dr. Ralf Stannarius
Prof. Dr. Eugene Terentjev

eingereicht am: 31.07.2009

verteidigt am: 22.02.2010

Contents

Motivation

Liquid crystalline elastomers (LCEs) combine rubber elasticity with anisotropic optical, mechanical and electrical properties of liquid crystals. The polymeric network couples the orientation of mesogenic groups with the mechanical deformation of the elastomer. For instance, mechanical deformation of a nematic LCE, perpendicular to the director, can change the orientation of mesogenic molecules [1, 2]. Deformation of a LCE parallel to the director can change the orientational order parameter of mesogens [3], and vice versa, changing of the orientational order parameter at the isotropic-smectic or isotropic-nematic phase transition can lead to a macroscopic deformation [4-6]. Moreover, the orientation of mesogens in some LCEs can be changed by an external electric field, and consequently the shape of these elastomers can be manipulated by an electric field [7-9]. Even such LCEs have been synthesized in which the nematic-isotropic phase transition can be induced by a light irradiation and their shape can be controlled just by a light irradiation [10, 11].

It has to be noted that mechanical properties of LCEs are usually quite different from those of conventional isotropic rubbers and highly anisotropic [3, 12-14]. An additional internal degree of freedom in nematic elastomers, the rotation of the director, makes possible a so-called soft or semi-soft elasticity [15-17], originally proposed by Golubovic and Lubensky [18]. An ideal soft deformation can be performed without the change of the free-energy of an elastomer and hence at zero stress. However, in reality, a very low but non-zero stress is required for this deformation, in this case one can speak of a semi-soft elasticity [17, 19].

The deformation of a smectic elastomer parallel to the smectic layers is opposed by the elastic modulus of the same order as in a conventional isotropic rubber [6, 12]. In this case smectic layers don't influence the elastic modulus and it's defined only by the entropy elasticity of polymeric chains $\mu \sim n_S k_B T$, where n_S is the number of chain strands per unit volume.

If deformation is perpendicular to the smectic layers, in addition to the elasticity of polymeric chains, the elastic energy of a deformed elastomer has to include term which is enthalpic in nature and proportional to the layer compression modulus. Experimental measurements confirm that for some smectic elastomers, elastic moduli perpendicular to the layers can be one or two order of magnitude higher than moduli parallel to the layers [6, 12]. But the anisotropy of elastic moduli isn't always so high, for some smectic elastomers the elastic moduli perpendicular to the layers just four times larger than the moduli parallel to the layers have been measured [14, 20].

Due to the coupling of microscopic parameters with the conformation of a polymeric network and therefore with the shape of a sample, LCEs are perspective candidates for sensor [21] and actuator applications and they even were proposed as materials for the creation of artificial muscles [22-24]. These unique properties of LCEs made them an object of intensive investigations.

Elastic moduli, deformational behaviour and the temperatures of the phase transitions of LC elastomers depend on many factors, such as; the density of crosslinkers [25], the temperature of crosslinking (in which phase the polymeric network was crosslinked), orientational order of the mesogens, which in its turn depends on temperature and external forces such as electric and magnetic fields and mechanical deformations.

The properties of nematic elastomers are much better understood than the properties of smectic elastomers. There is a large number of experimental investigations which help to understand the correlation between the properties of nematic elastomers and their structure, for instance [1, 3, 26-30]. Moreover, continues and molecular theories have been created that explain the deformational behaviour of nematic elastomers and provide suitable description of experimental results [31-34].

Smectic elastomers are a much more complicated system and their behaviour is less understood. Because of their complex structure, there are very few attempts to describe deformation of smectic elastomers from a molecular point of view [35-38]. However, the continuum theory of smectic elastomers is available, and can be used for the description of mechanical response at least at small deformations [33, 39].

Despite the numerous experimental investigations of smectic LCEs, the influence of chemical structure and preparation conditions is still not completely clear. Observations made for materials with different chemical structures contradict each other in some points [1, 12-14, 40-44]. As already was pointed out, mechanical properties of smectic elastomers are anisotropic, and the ratio of the elastic modulus in the layer plane to the modulus perpendicular to the smectic layers in some smectic elastomers can reach almost two orders of magnitude [6, 12], while other smectic elastomers show a much smaller anisotropy [14, 20]. Experimental investigations of the deformational behaviour of the elastomers investigated in this work revealed that the smectic layer structure does not have any noticeable influence on the elastic moduli of the elastomer [45, 46].

The main goal of this thesis is to carry out a detailed study of the behaviour of the free-standing smectic elastomer films described by Stannarius et al.[42-48]. In these elastomers, deformation parallel to the smectic layer leads to the compression of the film perpendicular to the smectic layers, while usually the thickness of the film perpendicular to the smectic layer does not change in other smectic elastomers stretched parallel to the smectic layer plane [12-14, 40]. Using

optical reflectometry the thickness changes of free-standing smectic LCE films have been measured. As most available method, optical reflectometry was used for different elastomers with different chemical structures. Also, for one of the LCEs under investigation, X-ray and polarized FTIR-spectroscopy measurements have been used for the detailed studying of the compression of the smectic LCE film perpendicular to the smectic layers. These measurements can help better understand the mechanism of the deformation of the smectic elastomers on the molecular level.

Also, an attempt has been made to measure the elastic moduli parallel and perpendicular to the smectic layers. For this purpose the elastic forces required for the deformation of free-standing smectic elastomer balloons and free-standing smectic elastomer films have been measured. In the first case, elastic modulus perpendicular to the smectic layers gives contribution to the elastic energy, while for the free-standing smectic elastomer films, main contribution in to the elastic energy of deformed elastomer has to be from the elastic modulus parallel to the smectic layers.

Studying of the deformation of free-standing films using different experimental technique have to schedule the light on the behaviour of elastomers studied by Stannarius at al. [42-46]. Understanding of the reasons responsible for the behaviour different from the elastomers described by Finkelmann at al. [1, 12-14, 40] can be very important for a deeper comprehension of the correlation between the structure of smectic LC elastomers and their properties

Chapter 1 Introduction

1.1 Liquid crystals

Liquid crystals (LCs) are unusual materials. They represent a state of matter that is intermediate between a crystal solid which possesses translational and orientational order (in case of non-spherical molecules) and a conventional liquid which is completely isotropic and possesses neither translational nor orientational order. Liquid crystals reveal some degree of fluidity, but at the same time, they are anisotropic and physical properties of the substance in the liquid crystalline state depend on the chosen direction. Some liquid crystalline phases have not only an orientation order but also a translational order in one or two dimensions [49, 50]. The liquid crystalline or mesomorphic behaviour was discovered by Reinitzer in 1888 when he observed two melting points of cholesterol ester [51, 52]. During heating, at first the substance melts in to a turbid liquid, and after that, at some temperature the cloudy liquid becomes transparent, this phenomenon was reversible and could be observed also by cooling. Moreover, some spectacular colour effects could be observed near both transition points [51, 52].

Otto Lehmann was the first who was trying to understand this phenomenon. He found that the opaque liquid phase is birefringent and had suggested that the turbid liquid has all attributes of crystal and at the same time posses some fluidity. He believed that he had discovered “crystals that flow” [52, 53]. But it was completely unclear why some substances have mesophases while others do not. The answer to this question was given by the German physicist Vorländer, he had systematically analyzed large number of the substances that have mesomorphic phases, and had come to the conclusion that mainly the substances with long rod-like molecules reveal mesophases [52, 54, 55]. But real understanding of the nature of LCs had required several decades of intensive research [52].

As was already noted, in some substances liquid crystalline phases reveal themselves only in certain temperature interval [49, 50], while in others, LC state can be reached only at certain concentration of solvent [30, 56]. The former are called thermotropic liquid crystal and the latter lyotropic liquid crystals. Since this work deals only with thermotropic liquid crystalline polymers and elastomers, lyotropic LC will not be discussed here.

One of the most important prerequisites for the appearance of mesophases is the anisotropic shape of molecules. The most typical liquid crystals have rod-like molecules and called calamitic liquid crystals. Substances with disc-like molecules can also exhibit mesophases. Such substances

are called discotics or discotic liquid crystal. There are other types of mesogenic molecules but they will not be discussed here, for more details see [49].

Nematic liquid crystals don't possess a long-range translation order, but only an orientational order. The long axes of molecules in the nematic phase tend to align in one direction which is commonly designated by a unit vector **n** also called director (Fig. 1.1a). This phase has a symmetry axis C_∞ parallel to the director, but up and down directions of the director are equivalent in the nematic phase, and therefore the symmetry of the nematic phase is $D_{\infty h}$.

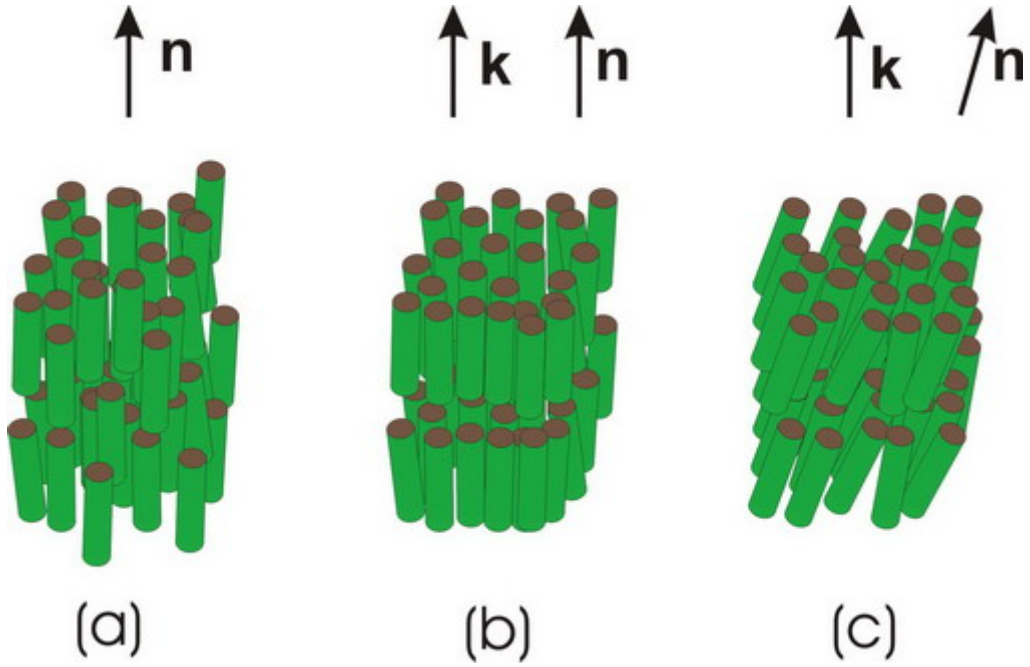

Figure 1.1: The arrangement of molecules in the nematic (a), smectic A (b) and smectic C (c) phases.

The X-ray diffraction on the oriented nematics shows only diffuse scattering, there are two diffuse spots at $\boldsymbol{q} = q_0\boldsymbol{n}$ with $q_0 = 2\pi/l$, where l is the molecule length, and two diffuse arcs in a wide-angle region about $\boldsymbol{q} = q_1\boldsymbol{n}\times\boldsymbol{k}$ with q_1 approximately equal to $2\pi/a$, where a is the distance between neighbouring molecules (Fig. 1.2a).

Smectic phases in addition to an orientational order possess a one-dimensional translational order. In the smectic A phase molecules form well defined layers and the average orientation of the long axis of molecules is parallel to the layer normal Fig. 1.1b. There is no translational order in the layer plain and positions of the centres of the molecules are not correlated within the smectic layers, therefore, in the layer plane smectic phase is similar to a 2-dimensional liquid.

The layered structure of the smectic phase is equivalent to the mass density wave perpendicular to the layers, and the layered smectic structure can be described by a sinusoidal modulation of the average molecular number density,

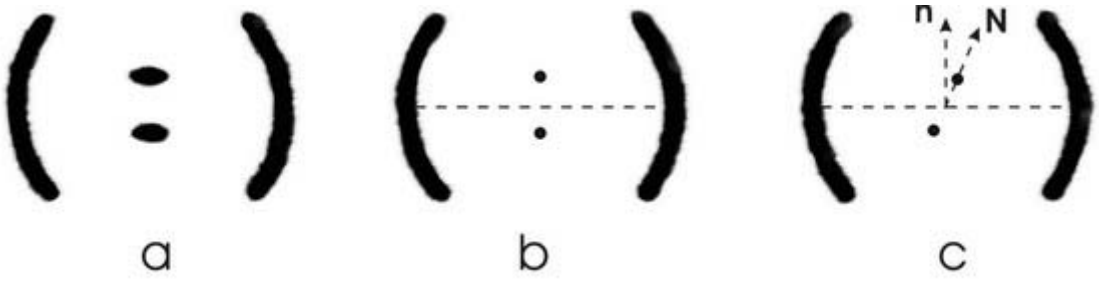

Figure 1.2: Schematic representation of X-ray intensity scattering profiles of (a) the nematic, (b) smectic A and (c) smectic C phases.

$$\langle n \rangle = n_0 + 2n_{q0}\cos(q_o z) \tag{1.1}$$

where $q_0 = 2\pi/l$ and the z axis is perpendicular to smectic layers [57].

Thermal fluctuations in 1-dimension destroy a long-range translational order and lead to quasi-long-range order in the smectic phase. The Bragg peaks of a smectic structure are not delta-functions but power law singularities, thus they are often called quasi-Bragg peaks [49, 58]. The X-ray diffraction patter of an oriented smectic shows two quasi-Bragg peaks at $\boldsymbol{q} = q_0\boldsymbol{n}$ with $q_0 = 2\pi/l$, where l is the smectic layer thickness, and like in case of nematics two diffuse arcs in the wide-angle region about $\boldsymbol{q} = q_1\boldsymbol{n}\times\boldsymbol{k}$ with q_1 approximately equal to $2\pi/a$,where a is the distance between neighbouring molecules [57].

Smectic A phase is not the only layered phase, in some materials, molecules in the smectic layers are tilted with respect to the smectic layer normal, that type of smectics is called smectic C phase. Locally all molecules are tilted in one preferred direction, i.e. their projections on the smectic layer plane tend to be aligned in one direction denoted by the unit vector **c,** which is called a **c**-director. Due to the tilt of the molecules the symmetry of the SmC phase is lower than that of SmA phase. In case of the SmA phase the local symmetry is the same as the symmetry of nematics $D_{\infty h}$ and local symmetry of the SmC phase is C_{2h}. Typical X-ray diffraction patter of a SmC phase is shown in Fig. 1.2c.

SmA and SmC phases are the simplest examples of smectic phases. There is a large number of modifications of the SmA phase and tilted smectic phases, but they will not be discussed here. A detailed description of different smectic phases can be found for instance here [49, 50, 59] .

In nematic and smectic-A phases the long axes of molecules tend to be aligned parallel to one direction denoted by a director. But in reality molecules are tilted on different angles with respect to the director. The orientation of the molecules is described by an orientational distribution function (ODF) $f(\theta, \varphi)$ where θ is the angle between the long axis of the molecule and director, angle φ is azimuthal angle around **n** [49, 60].

In conventional uniaxial nematic and smectic-A phases $f(\theta, \varphi)$ is independent of φ due to the symmetry of the phases. These phases have local symmetry $D_{\infty h}$ and therefore are cylindrically symmetric about **n.** Presence of the symmetry plane perpendicular to **n** makes the direction **n** and –**n** equivalent, therefore $f(\theta) = f(\pi-\theta)$. In this case, the ODF $f(\theta)$ can be expanded in terms of even Legendre polynomials $P_{2L}(\cos\theta)$:

$$f(\theta) = \sum_{L=0}^{\infty} (2L+1) S_{2L} P_{2L}(\cos\theta) \tag{1.2}$$

where the expansion coefficients S_{2L} are the scalar orientational order parameters. It is more convenient to characterise an orientational order not by a distribution function but by one numerical parameter. The orientation of individual molecule is described by the unit vector **a** parallel to the molecule long axis and it seams plausible to take an average projection of **a** on the director **n** as a characteristic of orientational order.

$$\left\langle \vec{a} \cdot \vec{n} \right\rangle = \left\langle \cos\theta \right\rangle = \int f(\theta) \cos\theta d\Omega \tag{1.3}$$

but due to the symmetry properties of the distribution function $f(\theta) = f(\pi-\theta)$ the average value of projection vanishes [49]. The first orientational order parameter giving a non-trivial answer is the Hermans-Tsvetkov orientational order parameter which is defined as the average value of the second Legendre polynomial [60]:

$$S \equiv S_2 = \frac{1}{2}\left\langle \left(3\cos^2\theta - 1\right) \right\rangle = \int f(\theta)\left(3\cos^2\theta - 1\right) d\Omega \tag{1.4}$$

In the ideal case when all molecules are parallel to the director, $f(\theta)$ has non zero values at $\theta = 0$ and $\theta = \pi$, for that values of θ, $\cos\theta = \pm 1$ and therefore S = 1. In an isotropic phase the orientation is random and $f(\theta)$ does not depend on θ, $\left\langle \cos^2 \theta \right\rangle = 1/3$, and hence S = 0. Thus, S is a suitable parameter for the characterisation of the orientational order. Typical experimental values of S, in nematics, lay in the range between 0.4 and 0.7.

1.2 Liquid crystalline polymers and elastomers

Along with low molecular mass compounds, polymers and elastomers can reveal liquid crystalline phases. Up to the present moment, polymer and elastomer counterparts of nematics, cholesterics and smectics have been synthesized. Different possibilities to obtain LC phases in polymers and elastomers will be described below.

1.2.1 Types of LC polymers

Polymer chains of linear polymers are form anisotropic and that is one of the main prerequisites for the formation of LC phases. If the chains are rigid enough and the persistence length is long enough, such chains can be mesogenic units themselves. Hence, under certain conditions such polymers are able to form LC-phases. However, the melting temperatures of rigid polymers usually are so high that they decompose before LC-phases can be reached. LC-phases in such polymers can be obtained by addition of an appropriate solvent [61]. In order to decrease melting temperatures and shift LC-phases to lower temperatures the order of crystalline phase has to be frustrated, for instance, by an attachment of flexible said chains [62] or by a random distribution of different segments in random copolymers [63]. Detailed discussion of the structural variations of LC polymers can be found for instance in the review articles by Sek [64] and Shibaev [65, 66]. All these methods allow to decrease melting temperatures of polymers to some degree, but the turning point in the design of LC polymers was the concept of spacers. Mesogenic molecules linked with each other head-to-tail by sufficiently flexible linking elements form thermotropic LC main-chain (MC) polymers (Fig. 1.3b and d) [67, 68].

Another way to obtain thermotropic LC elastomers with mesophases at sufficiently low temperatures is to attach mesogenic molecules as side chains to a flexible polymeric backbone. This type of LC polymers is called side-chain (SC) liquid crystalline polymers (Fig. 1.3a and c). Such

structure has to decouple the orientation of mesogens, which tend to orient themselves parallel to each other, from the conformation of a polymeric backbone which tends to adopt an isotropic coil conformation. Many from the first synthesised side-chain polymers did not revealed LC phases because the mesogens were directly attached to the polymeric backbone and the orientation of mesogens was not decoupled from the backbone orientation. As in case of main-chain LC polymers, this problem was solved by an introduction of a flexible spacer between mesogenic molecule and a polymeric backbone. First observations of the LC phases in side-chain LCPs were reported approximately at the same time by two different groups Finkelmann et al. [69, 70] and Shibaev et al. [71, 72] .

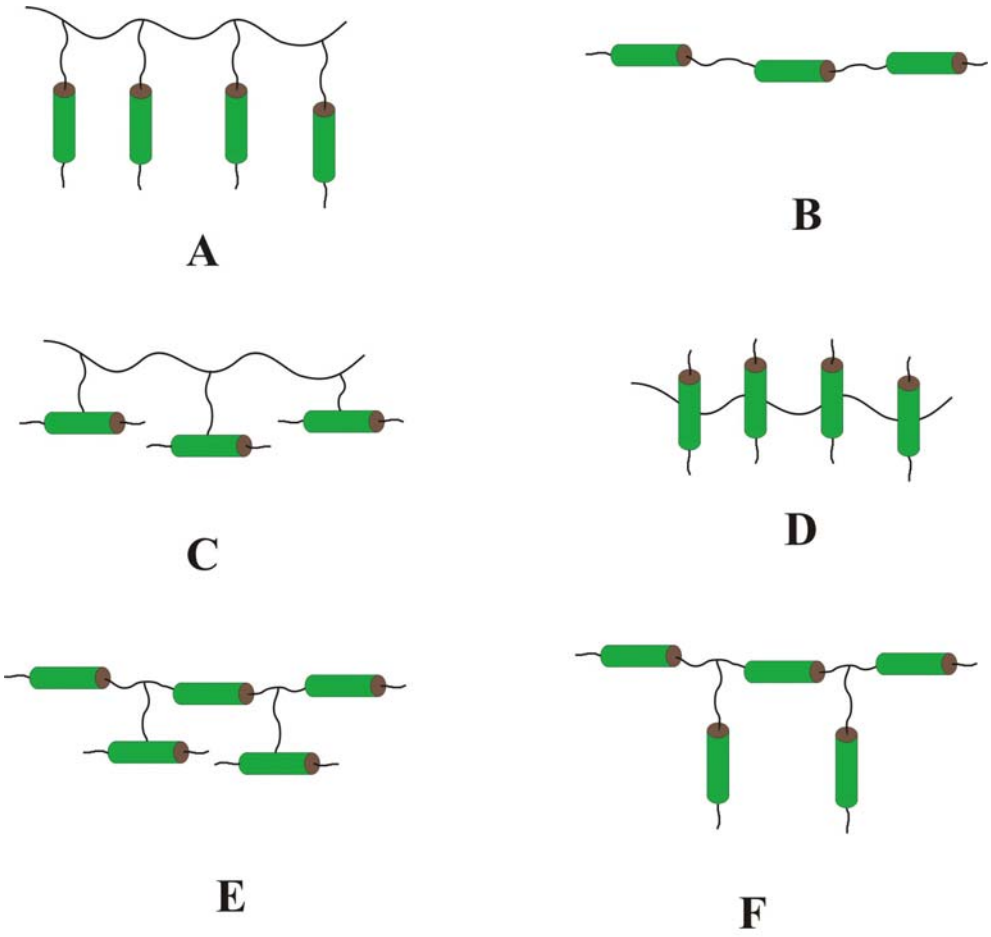

Figure 1.3: Different types of LC polymers, (a) and (c) side-chain polymers with and-on and side-on connection respectively. (b) and (d) main-chain polymers with and-on and side-on connection respectively. (e) and (f) side-chain polymers with end-on and side-on connection respectively.

The variety of LC polymers is not restricted just to main-chain and side-chain elastomers, in the course of a search for polymers with new properties, combined main-chain/side-chain liquid crystalline polymers and elastomers have been synthesized [73]. As it follow from their name, in

this type of polymers rigid mesogenic moieties are included in the main-chain and attached as a side groups as well see Fig. 1.3e and f.

First LC polymers were based on rod-like mesogens but just few years after side-chain LC elastomers with disc-like mesogens were synthesized [74].

All side-chain LC polymers and elastomers are based on the same general structure, mesogenic molecules are attached as a side chains to a polymeric backbone, but they can be realized by different chemical structures. A great variety of LC polymers with different chemical types of backbones, mesogens and spacers have been synthesized [30, 75].

Although, the type of the mesogens (their chemical structure) and spacer are the main factors defining the temperatures of phase transition and other properties of side-chain LCPs, the type of polymeric backbone has an influence on properties of LCP [30]. Not only the type of the spacer and mesogens can be changed, also, the type of the attachment, for instance, the mesogens can be connected “end-on” or “side-on”. Fig. 1.3 shows different types of main-chain and side-chain LC polymers.

The type and the length of spacers and volume fraction of rods influence the phase stability. The change of the spacer length leads to a so-called odd-even effect, in case when spacer has odd number of (CH_2) groups, pendant rods prefer to be perpendicular to the backbone, if the number of (CH_2) groups is even, mesogenic groups tend to be parallel to the polymeric backbone. This effect is stronger pronounced for shorter spacers. Usually in order to obtain a smectic order in LC elastomers longer spacers are required than the ones for the nematic phase. The long spacers provide enough mobility of the mesogenic side groups to make the micro phase separation and formation of the smectic layers possible.

1.2.2 Conformation of a polymeric backbone in LC polymers and elastomers

In main chain-polymer orientational order of the mesogens and anisotropy of polymer chain are directly connected (Eq. 1.5).

$$\left(\frac{l_{\parallel}}{l_{\perp}} - 1\right) = \alpha Q \tag{1.5}$$

Where $l_{\parallel}$ and $l_{\perp}$ are the components of the step length tensor in the direction parallel and perpendicular to the director and Q is the orientational order parameter. For the main-chain polymer the proportionality coefficient α is always positive and can have a quite large value [33].

In case of side-chain LC polymers the orientational order of the mesogens and polymer backbone are also mutually dependent, but the coefficient α is smaller than in case of main-chain polymers and dependence for the side-chain elastomer is more complicated [33].

Due to the coupling of polymeric network and orientation of the mesogenic molecules, the shape of the elastomer and orientation of the mesogens are interconnected. Therefore, the deformation of an elastomer can lead to reorientation of the director and vice versa, reorientation of mesogens can change the shape of elastomer. The later reveals itself in a spontaneous shape change at phase transition, for example, at isotropic-nematic or isotropic-smectic A phase transition.

The shape change at phase transition is defined by a shape of polymeric backbone in different phases which is usually described by a gyration tensor or gyration tensor spheroid. Chain conformation of ordinary polymers and polymeric backbones in isotropic phase of LC polymers and elastomers is spherical because all directions are equivalent and therefore the radius of gyration is the same in all directions and can be described by one parameter R_0. In nematic main-chain elastomers as the order parameter is increasing the rod-like segments tend to align parallel to each other and thereby the radius of gyration parallel to the director is increasing and the spheroid of gyration becomes an ellipsoid which is characterized by its three principal axes R_x, R_y, R_z with z axis parallel to the director. In uniaxial liquid crystalline polymers and elastomers $R_x = R_y$ and it is denoted by $R_\perp$ and R_z is denoted by $R_\parallel$. So in main-chain liquid crystalline elastomer with end to end connection of the mesogens $R_\parallel$ is always larger than $R_\perp$, such conformation is called prolate. In case of side-chain liquid crystalline polymer $R_\parallel$ can be larger or smaller than $R_\perp$ in the latter case the conformation is called oblate. Side-chain LCEs can have prolate or oblate backbone conformation; this depends on the type of attachment of the mesogenic groups, Fig. 1.3. End-on linking makes an oblate conformation energetically more favourable whereas side-on linking makes prolate conformation more favourable. Also in case of end-on linking the length of the spacer plays an important role. If a liquid crystalline elastomer has a prolate conformation in the nematic or smectic phase, then its length parallel to the director increases at the isotropic–nematic transition. If the backbone conformation is oblate then the length parallel to the director decreases at the isotropic–nematic transition. Therefore thermo-mechanical measurements which study the shape changes at the phase transition can help to determine whether the chain conformation is prolate or oblate in the liquid crystal phase.

The radius of gyration R_i is related to components l_{ij} of the step length tensor of the polymer $\langle RiRj \rangle = \frac{1}{3} l_{ij} L$, where L is the total length of the chain, also called the arc length. The spontaneous deformation is defined by the ratio of step length tensor components parallel and perpendicular to the director $\lambda = (l_{\parallel} / l_{\perp})^{1/3}$. The square root of this ratio $(l_{\parallel} / l_{\perp})^{1/2}$ can be directly measured by neutron scattering from the deuterated backbone [28].

1.2.3 Orientation of LC polymers by external forces

Usually in bulk samples of liquid crystalline polymers, if no special precautions have been taken, the director is not uniformly oriented and samples have a poly-domain structure. But, applying an external magnetic or electric field, the orientation of mesogens can be changed [76, 77], if the external magnetic field is strong enough uniform alignment of director in a nematic LC polymer can be achieved, as in low molecular mass nematic liquid crystals, and then the sample can be crosslinked in to a mono-domain nematic elastomer.

Also, uniform alignment of the mesogens can be obtained in LCP fibres spun from the nematic or isotropic melt [78-80]. The orientation of the mesogens in spun fibres is caused by anisotropic conformation of the polymeric backbone which the polymer adopts in the mesophases. The spinning process induces anisotropic conformation of the polymeric backbone and the radius of gyration parallel to the long axis is larger than perpendicular to it. Depending on the length of the spacer the conformation of the polymeric backbone in the mesophase can be prolate or oblate and mesogens tend to orient themselves parallel or perpendicular to the long axis of the fibre [81]. For the nematic or smectics LCP with oblate conformation, mesogens are perpendicular to the long axis of the fibre and randomly oriented in the plane perpendiculars to it, for the smectic LCP this means that smectic layers are parallel to the long axis of filament but their normals are randomly oriented in the plane perpendicular to the fibre long axis.

If the director of a liquid crystalline polymer has not been uniformly aligned before the crosslinking, then the obtained elastomer inherits a poly-domain structure of the precursor polymer, also elastomers crosslinked in the isotropic phase have a polydomain structure. A large number of attempts to align polydomain elastomers by magnetic or electric field have been done, but usually electric and magnetic fields turn out to be not strong enough to obtain a mono-domain structure in crosslinked samples.

1.2.4 Orientation of LC elastomers by mechanical deformation

In LC elastomers orientation of the mesogens is coupled with the orientation of the polymeric backbone which can be changed by a mechanical deformation, therefore mechanical deformation can be used as an external aligning field [78, 79, 81]. Uniaxial stretching of poly-domain nematic elastomers with prolate backbone conformation leads to uniform alignment of the director parallel to the stretching direction. It was shown by Küpfer and Finkelmann that uniform alignment obtained by mechanical deformation can be anchored by the second crosslinking [82]. The process of the alignment can be observed even with a naked eye: at large enough strain, opaque polydomain sample becomes transparent. The reorientation of the director takes place only after some threshold value of deformation. At small deformations, the mechanical response of the polydomain sample is linear, like in case with an isotropic rubber. When the threshold strain is reached, further deformation continues at constant stress and a stress plateau on the strain-stress diagram is observed. Appearance of a stress plateau can be explained by a rotation of the director in different domains towards the stretching direction. This deformation in nematic elastomers can be realized as soft-mode elasticity and therefore can be done at constant or almost constant stress. When all domains are oriented along the stretching direction stress again linearly increases with strain.

From symmetry considerations of nematic elastomers it is expected that uniaxial strain will induce uniform alignment of director only for the nematic with prolate conformation, in case of oblate conformation the director will be perpendicular to the stretching direction but randomly distributed in the plane perpendicular to it. But it was reported that in some LCEs with oblate conformation uniform alignment can be induced by uniaxial stretching, the director is perpendicular to the stretching direction and one of the surfaces of the sample with rectangular cross-section [81], the reason for the uniform orientation in the plain perpendicular to the stretching direction is not clear.

In smectic A liquid crystalline polymers, the polymeric backbone usually tends to be situated between the smectic layers, and therefore smectic LC polymers and elastomers usually have oblate configuration and uniaxial stretching of smectic elastomers is not an appropriate method for the preparation of smectic single crystal elastomers. Although, uniaxial stretching in smectic A phase aligns the smectic layers parallel to the stretching direction, but with the layer normals randomly oriented in the plane perpendicular to the stretching direction.

Because of the oblate conformation, smectic elastomers can not be aligned by a uniaxial stretching, but only by a uniaxial compression or equivalently by a symmetric biaxial stretching.

Uniaxial compression leads to prolate configuration of the polymer backbone and aligns the director parallel to the compression direction and hence smectic layers perpendicular to it.

In case when liquid crystal elastomer has a prolate nematic phase between smectic and isotropic phase, such material can be aligned by uniaxial stretching in the nematic phase and then cooled down in to the smectic phase. During cooling the homogeneous alignment of the director preserves and smectic layers are spontaneously forming perpendicular to the stretching direction. Even if there is no nematic phase between smectic and isotropic phase, it could be possible to obtain a monodomain sample by stretching a polydomain smectic elastomer in the isotropic phase and subsequent slow cooling down in to a smectic phase [80]. Also smectic monodomain samples have been obtained by application of a uniaxial mechanical stress in a swollen state and subsequent deswelling [40, 83]. Smectic monodomain LCEs obtained by this methods have a prolate conformation of polymeric backbone even if the precursor polymer have an oblate backbone conformation. That can be explained by the existence of nematic order below the isotropic transition or by the existence of nematic phase in a very narrow temperature interval. Nematic order leads to a prolate conformation of a backbone. Although at a following phase transition into smectic A phase the polymeric backbone tends to adopt equilibrium oblate conformation this tendency is opposed by the high elastic modulus perpendicular to the layers [83].

In case of tilted smectic elastomers, such as smectic C elastomers, uniaxial stretching is not sufficient for the alignment of the mesogens and smectic layers. After uniaxial deformation, the director is oriented parallel to the stretching direction but smectic layer are randomly oriented on the cone surface. In order to align smectic layers an additional uniaxial deformation at some angle to the first deformation [84, 85] or shear deformation has to be applied [86].

Although, an uniaxial compression or equivalently a biaxial stretching are the most natural methods for the orientation of smectic A elastomers with prolate conformation of polymeric backbone and it was proposed quite a long time ago, these methods were not realized until 2004 [87] because of the technical difficulties. To be exact, this method does not use uniaxial compression but anisotropic deswelling which firstly was proposed for the macroscopic alignment of cholesteric elastomers [88]. During the anisotropic deswelling the LC gel is allowed to deswell only in one direction, for instance z-direction, in two other directions in xy-plane, dimensions of the gel have to be constant. Such anisotropic deswelling in one direction is equivalent to a uniaxial compression and leads to an oblate backbone conformation. At the same time transition from the isotropic in to smectic phase takes place and smectic layers form spontaneously perpendicular to the deswelling direction. As expected, smectic liquid single crystal elastomers obtained by this method

have an oblate conformation of the polymeric backbone [87] in contrast to the smectic SLCEs oriented by the uniaxial stretching [40, 80].

1.2.5 Anisotropy of the nematic mono-domain deformation

The deformational behaviour of nematic monodomain elastomers strongly depends on the stretching direction. In case of the nematic elastomer with prolate configuration of the polymeric network stretching parallel to the director increases the anisotropy of the network. Due to the coupling of the mesogen orientation with the orientation of the network, the orientation of the director doesn't change and the orientation order parameter can be increased.

If the stretching direction is perpendicular to the director, stretching leads to the rotation of the director in such a way, that the angle between director and deformation direction is decreasing. Due to the symmetry of nematic elastomers, clockwise and counter clockwise rotations are equivalent. But, rotation in one direction would cause a large shear deformation which is not compatible with the border conditions when the both sides of the elastomer are fixed and have to be perpendicular to the stretching direction. Thus, the deformation of a nematic elastomer with fixed edges leads to the formation of a stripe texture with rotation of the director in neighbouring stripes in opposite directions [1, 26, 89].

1.2.6 Anisotropy of the smectic mono-domain deformation

Deformation of smectic elastomers is more complicated and can depend on the details of chemical structures and preparation conditions of the monodomain. Different types of deformation have been described in works of Nishikawa et al.[6, 12, 40] and Komp et al. [14, 20] from the group of Prof. Finkelmann.

Elastomers which were studied by Nishikawa are side-chain LC elastomers with end-on attachment of the mesogenic groups. Thermoelastic behaviour indicates that the polymeric network has prolate configuration. Stretching of the elastomer perpendicular to the director doesn't induce an orientation of the director like in nematic elastomers. The elastic modulus for the deformation perpendicular to director is of the same order as the elastic modulus of isotropic rubber $E_z = 1.4 \times 10^5$ N/m^2. Under deformation up to 100% the smectic layer structure remains unchanged and the thickness of the smectic layers and the thickness of the sample perpendicular to smectic layers

(parallel to the director) don't change [12]. The volume of the sample is constant at any value of deformation and the stretching deformation is compensated by compression in the smectic layer plane. This behaviour is similar to the deformation of smectic films of low molecular mass liquid crystals. During stretching, molecules freely move in the layer and the thickness of the smectic layers and of the film are constant. Due to this similarity that phenomenon was called in-plain fluidity [12].

Stretching of such elastomer parallel to the director reveals threshold behaviour. At small deformations the elastomer shows a high elastic modulus which is almost two orders of magnitude higher than for the deformation perpendicular to the director $E_z = 1.0 \times 10^7$ N/m^2. When the deformation exceeds a threshold of about 3-5%, the elastic modulus decreases and becomes of the same order as perpendicular to the director. Above the threshold, the sample becomes opaque. X-ray measurements revealed, that above the threshold, the deformation causes rotation and break-down of the smectic layers [40].

The LCEs studied by Komp are also side-chain LC elastomers but with a side-on attachment of the mesogenic groups. The stress-strain dependence of these elastomers is similar to the stress-strain dependence of the elastomers studied by Nishikawa. The deformation parallel to the director reveals threshold behaviour with a very high modulus before the threshold and much lower modulus above the threshold. Despite the similarity of the stress-strain diagram the deformational behaviour of these two types of elastomers turns out to be quite different at more detailed examination. The elastic moduli of the elastomer with side-on attachment of the mesogenic molecules along and perpendicular to the director are larger than corresponding moduli of the elastomer with an end-on attachment. Nishikawa et al. has measured $E_z = 1.0 \times 10^7$ N/m^2 parallel to the director and $E_x = 1.4 \times 10^5$ N/m^2 perpendicular to the director. The elastomer studied by Komp have $E_z = 1.4 \times 10^7$ N/m^2 parallel to the director and $E_z = 3.8 \times 10^6$ N/m^2 = perpendicular to it. These values show that the elastomer with end-on attachment is more anisotropic, the ratio $E_z/E_x = 75$ is much larger then the value for the Komp elastomer where $E_z/E_x = 3.7$. Another difference is that the elastic moduli of the Komp elastomer are highly temperature dependant while the moduli measured by Nishikawa are almost temperature independent in a smectic-A phase.

The most important difference between the two types of elastomer is the influence of the deformation on orientation of the smectic layers. Like in case of Nishikawa's materials, deformation of the elastomers studied by Komp perpendicular to the director doesn't cause reorientation of the smectic layers. The maximal deformation that can be reached is about 40-45%. After that the sample usually breaks down. The thickness of the sample perpendicular to the smectic layers remains constant up to 20% deformation. After that it's slightly decreasing with increasing

deformation. The compression perpendicular to the smectic layers ε_z reaches approximately 4-5% at when the stretching deformation ε_x is about 40%. X-ray measurements reveal only a very small decrement of the smectic layer thickness with increasing stretching deformation and the maximal layer thickness change is about 2% at $\varepsilon_x \approx 40\%$.

Deformations parallel to the director of elastomers studied by Komp don't cause reorientation of the director or break down of the smectic layers even above the threshold, even at very large deformation parallel to the director sample remains transparent. X-ray measurements have not revealed any rotation of the smectic layer for the deformation up to 80%. This unusual behaviour was explained by a particular defect structure in the smectic layers which makes possible creation of new smectic layers and therefore deformations parallel to the director do not induce rotation or break down of the layers [14, 20].

Recently experiments on SLCE with an anisotropic of elastic modulus properties intermediate between the Komp's and Nishikawa's elastomers have been reported, the ratio of elastic modulus is $E_z/E_x \approx 10$ [13]. This LCE is a side-chain LCE which consists of poly(methylsiloxane) backbones, two end-on attached of the mesogens carrying fluorinated tails and bifunctional isotropic crosslinker [13]. This material also exhibits high elastic modulus parallel to the director $E_z = 1.4 \times 10^7$ N/m^2, elastic modulus parallel to the layers is approximately two times higher then in isotropic phase, that is attributed to the high concentration of defects in smectic layers. The deformation parallel to the smectic layers reveals in-plane fluidity like in two above described elastomers, the orientation of the mesogens don't change and the thickness of the smectic layers is constant. X-ray measurements do not reveal rotation of the layers during deformations parallel to the director, like in case of Nishikawa's elastomers, but the intensity of smectic reflexes in the small angle region and the correlation length strongly decrease, indicating a break down of the smectic layers.

Although, the described above elastomers have a quite different smectic order [12-14, 40]; highly correlated Nishikawa's elastomers or elastomers with strongly frustrated layers prepared by Kramer et al. [13], all of them have very high elastic moduli parallel to the director. Yet response of the smectic layers to deformations parallel to the director is different in all three cases. In case of the highly anisotropic Nishikawa's elastomers [40] deformation parallel to the director induce break down of some parts of the layer while other parts preserve smectic order and only rotate. Break down of the layers without rotation was found during deformation of the elastomers with the intermediate anisotropy of the elastic moduli ($E_z/E_x \approx 10$) and highly frustrated smectic layers described by Kramer [13]. The elastomers described by Komp [14] deform without the rotation or

break down of the layers. The defect structure of these elastomers makes possible the creation of new smectic layers for the compensation of the deformation parallel to the director.

Summarizing these experimental observations, the conclusion can be drawn that the response of the smectic layers to deformation is defined not by the elastic modulus but by the anisotropy of elastic moduli.

Measurements on LCSE demonstrating completely different behaviour from elastomer described above have been reported [42-47, 90]. Optical reflectometry measurements revealed that the stretching of the free-standing films in the SmA phase parallel to smectic layers induces a compression of the film thickness [47]. Measurements of the film compression by optical reflectometry and small angle X-ray scattering prove that the compression of the film is caused by compression of the smectic layer. The measured Poisson ratio is isotropic and close to ½ [44, 47]. The question about the origin of completely different behaviour of the elastomers demonstrating in-plane fluidity and elastomer in which deformations parallel to the smectic layers lead to compression of the film and smectic layers is unsolved so far.

Chapter 2 Experimental methods

2.1 Compounds and their phase behaviour

The LC polymers used in this work for the preparation of LCEs had been provided by the research group of Professor R. Zentel. The notations, phase sequence and phase transition temperatures of the uncrosslinked polymers are presented in the Table 2.1. All these LCPs are side-chain LCPs which consist of a siloxane backbone, end-on attached mesogens and cross-linking groups Fig. 2.1. The crosslinker groups have the same length and the same structure as mesogens except for an additional terminal photo reactive group. Polymers 1-3 are random side-chain copolymers, while polymer 4 – BR153B is a homopolymer.

Name	Lab Name	x	y	z	Phase sequence
1	CT86	0.95	0.05	2.7	SmX 65°C SmC* 95–96°C SmA 125°C Iso
2	BR162A	0.95	0.05	2.9	SmX 45°C SmC* 95°C SmA 140°C Iso
3	BR162H	0.9	0.1	2.9	SmX 45°C SmC* 100°C SmA 145°C Iso
4	BR153B	0.93	0.07	0	SmX 88°C SmC* 166°C SmA 199°C Iso

Table 2.1 Compounds and their phase behaviour

Polymeric backbone, mesogenic and crosslinker groups are the same in case of homopolymer and copolymers, the only difference is that in a homopolymer all backbone segments are substituted with mesogens or crosslinkers while in the copolymers some backbone segments are not substituted with side chains. The ratios of mesogen substituted (x), crosslinker substituted (y) and unsubstituted siloxane backbone units (z) for the different precursor polymers are presented in the Table 2.1. The synthesis of the precursor polymers has been described in detail elsewhere [46, 91].

It has been found that different chemical nature of the mesogens and polymeric backbone leads to a micro-phase separation in smectic phase. Mesogens segregate into smectic layers and siloxane backbone are mainly sandwiched between neighbouring layers [92]. Due to such layered structure the length of the cross-linking group plays an important role in formation of the network topology. In case when a crosslinker and mesogenic group are of the same length, they are

compatible with the layer structure and connect different siloxane layers, such cross-linking is known as interlayer cross-linking.

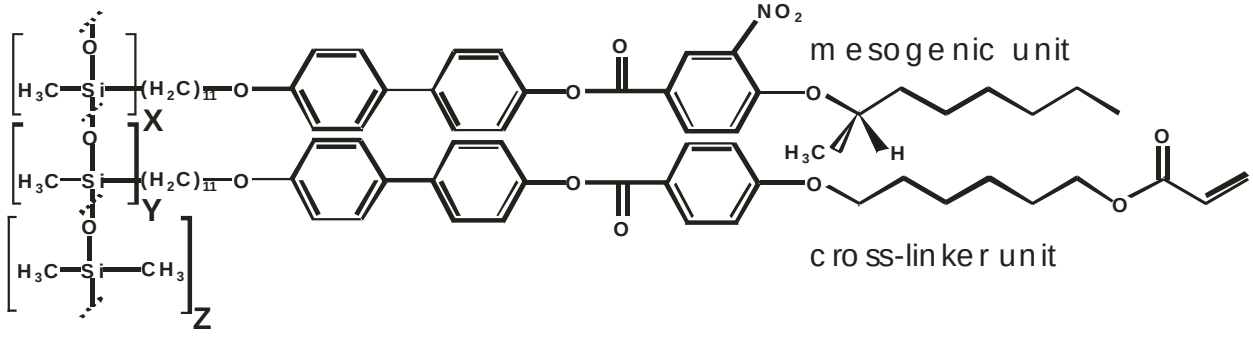

Figure 2.1: Chemical structure of the precursor polymers.

Due to the cross-linking between different layers network obtained after a cross-linking has three-dimensional topology. If the length of a crosslinker is much smaller then the length of the mesogen, crosslinking between two neighbouring layers is incompatible with smectic structure and would induce defects which increase the free-energy and therefore such crosslinking is energetically unfavourable. Cross-linking inside one layer is formed in such LCPs, and such network is mainly two-dimensional [46]. This type of crosslinking is also called intralayer crosslinking. Coupling between orientation of the mesogens and polymeric network is much stronger in 3D network formed by interlayer crosslinkers then in the case with interlayer crosslinkers, for this reason only elastomers with interlayer crosslinkers have been chosen for the investigations.

2.2 Preparation of the free standing elastomer films

Free-standing elastomer films have been prepared by crosslinking of free-standing LCP films in the smectic A phase. The scheme of the set-up used for the preparation of free-standing LC polymer films is shown in Fig. 2.2. The main part of the set-up is a frame with one movable edge. The temperature of the samples is controlled by a Linkam heating stage THMS 600. For the film preparation opposite edges of the frame are moved together so that only a very narrow gap between them remains, this gap is filled with a small amount of precursor LC polymer. The position of the movable edge is controlled by a microscrew. By drawing apart the movable edge from the frame edge a film of required size can be prepared. In the SmA phase and at lower temperatures the viscosity of the polymers is too high for the preparation of free-standing films, therefore films were

prepared at temperature close to a bulk SmA-Isotropic phase transition, usually at temperature 5-10°C above the transition temperature. Then the film is cooled down into the SmA phase and cross-linked by UV light irradiation, a 250 W Panacol-Elosol UV point source UV-P 280 has been used for irradiation. The time of UV irradiation is usually 2 hours, irradiation was performed in two steps, in the first step, two side edges of the free standing film are shielded from UV exposure with an opaque mask (Fig. 2.2). After the first crosslinking, the sample consists of an elastomer stripe in the middle and two liquid parts at both sides of this stripe, these liquid parts can be easily removed. When uncrosslinked material on the sides is removed some amount of still liquid material can gather on the edge of crosslinked film forming an edging consisting from unoriented material. For this reason film is crosslinked for the second time for one hour. This method allows to prepare free standing elastomer film fixed at two opposite edges [47].

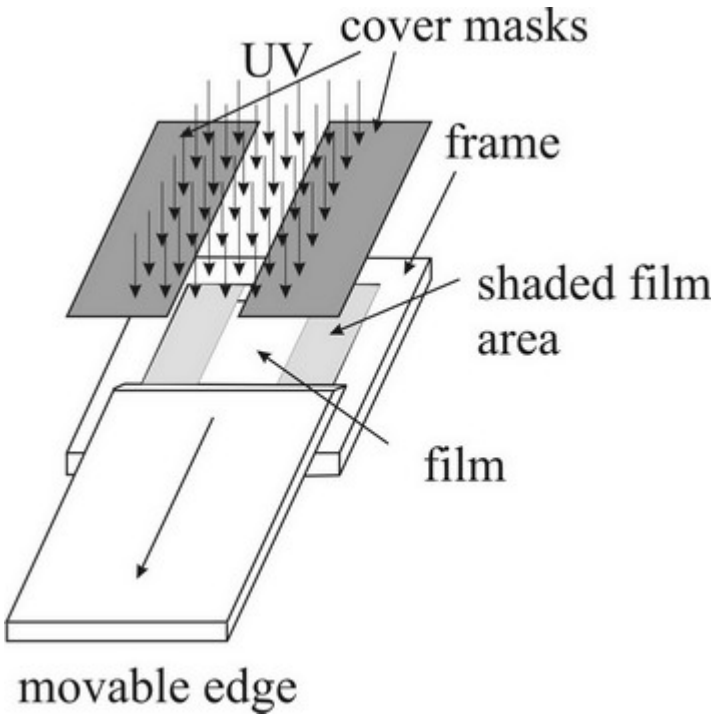

Figure 2.2: Schematic representation of the film stretching set-up.

The minimum exposure time for a complete crosslinking of LC polymer films has not been tested, it may be sufficient to irradiate the sample for a much shorter time.

Often, immediately after drawing LCP films have a very inhomogeneous thickness (Fig. 2.3). The homogeneity of the film thickness can be improved by an alignment at the temperature close to SmA – Isotropic phase transition. At this temperature polymer is less viscous than in smectic phase which makes the flow of material in the layer plain possible. Small regions with the

same thickness tend to coalesce and form large regions with a homogeneous thickness. At low temperatures polymer viscosity is much higher than in the isotropic phase and flow of the material is negligible on the time scale of the experiments and only diffusion tends to smooth thickness variation. A long time exposure to high temperatures leads to thermo-activation of some amount of crosslinkers, and this turns the LCP film into the slightly crosslinked elastomers and prevent a further homogenisation of the film thickness. This becomes especially obvious for the homopolymer with high SmA – Isotropic transition temperature. After a few hours at this temperature homopolymer is not longer fluid and any attempt to change the size of the film leads to its rupture.

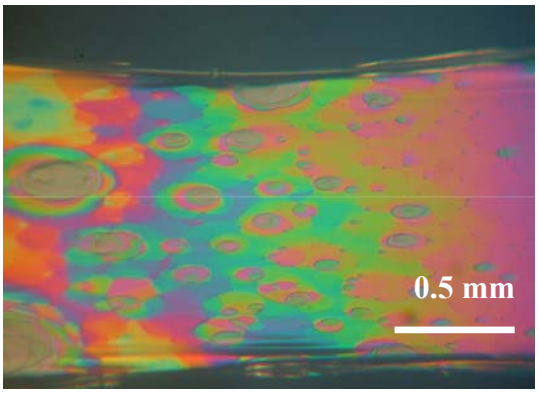

Figure 2.3: Free-standing LC elastomer film prepared by cross-linking of a free-standing LCP film.

The "diluted" LC polymer films can be further drawn even after one or two days at SmA – isotropic phase transition temperature. This makes the preparation of the film with homogeneous thickness very difficult even in case of copolymers and impossible in case of the homopolymers.

2.3 Preparation of the free standing elastomer balloons

Elastomer balloons (Fig. 2.4) were prepared by a photo crosslinking of LC polymer bubbles using UV irradiation. In order to prepare a smectic bubble, free-standing film is drawn on the top open end of vertically standing capillary which is placed into a copper thermo box (Fig. 2.5) for a temperature control, and then the film is inflated into the smectic bubble by slow blowing of a small volume of air into the capillary using a microliter syringe.

The temperature inside the heating box is regulated by a temperature controller with an accuracy 0.1°C, maximal temperature which can be attained inside the heating box is about 210°C.

As well as in case of free-standing films, optimal temperature for the preparation of smectic bubbles is 5-10°C above the bulk smectic A – isotropic transition.

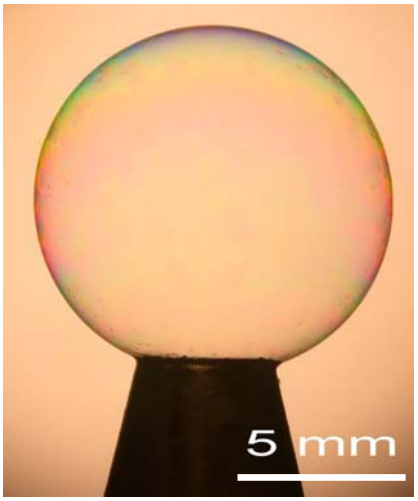

Figure 2.4: An elastomer balloon prepared by cross-linking of a LCP bubble in SmA phase.

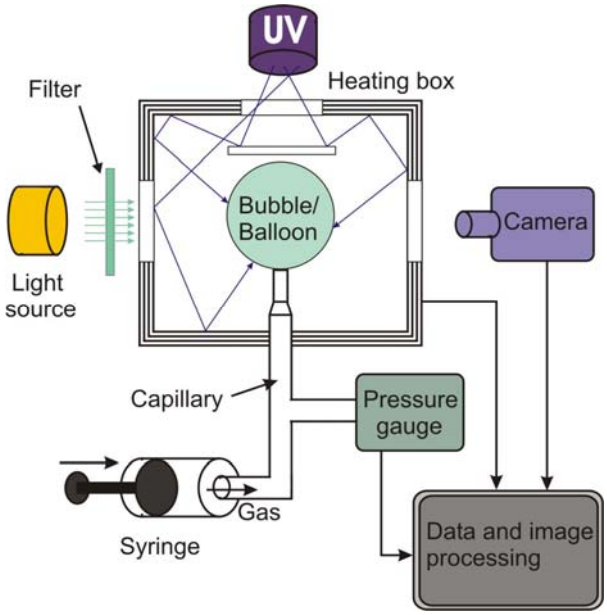

Figure 2.5: Experimental set-up used for the preparation of LC elastomer balloons and measurements of stress-strain dependence for LC elastomer balloons in different mesophases.

For the optical observation, the bubble is illuminated with parallel light and photos are made by Nikon Coolpix 990 digital camera. In order to prevent bubbles from uncontrolled crosslinking, borosilicate glass with a cut-off wavelength 320 nm have been used. The bubble radius could be measured with an accuracy of 0.01mm using image-processing software. The pressure difference between the pressure inside the bubble and the ambient atmospheric pressure is measured by a very

sensitive capacitative pressure gauge (absolute accuracy about 2 Pa, relative accuracy 0.1Pa). The film thickness is determined optically from the transmission images. As in case of free-standing film, the thickness of the smectic bubbles is not homogeneous, usually the upper part of the bubble is thinner than the bottom part (Fig. 2.4).

LCP bubbles have been slowly cooled down into the smectic A phase and then crosslinked by UV light irradiation. Bubbles have been irradiated by UV light through a quartz-glass window in the top of the heating box. Direct irradiation lead to inhomogeneous illumination and the crosslinking rate is different in the different parts of the bubble and such bubbles usually collapse. To provide uniform illumination, the direct UV beam was blocked and inner walls of the heating box had been covered with randomly reflecting material. Exposure times between 1 and 2 hours had been used.

2.4 Optical microscopy

Optical microscopy and polarizing optical microscopy (POM) along with X-ray methods and differential scanning calorimetry (DSC) is one of the most important methods for the characterisation of liquid crystals, liquid crystalline polymers and elastomers.

A typical set up of a polarizing microscope usually consists of a light source, polarizer, sub stage iris, condenser, rotation stage, hot stage with sample, objective, analyzer and eyepiece. In some cases additional components such as a compensator and Bertrand lens for conoscopic observations can be included. By the orthoscopic observations, polarization effects together with the image of a sample are observed, while by the conoscopic observation only interference from a sample is observed [93]. Orthoscopic observations with crossed polarizers give an opportunity to define whether the sample under investigation is anisotropic or not. Some microscopes with second light source give an opportunity to perform a reflected light microscopy.

Many LC phases have their own distinct optical textures and can be identified by the POM observations, therefore studying of the liquid crystal textures at different temperatures can help to detect different liquid crystalline phases and temperatures of the phase transitions between them. Different patterns or textures and defect observed under POM allow not only to detect different mesophases but also to define an orientation of the nematic or smectic director [94].

In our experiments a microscope Carl Zeiss Axioskope 40 had been used. Photos were made by Nikon Coolpix 990 digital camera. In order to control the temperature the setup for the film preparation and drawing was placed in to a Linkam heating stage THMS 600.

2.5 Optical reflectometry

Optical reflectometry can be used for the measurement of the thickness of thin transparent films. The optical reflectometry method is based on the interference between two beams reflected at the top and bottom surface of the film. If a film with the thickness of a few hundred nanometres is irradiated by a white light its reflection image appears coloured and the interference colours depend on the film thickness. If the same film is irradiated with a monochromatic light, some regions of the film will be dark, while other regions bright.

For the free-standing films with a small reflection coefficient, the interference can be observed only in reflection but not in transmission, because the intensities of the first and second reflected beams are approximately the same while the intensity of the beam which comes through is much higher then that of the beam which comes through after two reflections.

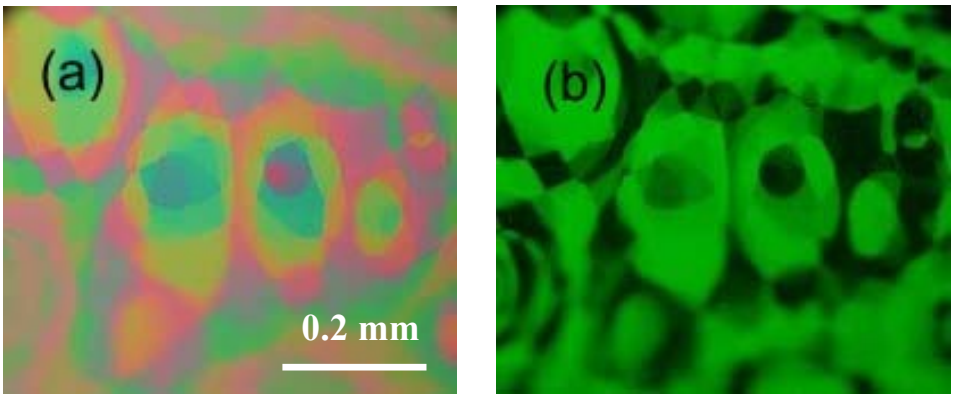

Figure 2.6: Reflection microscopy images of the thin free-standing smectic LCE film, obtained with (a) white light, (b) monochromatic light with the wave length λ = 547 nm.

The intensity of the third and higher order reflected beams is usually much lower than that of the first two; therefore it is often enough to consider the interference of the first and the second reflected beam and the contribution of higher order reflected beams can be neglected. The exact formula for the film reflectivity which takes into account multiple beam interference is [95]:

$$R(\lambda) = \frac{4r^2/(1-r^2)^2 \sin^2 \Delta\varphi}{1+4r^2/(1-r^2)^2 \sin^2 \Delta\varphi} \qquad (2.1)$$

where $\Delta\varphi = 2\pi n_0 \frac{d_{film}}{\lambda}$, d is a film thickness, λ is a wavelength and r is an amplitude reflection coefficient. The amplitude reflection coefficient is equal to the ratio of E-field vector of incident beam E_{0i} and reflected beam E_{0r} and it depends on the angle of incidence. The reflection coefficient $r_\perp$ when the E vector is perpendicular to the plane-of-incidence differs from the reflection coefficient $r_\parallel$ for the case when the E lies parallel to the plane-of-incidence.

$$r_\perp \equiv \left(\frac{E_{0r}}{E_{0i}}\right) = \frac{n_i \cos\theta_i - n_t \cos\theta_t}{n_i \cos\theta_i + n_t \cos\theta_t} \tag{2.2}$$

$$r_\parallel \equiv \left(\frac{E_{0r}}{E_{0i}}\right) = \frac{n_t \cos\theta_i - n_i \cos\theta_t}{n_t \cos\theta_i + n_i \cos\theta_t} \tag{2.3}$$

where, θ_i and θ_t are the angles of incidence and transmission, n_i and n_t are the refractive indexes of the ambient media and of the film respectively.

At nearly normal incidence $\theta_i \approx 0$ $r_\perp$ is equal to - $r_\parallel$

$$\left[r_\parallel\right]_{\theta_i=0} = \left[-r_\perp\right]_{\theta_i=0} = \left[\frac{n_t \cos\theta_i - n_i \cos\theta_t}{n_t \cos\theta_i + n_i \cos\theta_t}\right]_{\theta_i=0} \tag{2.4}$$

In the limit when θ_i tends to 0, $\cos\theta_i$ and $\cos\theta_t$ boss approach one, and hence

$$\left[r_\parallel\right]_{\theta_i=0} = \left[-r_\perp\right]_{\theta_i=0} = \frac{n_t - n_i}{n_t + n_i} \tag{2.5}$$

The absolute values of the $r_\parallel$ and $r_\perp$ become equal due to the fact that the plane-of-incidence is not defined when $\theta_i = 0$ and $\theta_t = 0$. In the case of free-standing film n_i is the refractive index of air and it is equal to one. We are interested only in the absolute value of the r, because in the Eq. 2.1 appears only second or fourth power of r, therefore we get:

$$r = \frac{n_0 - 1}{n_0 + 1} \tag{2.6}$$

n_0 is the effective refractive index, which corresponds to the ordinary refractive index of the mesogens in the smectic A phase.

Comparison of the results of X-ray and reflectometry measurement of compression of free-standing smectic elastomer films confirms that this approximation is valid for the SmA phase and even a good approximation for the SmC* phase of the material under investigation [42]. For a small value of ρ an approximate formula can be used:

$$R(\lambda) = 4r^2/(1-r^2)^2 \sin^2 \Delta\varphi \qquad (2.7)$$

Using this formula the phase difference for any point of the film can be found from experimental reflectivity dependence obtained with monochromatic light. However, the values of the phase difference obtained using Eq. 2.7 are not unambiguous, because phase difference values $\Delta\varphi$ and $\Delta\varphi \pm n\pi$, where n is an integer number, correspond to the same value of reflectivity. Therefore, in order to find the value of the phase difference unambiguously the order of the interference maxima and minima n has to be found. The order of the interference maxima and minima has been found using the reflectivity images obtained with white light.

Knowing the phase difference, optical path can be easily found $2\pi d_{(opt)}/\lambda = \Delta\varphi$ and the film thickness for the given refractive index is $d_{film} = d_{(opt)}/n_0$. Since the refractive index is not exactly known, we use the approximate value $n_0 = 1.5$ for the thickness calculations.

The error in the calculation of the $\Delta\varphi$, results from the experimental error in the measurement of the reflectivity at given wave length. Because $R(\Delta\varphi)$ at fixed wave length is not linear but proportional to $\sin^2(\Delta\varphi)$, the experimental uncertainty also depends on the position on the reflectivity curve: the uncertainty is the largest close to maxima and minima of the reflectivity curve, and it is the smallest where R = 1/2 R_{max}. The film thickness can be evaluated with an accuracy of ±35 nm close to maxima and minima of the reflectivity function and ±20 nm where the reflectivity is equal to ½ of the maximal value.

2.6 X-ray diffraction

2.6.1 Experiments on non-oriented material

The temperature dependence of the smectic LC elastomer and polymer have been measured using X-ray scattering measurement on bulk not-oriented LC elastomers and polymers. A thin glass capillary was filled with the substance under investigation in the isotropic phase. The thickness of the capillary was 0.5 mm. For the temperature control the capillary was placed into a heating-stage "INSTEK". The temperature was regulated with the accuracy 0.1°C. The Co Kα (λ=1.79Å) source in connection with Hi Star (Siemens AG) two dimensional area detector have been used (Fig 2.7). Diffractogram were recorded at different temperatures with interval 5 or 10°C. After that the substance was cross-linked in SmA phase by irradiation by UV light and the same procedure was repeated for the crosslinked material.

2.6.2 Experiments on oriented samples

Samples for the X-ray measurements were prepared by irradiation of free-standing films of the photo-crosslinkable polymer in the SmA phase, see section 2.5. This method allows us to obtain freestanding films fixed at two opposite edges [1, 6]. For the measurement of the smectic layer thickness dependence on deformation the film was stretched in discrete steps and after each step the thickness of the smectic layers was measured.

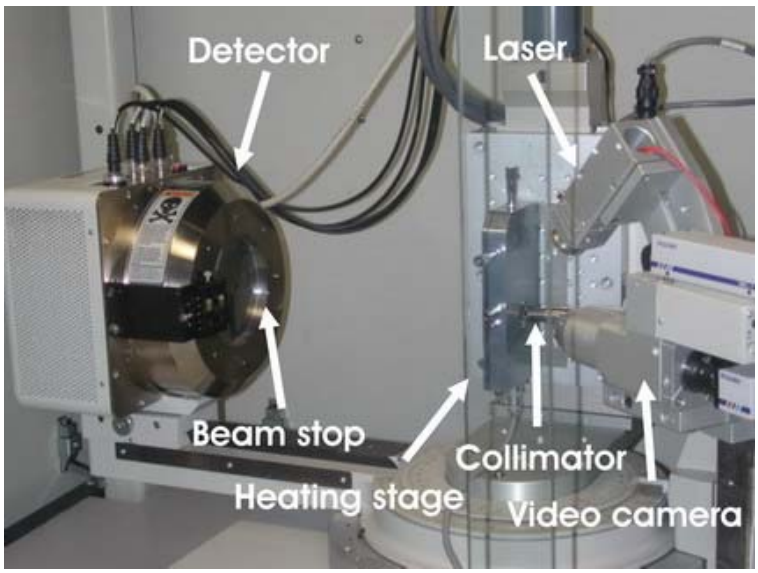

Figure 2.7: X-ray setup.

2.7 Polarized Fourier transform infrared spectroscopy

The Polarized Fourier transform infrared (FTIR) spectroscopy is a widely used method for the investigation of organic substances. The Fourier transform infrared spectroscopy provides the information concerning chemical composition of the substance under investigation, to be exact; it provides information about what chemical bonds are present in the substance. Infrared spectroscopy is a technique based on absorption of IR-radiation by molecules of the investigated substance, different molecules or more precisely defined different molecules bonds have different characteristic frequencies of vibration and absorption of the energy take place only at these frequencies. Therefore absorption spectrum of a substance is so to say a "fingerprint" of the substance. Polarized Fourier transform infrared spectroscopy allows not only to define the chemical composition of the sample but also the orientation of the molecules. Absorption of the energy depends on mutual orientation of the IR beam and molecular transition dipole moment. In case of Polarized FTIR spectroscopy linear polarized light is used and from the dependence of the absorption on the orientation of the polarizer the average orientation of the molecules can be defined.

2.7.1 The Michelson Interferometer

The most important part of the FT spectrometer is an interferometer. Most of contemporary FT spectrometers use the classical two-beam Michelson interferometer [96, 97], it is schematically shown on Fig. 2.8. It consists of two mutually perpendicular mirrors, one fixed mirror M1 and a movable mirror M2. Beam splitter, semi-transparent mirror, which bisects the angle between two mirrors splits the beam from the lights source with intensity I_S into two. Transmitted part of the beam travels to the fixed mirror M2 through the distance L, after reflection it travels back and reflected one more time on the beam splitter at that moment total path length is $2L$.

The second part which is reflected at the beam splitter travels in direction of the movable mirror M1 and back to the beam splitter where it meats the first part. Since, the mirror M1 isn't fixed and can be moved back and forth around zero position L by a distance x, the total path length of the second beam to the beam splitter where the two parts of the beam recombine will be $2(L+x)$. An optical path difference for the two parts of the beam will be $\delta = 2x$. Intensity measured by detector I_D is produced by interference of two beams E_1 and E_2.

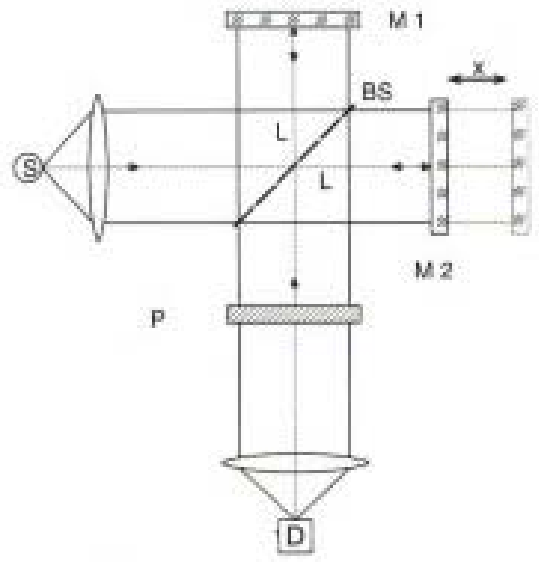

Figure 2.8: Schematic representation of the Michelson interferometer [98].

Intensity I_D can be divided in to two parts, first one is I_{DC} which is constant and the second one I_{AC} is a function of δ. Only a modulated part I_{AC} is important in spectroscopic measurements and it is usually referred to as interferogram. In order to obtain FT-IR spectrum an interferogram with and without a sample have to be measured and then have to be transformed into spectra of the source with sample absorption and without sample absorption. The ratio of the first one and the second is the IR transmission spectrum of the sample [98].

2.7.2 Dependence of the IR light absorbance on a polarization angle.

The absorbance of linearly polarized IR light is proportional to the scalar product of polarization vector $\vec{\varepsilon}$ and molecular transition dipole moment $\vec{\mu}$ [99].

$$\frac{dI}{Idl} = -k(\vec{\varepsilon} \cdot \vec{\mu})^2 \tag{2.8}$$

Due to a large number of molecules in the measured spot, the measured absorbance is proportional to an average value of scalar product over all molecules in the region of light transmission.

$$\frac{dI}{I \cdot dl} = -k_a \left\langle (\vec{\varepsilon} \cdot \vec{\mu})^2 \right\rangle = -k_a \sum_{i,j \in \{x,y,z\}} \varepsilon_i \varepsilon_j \left\langle \mu_i \mu_j \right\rangle = -\frac{1}{L \ln 10} \hat{A}(\vec{\varepsilon}) \tag{2.9}$$

Where $\hat{A}(\vec{\varepsilon})$ is an absorbance ellipsoid defined as a symmetric second-rank tensor. The expression $\langle \mu_i \mu_j \rangle$ is the mean product of components of transition moment in x, y, z coordinate system. Eq. 2.9 defines the change of the intensity when polarized light comes through a layer of thickness d*l*. In order to obtain the intensity for the case of finite thickness L Eq. 2.9 has to be integrated over the thickness of the sample from 0 to L and we will get the following equation:

$$I = I_0 e^{-k_a L\langle(\vec{\varepsilon}\cdot\vec{\mu})^2\rangle} = I_0 10^{-kL\langle(\vec{\varepsilon}\cdot\vec{\mu})^2\rangle} = I_0 10^{-\hat{A}(\vec{\varepsilon})} = I_0 10^{-kL\sum_{i,j\in\{x,y,z\}}\varepsilon_i\varepsilon_j\langle\mu_i\mu_j\rangle} \tag{2.10}$$

where $k = k_a/\ln 10$.

The change of orientation of polarization vector is realized by rotation of a polarizer in the plane perpendicular to the beam propagation direction. Assuming that direction of propagation is parallel to y axis of the laboratory coordinate system then the polarization vector will depend on the angle of polarizer as follows: $\vec{\varepsilon}(\Omega) = (\sin\Omega, 0, \cos\Omega)$.

The dependence of extinction $A = -\log(I/I_0)$ on the polarizer angle can be obtained from equation Eq. 2.10:

$$\begin{aligned} A(\Omega) &= -\log(I/I_0) = kL(\sin^2\Omega\langle\mu_x^2\rangle + \cos^2\Omega\langle\mu_z^2\rangle + 2\sin\Omega\cos\Omega\langle\mu_x\mu_z\rangle) \\ &= A(\Omega_0)\cos^2(\Omega-\Omega_0) - A(\Omega_0+90°)\sin^2(\Omega-\Omega_0) \end{aligned} \tag{2.11}$$

where $A(\Omega_0)$ and $A(\Omega_0+90°)$ define the main axes of the (time-averaged) projection of the absorbance ellipsoid in the layer plane, Ω_0 describes the mean bond orientation in the film plane and Ω is the orientation of the polarizer. This formula can be used for the analysis of the molecular bonds orientation. In order to find the main parameters of the absorbance ellipsoid: main axes, Ω and Ω_0 Eq. 2.11 was represented in a form more convenient for the fitting procedure[44]:

$$A_\nu(\Omega) = a + b\cos 2(\Omega - \Omega_0) \tag{2.12}$$

where the following parameters were introduced: $a = (A(\Omega_0) + A(\Omega_0+90°))/2$ and $b = (A(\Omega_0) - A(\Omega_0+90°))/2$.

2.7.3 Experimental setup

Polarized Fourier transform infrared (FTIR) spectroscopy is performed with an FTS-6000 FTIR (Bio-Rad) spectrometer in combination with an IR microscope (UMA-500 Bio-Rad). The size of the region chosen for the measurement is 250 μm × 250 μm. The polarized IR beam propagates perpendicular to the film surface and to the smectic layers. The dependence of the IR spectra on the polarizer angle φ is measured with 9° steps from 0° to 180°. IR spectra are recorded with a spectral resolution of 4 cm^{-1}.

The films are uniaxially stretched in discrete steps (Fig. 2.2) and measurements were repeated after each step. The average in-plane strain is determined from the distance of the two fixed edges of the film. The temperature of the samples is controlled by a Linkam heating stage THMS 600.

Chapter 3 Mechanical Properties

In this chapter the results of elastic moduli measurements of LCEs in different mesophases are presented. The elastic moduli have been measured using two different measurement methods. The first one is based on the deformation of free-standing elastomer balloons and the second one on the uniaxial stretching of free-standing films.

Smectic LCEs are highly anisotropic materials [12-14, 83], but the anisotropy of elastic properties reveals itself only in monodomain samples with the uniform orientation of the director. Polydomain samples consist of a large number of domains with different orientations of the director. Due to the random orientation of domains, anisotropy averages out and physical properties do not depend on the measurement direction. For this reason, monodomain samples have to be used for the measurement of the anisotropic elastic properties. For the preparation of monodomain smectic A LCE films with a uniform orientation of the smectic layers, the orientational effect of the surface between LCP and air has been used. During the drawing of a free-standing LCP film, smectic layers are oriented parallel to the film surface, only the structure with smectic layers parallel to the film surface is stable. Because in the smectic A phase the nematic director is perpendicular to the layers the uniform orientation of the layers corresponds to the uniform orientation of the director. It is not true for the smectic C or smectic C* phase. In the smectic C phase, even if the smectic layers are uniformly oriented, the smectic C director can be randomly oriented in the layer plane.

After the preparation of a free-standing smectic A LCP film with uniform orientation of the director, it can be crosslinked into a monodomain free-standing elastomer film. Only films with smectic layers parallel to the film surface can be prepared using this technique. Therefore in the uniaxial stretching experiments with free-standing smectic elastomer films, only elastic modulus parallel to the smectic layer can be measured.

This problem can be overcome by the experiments with free-standing elastomer balloons [45, 46]. As in free-standing smectic elastomer films, in the elastomer balloons smectic layers are parallel to the film surface [45]. Increasing of the balloon radius leads to a uniform biaxial stretching in the layer plane. The volume of the film has to be constant during the deformation, because of a large bulk elastic modulus (10^9-10^{10} Pa), hence, the uniform stretching in the layer plane has to be compensated by the film compression perpendicular to the film surface. If the elastic modulus perpendicular to the layer is much higher than in the layer plain, then the main contribution into the elastic energy of a deformed smectic elastomer balloon is due to the layer

compression and the elastic response of the elastomer balloons in the smectic phase is defined by the layer compression modulus. In the isotropic phase smectic layer structure disappears and elastic energy of the same elastomer balloons in the isotropic phase is defined only by the isotropic rubber modulus. Therefore, it is expected that smectic elastomer balloons will be much "softer" in isotropic phase. This means that for the same excess pressure inside a balloon, deformation in the isotropic phase has to be larger than in the smectic phase.

The elastic modulus parallel to the smectic layers is expected to be of the same order as in isotropic phase of the same material. But experimental investigations demonstrate that elastic moduli parallel to the smectic layers strongly depend on the chemical structure of the elastomer. While in some materials elastic moduli in the layer plane are very close to the elastic moduli in isotropic phase [1, 12] in other materials they can be up to ten times higher than that of isotropic phase [14].

3.1 Smectic elastomer balloons

If the internal pressure in an elastomer balloon is changed, the radius of the balloon has to change to a new value which corresponds to equilibrium between an excess pressure and elastic forces in the deformed balloon. Fig 3.1 shows the dependence of the elastomer balloon radius on the excess pressure inside the balloon, measured in the SmA phase.

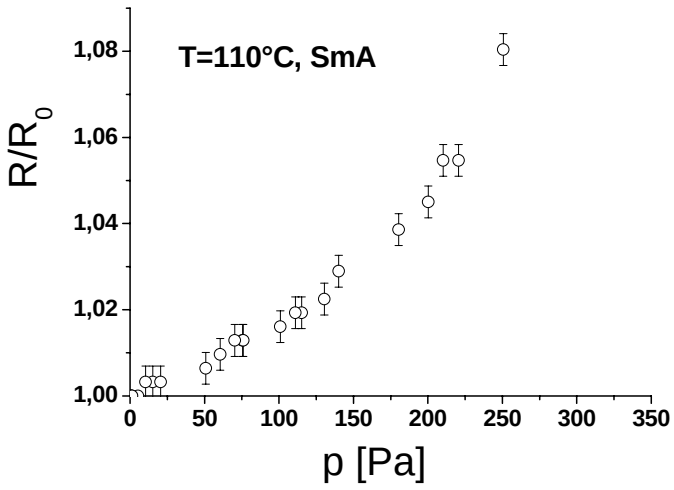

Figure 3.1: Pressure-radius relation for the elastomer diluted LC polymer (CT86) crosslinked in the SmA phase at T=110°C. The measurement temperature is 110°C in the SmA phase.

The elastomer balloon is prepared by crosslinking of the LCP bubble, prepared from the diluted LC polymer CT86 (see section 2.1), in SmA phase at T = 110°C, the time of a UV irradiation was 2 hours. In these particular measurements the radius of the balloon after the crosslinking is 2.71 mm and the thickness in the equatorial plane is approximately 2 μm.

For the measurement of the radius - pressure relation, the internal excess pressure was not changed in steps from the minimal to the maximal value, instead the pressure inside the elastomer balloon was randomly changed and the corresponding equilibrium radius was measured. The maximal deformation that was reached in these experiments was about 10%. The maximal deformation was not restricted in this case by a rupture of the balloons or by the plastic deformation as usually, but by the disconnection of the elastomer balloons from the capillary at high pressure. Maximal deformation that can be reached depends on how strong is the adhesion force between the capillary surface and the elastomer balloon. For different elastomer balloons this maximal value is different and in some cases the deformation of elastomer balloons up to 30% can be reached [45].

Because, the deformational behaviour is nonlinear (Fig. 3.1), it has to be described by a non-linear model. For this purpose the phenomenological Mooney-Rivlin model can be used [45, 46, 100]. This model was developed for the description of large deformations of isotropic materials such as a rubber for instance. In this model the strain-energy of a deformed body depends on three invariants I_1, I_2, I_3 of Cauchy tensor λ_{ij} and three temperature dependant material coefficients C_1, C_2, C_3:

$$f_{el} = C_1(I_1 - 3) + C_2(I_2 - 3) + C_3(I_3 - 1) \tag{3.1}$$

These well-known invariants have the following form:

$$\begin{aligned} I_1 &= \lambda_{xx}^2 + \lambda_{yy}^2 + \lambda_{zz}^2 \\ I_2 &= \lambda_{xx}^2\lambda_{yy}^2 + \lambda_{yy}^2\lambda_{zz}^2 + \lambda_{zz}^2\lambda_{xx}^2 \\ I_3 &= \lambda_{xx}^2\lambda_{yy}^2\lambda_{zz}^2 \end{aligned} \tag{3.2}$$

The first coefficient C_1 is a temperature dependent constant, $C_1 = N^*kT/2$ and it represents the free energy of an ideal polymer network, where N^* is the number of polymer chains per unit volume and k is the Boltzmann constant. The coefficient C_3 is connected with volume changes of the material i.e. it is an analogue of a bulk modulus. The third coefficient C_3 is much larger for polymers or

rubbers than the former two coefficients and therefore such materials can be treated as incompressible and Eq. 3.1 takes the following form:

$$f_{el} = C_1(I_1 - 3) + C_2(I_2 - 3) \tag{3.3}$$

Accordingly to that equation just as two constants are required to characterise infinitesimal deformations of a conventional elastic material, also two constants are required to characterise large deformations of a soft material [100]. The relation between the excess pressure and radius of the balloon can be derived from the Eq. (3.3) [45, 46]:

$$p = \frac{4D_0}{R_0}\left[C_1\left(2\frac{R_0}{R} - \frac{R_0^7}{R^7}\right) + C_2\left(\frac{R}{R_0} + 2\frac{R_0^5}{R^5}\right)\right] \tag{3.4}$$

For small deformations, $\varepsilon = (R - R_0)/R_0 << 1$ ($R - R_0 << R_0$) this equation can be reduced to a linearized form

$$p \approx \frac{4D_0}{R_0} 6(C_1 + C_2)\frac{\delta R}{R_0} = \frac{4D_0}{R_0} 6C\varepsilon \tag{3.5}$$

where the coefficient $C = C_1 + C_2$.

Mooney-Rivlin model describes the deformation of an isotropic rubber. But, if a smectic elastomer is deformed perpendicular to the smectic layers, an additional contribution into the elastic energy arises from the compression of the smectic layers. Inflation of the elastomer balloon produces a uniform stretching in all directions in the layer plane. Because of the high bulk modulus, volume of the film conserves during deformation, therefore uniform stretching in all directions in the layer plane causes the compression of the film perpendicular to the layer. If the compression of the film induces the compression of the smectic layers then an additional term has to be added to the free energy expression [33, 45, 46, 49]:

$$f_{sm} = \frac{1}{2}B\left(\frac{du}{dz}\right)^2 \tag{3.6}$$

where *u* is the smectic layer displacement. This term leads to an additional contribution to the p(R) curve [46].

$$p = \frac{2D_0}{R_0} B\left(\frac{R_0^5}{R^5} - \frac{R_0^7}{R^7}\right) \approx B\frac{4D_0}{R_0}\varepsilon \tag{3.7}$$

In the isotropic phase smectic layer structure disappears, hence this term has to be included only for the smectic phases.

Because for the calculation of the elastic modulus some average value of the film thickness is used and uncertainty in the film thickness is the largest error source in the calculation of elastic moduli from the strain-stress curves, it is more convenient to introduce the specific modulus $\widetilde{C}_i = (4D_0 / R_0)C_i$, which can bee directly compared for the stress-strain curves measured for the same elastomer balloon at different temperatures.

The experimental pressure-radius curve measured in the isotropic phase Fig. 3.2a has been fitted by Moony-Rivlin model Eq. (3.1) – the solid line on the graph (Fig. 3.2). The coefficient C_2 was set to zero, this corresponds to an ideal rubber behaviour. The fit with Mooney-Rivlin model is in a good agreement with experimental curve, the fit parameter was set to $\widetilde{C}_1 = 680Pa$. In the SmA and SmC* phases experimental p(R) curves qualitatively have the same shape as in isotropic phase. But, they can not be fitted by Moony-Rivlin model with any parameters C_1 and C_2. Only the part of the curve for the small deformation $R/R_0 < 1.03$ can be fitted with Mooney-Rivlin model, $\widetilde{C}_1 = 1040Pa$ for the SmA phase and $\widetilde{C}_1 = 1200Pa$ for the SmC* phase, $\widetilde{C}_2 = 0$. But, it is impossible to fit the whole curve by the Mooney-Rivlin model with any chosen parameters $\widetilde{C}_1$ and $\widetilde{C}_2$. This indicates that the layer structure of the SmA and SmC* phase gives some additional contribution into the elastic energy of the elastomer balloon which is not taken into account by the isotropic Moony-Rivlin model. The Mooney-Rivlin model provides a satisfactory fit for the balloon deformation in the SmX phase with the fit parameter $\widetilde{C}_1 = 1500Pa$. However, the reason for that is not a good agreement between the model and experiment, but simply because of the higher elastic modulus than in other phases, deformation is in linear regime and the experimental curve only slightly deviates from the linear behaviour.

With known parameters of the balloon, the thickness of the balloon D_0 and the radius at zero pressure R_0 the elastic modulus $E = 6C$ [45] can be calculated. Elastic modulus in the isotropic

phase (T=140°C) $E \approx 1.38$ MPa , in the SmA phase (T=110°C, R/R0 < 1.03) $E \approx 2.1$ MPa, in the SmC* phase (T=180°C, $R/R_0 < 1.03$) $E \approx 2.1$ MPa and in SmX phase (T = 50°C) E ≈ 3.0 MPa.

It has to be kept in mind that the thickness of the balloons is not homogeneous. Usually, all balloons are thinner at the top than at the bottom and even locally the film thickness varies slightly.

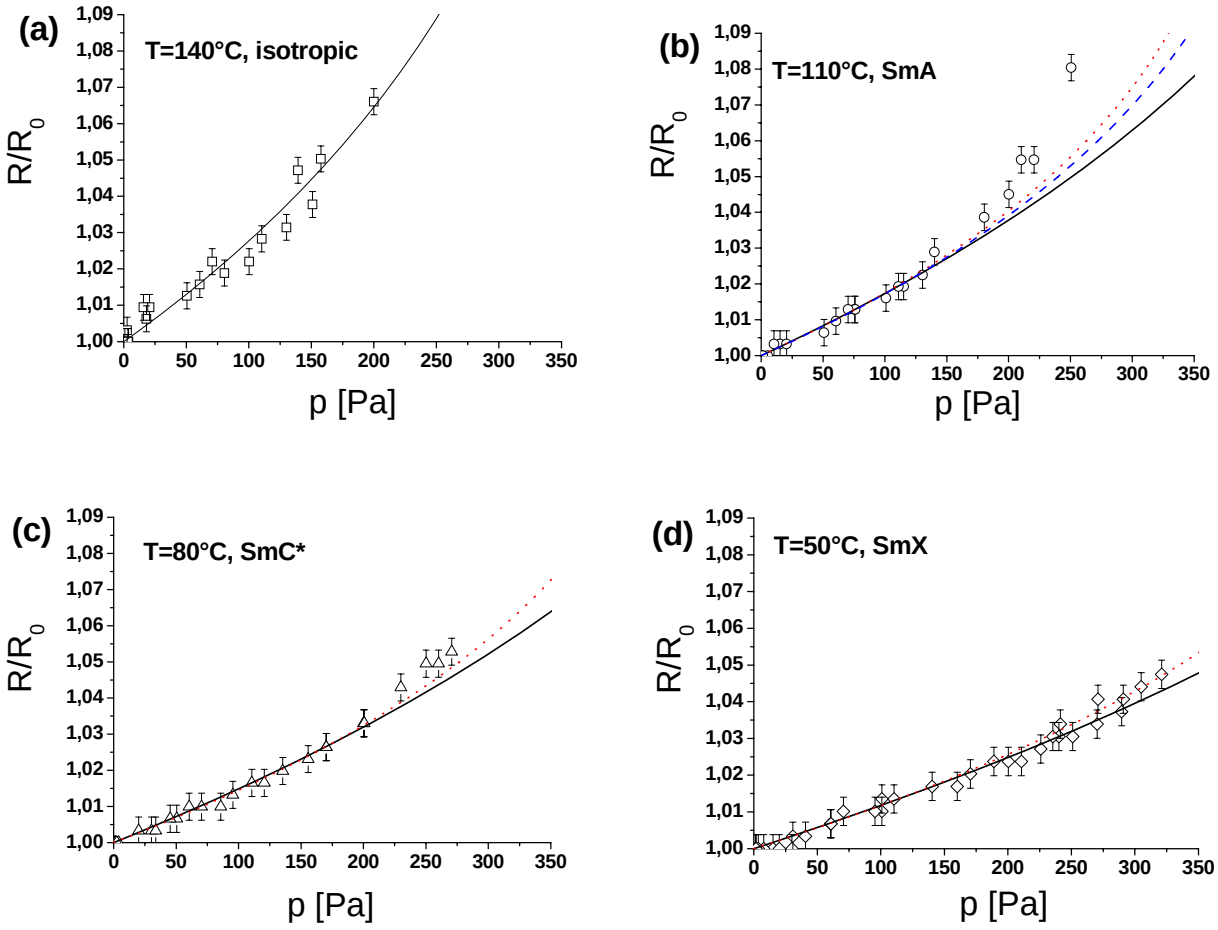

Figure 3.2: Pressure-radius relation for the elastomer CT86 cross-linked in the SmA phase at T=110°C. Measurement temperature 140°C in isotropic phase (a), 110°C in SmA (b), 80°C in SmC* (c) and 50°C in SmX (d). The solid curve indicate the behaviour calculated from the Mooney-Rivlin model with C_2=0 and fit parameters $\widetilde{C}_1 = 680Pa$ (a), $\widetilde{C}_1 = 1040Pa$ (b), $\widetilde{C}_1 = 1200Pa$ (c), and $\widetilde{C}_1 = 150Pa$ (d). The dot-curves indicate the behaviour expected from the layer compression model with fit parameters $\widetilde{B} = 3200Pa$ (b), $\widetilde{B} = 3800Pa$ (c), and $\widetilde{B} = 4600Pa$ (d) ($\widetilde{B} = (4D_0 / R_0)B$). The dash-curve indicates the behaviour expected from the Mooney-Rivlin model with an additional smectic layer compression term, the fit parameters are $\widetilde{C}_1 = 240Pa$ and $\widetilde{B} = 2500Pa$ (b).

But this in not important if the stress-strain curves measured with the same balloon but at different temperatures and experimental curves can be directly compared with each other. Therefore, the measurements of stress-strain dependences in different mesophases for the same

balloon provide very important information concerning the influence of phase structure on elastic properties of the elastomer. The gradient of the film thickness can be quite different for the different elastomer balloons and this hinders the comparison of the elastic modulus measured with different elastomers balloons and produces quite large error (25 %) [45] in the absolute value of the elastic moduli obtained from the experimental stress-strain curves.

Attempt to fit deformation in SmA and SmC* phases with the layer compression model Esq. (3.7) also gives a good fit only for small deformations. Smectic layer compression moduli obtained from that fit are close to the elastic moduli obtained from the Mooney-Rivlin fit. The layer compression modulus in the SmA phase (T=110°C, R/R0 < 1.03) $B \approx 2.17$ MPa, in the SmC* phase (T=80°C, $R/R_0 < 1.03$) $B \approx 2.57$ MPa and the SmX phase (T=50°C) $B \approx 3.1$ MPa .

As one can see neither the Mooney-Rivlin model (with any chosen parameters $\widetilde{C}_1$ and $\widetilde{C}_2$) nor the layer compression model provide a proper description of a smectic balloon deformation. Integrated model which combines Mooney-Rivlin model and the elastic energy of the smectic layer compression also can not fit the whole experimental curve – dash line on the Fig 3.2b. If the fit parameters C_1 and B chosen in such a way that the curve provides a proper fit for small deformations, than at large deformations it lies between the Mooney-Rivlin curve and the smectic compression curve.

What is the reason for the discrepancy between the experimental results and combined theoretical model? It seems that the model takes into account the main characteristic features of the smectic elastomers such as the nonlinear rubber elasticity and the elastic energy of the smectic layers compression.

The deformation of the smectic layers have to give prevailing contribution in to the elastic energy of a smectic elastomer because the layer compression modulus is much higher than the elastic modulus of the polymeric network. But, taking into account the measurement of elastic moduli parallel to director, conclusion can be made that at least for the stretching deformation perpendicular to the smectic layers, smectic layer structure defines the large elastic modulus only at small deformations [13, 14, 40]. When stress-strain curve deviates from a linear response different processes take place which soften the material. Depending on the chemical structures this can be a rotation of the smectic layers or a break down of the layers [13, 40]. Even if the smectic layer structure preserves and no rotation of the layers takes place the elastic modulus parallel to the director drastically decrease above the threshold deformation [14] which is usually 3-4%. After the threshold deformation elastic modulus perpendicular to the smectic layers becomes of the same order as the modulus measured parallel to the smectic layers or even smaller. Although only the results of stretching experiments are available and there is no experimental observation of the

deformational behaviour of the smectic elastomers compressed perpendicular to the smectic layers, it can be anticipated that at compression deformation, as in the case with stretching deformation, the smectic layer structure will be stable only at small values of deformation.

Therefore, we can expect that the layer compression modulus gives contribution into the elastic energy of the smectic elastomer balloons only at small deformations (5–6 %). At large deformation contribution from the smectic layer compression modulus diminishes and elastic modulus parallel to the smectic layer and perpendicular to it will have close value. In this case, for large strains, the deformational behaviour of an elastomer balloon has to be similar to non-linear deformation of isotropic rubber and the Mooney-Rivlin model has to be a proper description. Because elastic energy at small and large deformation depends on different contributions, experimental curve at small and large deformations has to be described by two different curves.

At small deformations it has to be the Mooney-Rivlin model with an additional term which takes into account compression of the smectic layers, if elastic modulus perpendicular to the layer is much higher than parallel to it, then smectic layers compression gives the main contribution and smectic layer compression term probably will be a good enough approximation. At large deformations the Mooney-Rivlin model has to be a proper model.

3.2 Uniaxial stretching of free-standing elastomer films

Although, a large smectic layer compression modulus is the characteristic feature of smectic elastomers; but it alone does note define the deformational behaviour of the smectic elastomers [13]. Different smectic LCEs with high layer compression moduli demonstrate different mechanisms of deformation when they are stretched parallel to the director [13, 14, 40]. It seems that the anisotropy of elastic moduli a more fundamental role, it defines which of these mechanism will be activated by deformation [13, 14, 40]. It is well known that the ratio between the elastic moduli perpendicular and parallel to the smectic layer depends on elastomer chemical structure and can vary from 3-4 times [14, 20] up to one hundred [6, 12].

The experiments with free-standing elastomer balloons presented above give an opportunity to measure the elastic moduli perpendicular to the smectic layers, to be exact, the elastic energy of a deformed elastomer balloon always includes the contributions of the elastic moduli parallel and perpendicular to the layers. If the elastic modulus perpendicular to the layer is much higher than the modulus parallel to it, then the main contribution will be from the layer compression modulus and

therefore the elastic moduli measured in these experiments are mainly defined by the smectic layer compression moduli.

Elastic moduli parallel to the smectic layer can be measured in simple uniaxial stretching experiments with free-standing films. The elastic modulus of a sample E is defined by the slope of the stress-strain curve: $E = \sigma / \varepsilon$, where σ is the applied stress and $\varepsilon = (l - l_0)/l_0$ is the strain caused by the stress (l_0 is the initial length of the film and l is the length of the stretched film). Hence, in order to define the elastic modulus of the film, the elastic force with which the film opposes to a deformation has to be measured at different values of strain.

In order to find out whether the smectic layer structure influences the elastic moduli parallel to the layers, the deformational behaviour of free-standing films at different temperatures has been studied.

Using a self-constructed setup for stretching experiments, stress-stain diagrams for the free-standing elastomer films have been measured. An elastomer film was fixed between two clamps, one of the clamps was connected to a digital analytical balance with 0.1 mg precision while the second clamp could be moved with a step-motor which was controlled by a computer. The minimal step length is 0.002 mm that is approximately 0.1% of the film length. The speed of deformation is ν = 0.002 mm/s, the relaxation time between two steps is 12 second. Therefore, the effective speed of deformation $\nu_{eff} \approx 0.00015$ mm/s. For the film length l_0 = 2.77 mm, the effective strain rate is $\dot{\varepsilon} = \delta\varepsilon / \delta t = \nu / l_0 = 5.4 \times 10^{-5}$ s^{-1}, where l_0 is the initial length of the film (strain rate is 0.0054 % per second). The initial film length at zero deformation has been measured using an optical long range microscope. Both, the step-motor and the digital balance are connected to a computer and after every deformation step the force acting on the clamp connected to digital balance and the change of the film length are recorded. In order to control the temperature of the film it has been placed inside a copper heating box. The temperature inside the heating box can be changed between room temperature and 210°C.

Measurements have been performed for two elastomers with a similar chemical structure CT86 and BR162A (see section 2.1). Several films have been prepared and stress-strain curves have been measured for different mesophases. All films demonstrate qualitatively similar behaviour (see Fig 3.3). Usually the thickness of free-standing films is highly inhomogeneous and some average value of the film cross-section area has to be used for the calculation of elastic moduli. The inaccuracy of the film cross-section leads to large errors in the values of the elastic moduli calculated from the experimental stress-strain curves. For this reason, only the results of the measurements on one free-standing film with the smallest thickness variations are presented here.

These measurements provide more precise quantitative results and they are most suitable for the calculation of elastic moduli.

A free-standing film, prepared from the smectic LC polymer BR162 (see section 2.1), was crosslinked in SmA phase approximately 15°C above the SmC*-SmA phase transition. Fig 3.3a shows the dependence of the force as a function of deformation. With the known geometrical parameters such as the film length l_0=2.77mm, film thickness $d_0 \approx$ 0,9μm and film width in the middle of the film $w_0 \approx$ 1.8mm (the cross-section area of the film $S = d_0 w_0 \approx 1.62 \times 10^{-9}$ m^2) the stress and strain values can be calculated from the measured force and the length change of the film. Fig. 3.3b shows the stress-strain diagram for the deformation of the elastomer film in the SmA phase.

Approximately up to 10 percent deformation, stress linearly depends on strain, after that it starts to deviate from a linear dependence. The strain at which stress-strain dependence start to deviate from a linear (Fig. 3.4) will be called below the threshold strain. Experiments with larger deformations demonstrate that after the threshold deformation stress-strain dependence is again approximately linear but with smaller elastic modulus Fig. 3.4. Using the relation between stress and strain $E = \frac{\sigma}{\varepsilon}$ elastic moduli can bee calculated from the linear part of the stress-strain curve. Because the stress-strain dependence above the threshold strain is almost linear, elastic modulus for this part of the curve can be also calculated using the same relation.

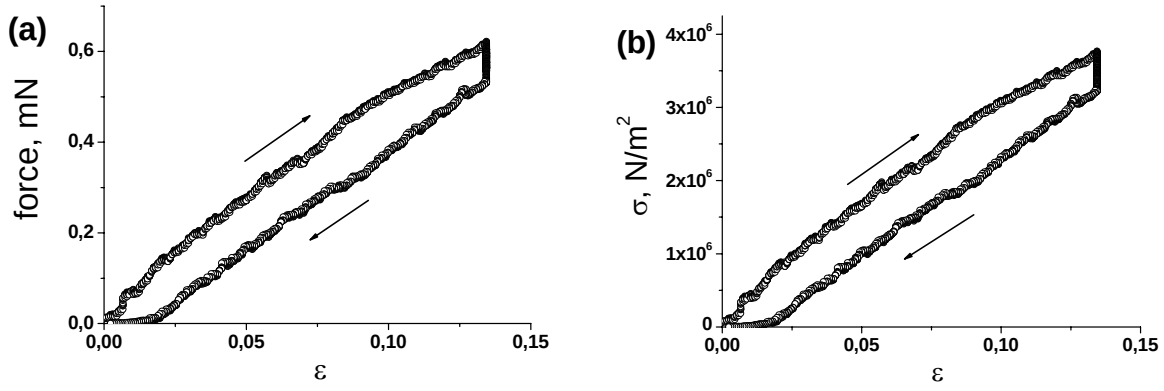

Figure 3.3: Stress-strain dependence for the elastomer BR162 A cross-linked in SmA phase (T = 116°C). a) The dependence of the measured force on deformation. b) Stress-strain dependence calculated from the Fig. 3.3a using geometrical parameters of the film.

For the stretching experiment in the SmA phase (Fig 3.4) elastic moduli for the small deformations are slightly different for the first and second stretching cycles, $E_1 = 3.06 \times 10^6$ N/m^2 and $E_1 = 2.62 \times 10^6$ N/m^2 for the first and second stretchings respectively.

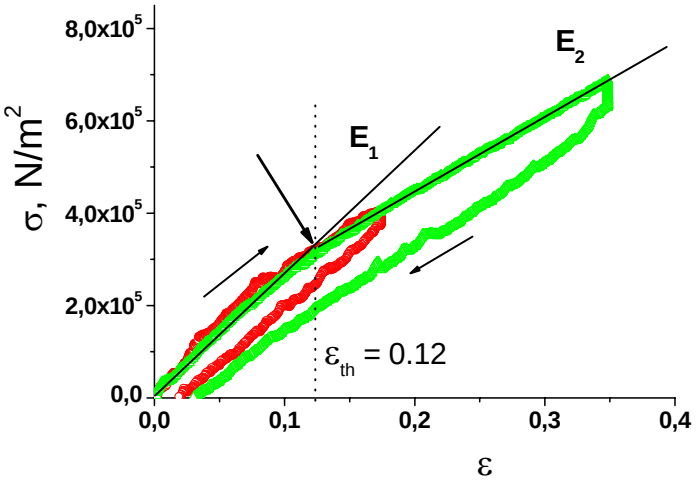

Figure 3.4: Stress-strain dependence for the elastomer BR162 A cross-linked in SmA phase. Two-repeated loading-unloading cycles with increasing maximal deformation are shown. The dashed line shows the threshold strain $\varepsilon_{th} \approx 0.12$.

Above the threshold deformation the elastic modulus becomes approximately two times smaller $E_2 = 1.6 \times 10^6$ N/m^2. Usually deformation parallel to the smectic layers is linear in a wide range of deformations [12-14]. Threshold behaviour is observed for the deformation parallel to the director, but in this case elastic modulus drastically decreases above the threshold strain. It can be ten times smaller than the modulus under the threshold deformation [12-14].

In order to determine the temperature dependence of the elastic modulus parallel to the smectic layer, stretching experiments have been performed at different temperatures. Fig. 3.5 shows the stress-strain dependence in the isotropic phase. The measurement temperature is 158°C, that is approximately 20°C above the SmA-isotropic phase transition. Qualitatively the stress-strain dependence in the isotropic phase is similar to the deformation in the smectic A phase (Fig. 3.4). The elastic modulus for the linear strain-stress regime is $E_1 = 2.39 \times 10^6$ N/m^2 and above the threshold strain $E_2 = 1.4 \times 10^6$ N/m^2. So, transition from the SmA phase in the isotropic phase does not induce a significant change of the elastic modulus parallel to the layer. But that is not a completely unusual situation. In some material elastic moduli parallel to the layers have almost the same value as in isotropic phase [6]. Also experimental observations of the elastic moduli in the smectic phase parallel to the layers ten times as high as in the isotropic phase have been reported [14]. Unfortunately it was impossible to perform measurements at higher temperature deeper in the isotropic phase.

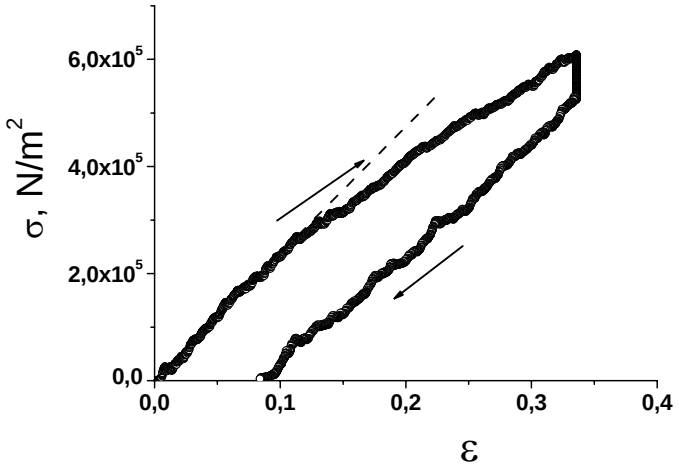

Figure 3.5: Stress-strain curves for the deformation in isotropic phase T = 158°C.

Stress-strain dependence in the SmC* phase looks qualitatively different from the stress-strain curves in the SmA and isotropic phases. The slope of the stress-strain curve at first linear stage is much steeper than in the isotropic and smectic A phases $E_1 = 1.86 \times 10^7$ N/m^2. At the same time, the threshold strain is smaller than in the isotropic and smectic A phases. In contrast with elastic modulus under the threshold strain elastic modulus above the threshold is $E_2 = 1.8 \times 10^6$ N/m^2 hardly changes in comparison with the moduli in SmA and isotropic phases.

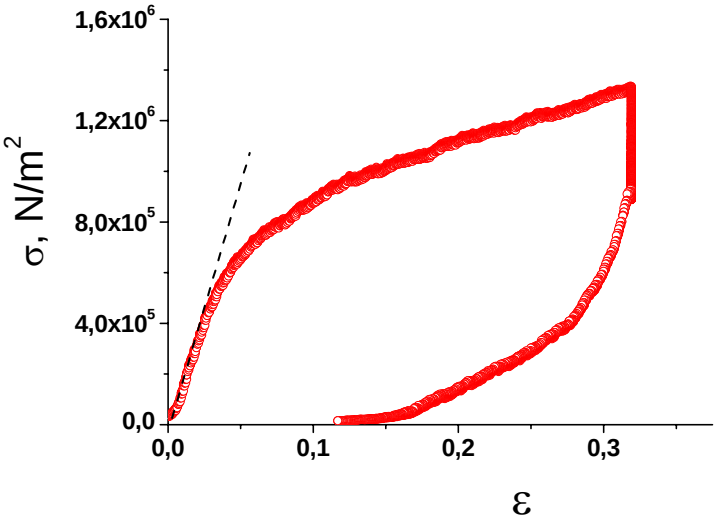

Figure 3.6: Stress-strain curve for the deformation in the SmC* phase, T = 52°C.

Another distinct feature is that the hysteresis in the SmC* phase is much stronger pronounced than in the isotropic and SmA phase. The maximal strain was approximately the same in all experiments in different phases. But the strain value when stress reaches zero value at shrinking of the film is different. In SmA phase this value is about 2-3%. In the isotopic phase this is about 10% and in SmC* phase this deformation is approximately 15%. In fact that is not the irreversible deformation in its usual sense, but some time is required before the film shrinks back to initial length. The relaxation to initial film length is much faster at high temperatures. In the isotropic and SmA phases only a few hours are required for the relaxation to the initial length. In the SmC* phase it can be few days, but if the film stretched in the SmC* phase, is warmed in to isotropic phase and then it is cooled down in to the SmC* phase, it recovers its initial length. That indicates that relaxation processes at low temperatures are much slower than in the SmA and isotropic phases. This can be the reason for the large hysteresis in the SmC* phase. Although, the strain rate is the same for all measurement, it is probably too fast for the measurements at low temperatures.

From the stress-strain measurement at different temperatures temperature, elastic moduli for different mesophases have been obtained. Fig 3.7 shows the temperature dependence of elastic moduli in the first linear regime E_1 - □ and above the threshold strain E_2 - ■. Usually the thickness of the film is not homogeneous and some average cross-section has to be chosen. This is one of the main error sources in the calculation of strain value. Also during preparation of the free-standing film some amount of liquid material from the area masked during cross-linking gather on the rand of the film increasing the cross-section area of the film. This will lead to over estimated elastic moduli, because the real cross-section area is larger than the value used in calculation of elastic moduli. But it is difficult to estimate the difference between the real cross-section area of the film and the cross-section area obtained just by multiplication of the film thickness by the film width.

From the comparison of the film area and the area of liquid material at the both sides of the film we can suppose that the maximal value of the unoriented material gathered on the two film sides can be approximately the same as the volume of material of the film. Therefore, the area of the film cross-section can be twice as large as estimated from the film thickness and its width.

That is the upper limit in the estimation of the film cross-section area. From that we can draw a conclusion that the real value of elastic moduli has to be between the experimentally obtained value E and E/2. In any case this value is close to the elastic moduli perpendicular to the smectic layers obtained in the experiments with the smectic elastomer balloons.

The measured values of the elastic moduli of the free-standing elastomer films and elastomer balloons indicate that in the material under investigation the anisotropy of elastic moduli parallel and perpendicular to the smectic layers is very low. On one hand this can mean that smectic

layer structure does not significantly increases the elastic moduli perpendicular to the smectic layers.

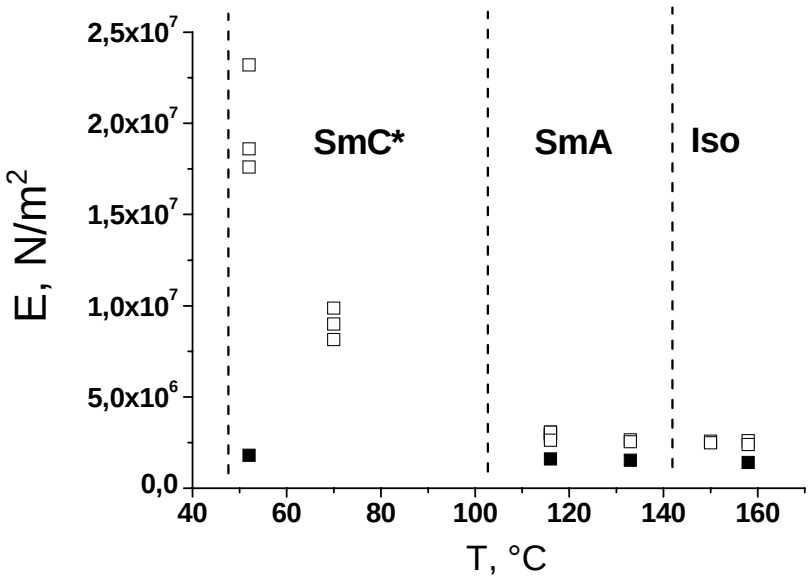

Fig 3.7: The temperature dependence of elastic modulus. Squares represent the elastic modulus before the threshold deformation and circles represent the elastic modulus after the threshold deformation.

But in fact the elastic moduli measured in experiments with elastomer balloons E = 2-3*10^6 Pa are very close to the elastic modulus parallel to the director measured for a highly anisotropic smectic elastomer (E=3.2*10^6 Pa) which shows in-plane fluidity behaviour [83]. For the smectic elastomer elastic with different chemical structure moduli in the range from 3.2* 10^6 Pa up to 1.4*10^7 Pa have been measured [12-14, 40, 83]. On the other hand anisotropic of elastic moduli can be diminished because of the high elastic modulus parallel to the smectic layers. Elastic moduli in the layer plane can be increased, in comparison with the moduli for the isotropic phase, because of defects in the smectic layer structure [13].

Low anisotropy of the elastic moduli parallel and perpendicular to the smectic layers can explain why in the elastomer studied here deformation of free-standing elastomer film parallel to the smectic layer induces compression perpendicular to the smectic layers. Because the elastic moduli parallel and perpendicular to the director have close values and deformation perpendicular to the layers is now longer penalized by high layer compression modulus it is more energetically favourable if deformations in the layer plane and perpendicular to the layer have close values.

Chapter 4 Optical reflectometry measurements

The measurements of the elastic moduli on elastomer balloons, described in the previous chapter, have not revealed any significant influence of the smectic layers on the mechanical properties of smectic elastomer. Although, the elastic moduli in the SmA phase are larger than in the isotropic phase, however, the difference between the moduli in the SmA phase and the moduli in the isotropic phase is small in comparison with the difference of the moduli in the SmA and isotropic phases found measured for many other smectic elastomers [12-14]. In the experiments with the elastomer balloons the changes of the film thickness can be only roughly estimated, because a curved shape of the elastomer balloons complicates the measurement of the film thickness. For the calculation of the elastic moduli compression of the balloon perpendicular to the surface was calculated from the volume conservation assumption. But, other mechanisms of deformation which do not induce the compression of smectic layers are also possible, for instance the rupture of smectic layers. For this reason, the information concerning the changes of the smectic film thickness during deformation is very important for the understanding of the mechanical properties of the smectic elastomers under investigation.

The thickness of free-standing elastomer films can be precisely measured using the optical reflectometry method. For the detailed description of the method see chapter 2.

This chapter presents the result of optical reflectometry measurements of the free-standing films compression during a uniaxial stretching parallel to the smectic layers. The main goal of these experimental investigations was to determine the influence of the structure of elastomers, density of crosslinking groups and preparation conditions on the deformational behaviour of free-standing smectic elastomer films. Using optical reflectometry the thickness of free-standing smectic elastomer films at different values of strain has been determined. From the optical images of the films, deformation along the stretching direction and perpendicular to it can be determined by measurement of the distance between two chosen points on the film surface.

4.1 Cross-linking of free-standing films

Crosslinking of smectic LCP in the smectic A phase preserves the smectic layer structure, this has been confirmed by X-ray measurement on oriented films and unoriented bulk elastomers [48, 101]. Optical observations reveal a noticeable difference in the surface structure of LCE films

crosslinked in the smectic phase and in the isotropic phase. While in the smectic phase thickness changes usually have distinct steps which can be attributed to the changes of the smectic layers number, in the isotropic phase thickness variations are smooth. AFM measurements at room temperature show distinct steps on the surface of films crosslinked in the SmA phase (Fig. 4.1), while in the films crosslinked in the isotropic phase the changes of the film thickness are smooth (Fig. 4.2). Crosslinking process freezes the structure of precursor free-standing LCP films. If the film before crosslinking in the SmA phase has distinct thickness steps they are preserved after crosslinking, even if crosslinked film is heated up into the isotropic phase the film thickness steps are still visible.

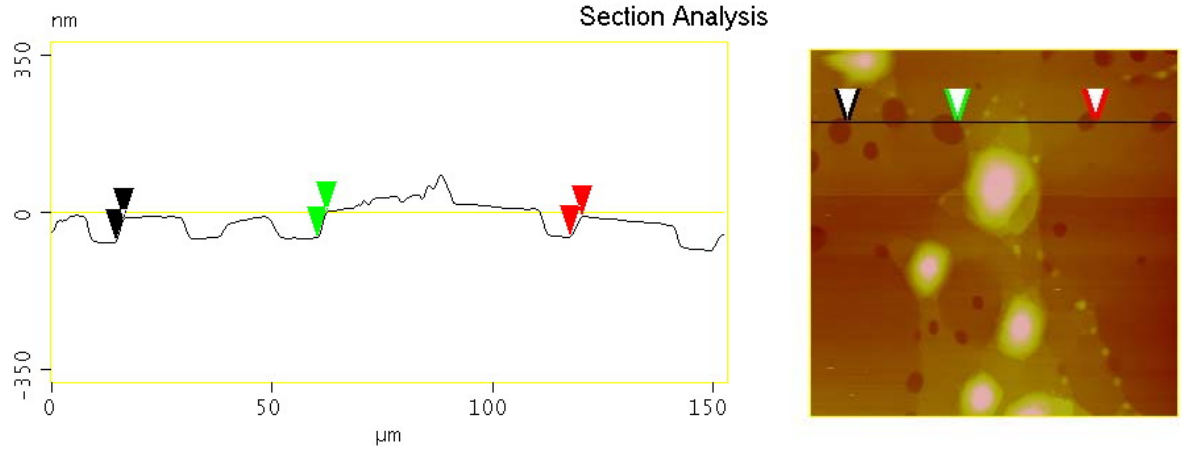

Figure 4.1: AFM measurement of the film surface profile at room temperature. The film has been crosslinked in the SmA phase.

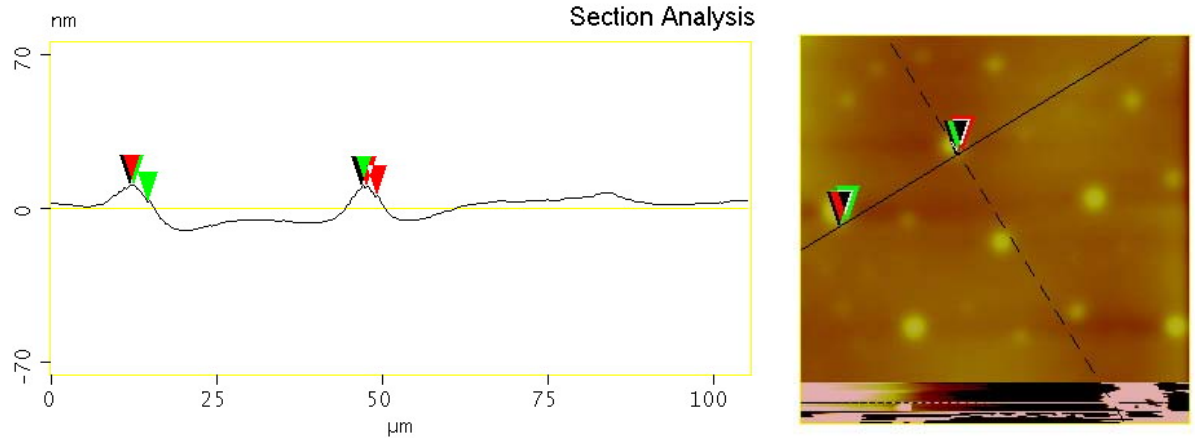

Figure 4.2: AFM measurement of the film surface profile at room temperature. The film has been crosslinked in the isotropic phase.

Optical observations reveal the changes of the optical film thickness during a crosslinking process (see Fig. 4.3). Using optical reflectometry method the influence of crosslinking on thickness of free-standing elastomer films has been studied. For this purpose the film thickness profiles before and after crosslinking have been calculated from the optical reflectometry data. The optical reflectometry measurements allow to find only an optical film thickness $d_{opt} = dn$ (where d is the film thickness and n is the refractive index of the film material), but not a real film thickness. In order to compare the film thickness before and after crosslinking the refractive index is supposed to has the same value before and after crosslinking ($n = 1.5$) and in this case the film thickness can be calculated as follows $d = d_{opt} / n$.

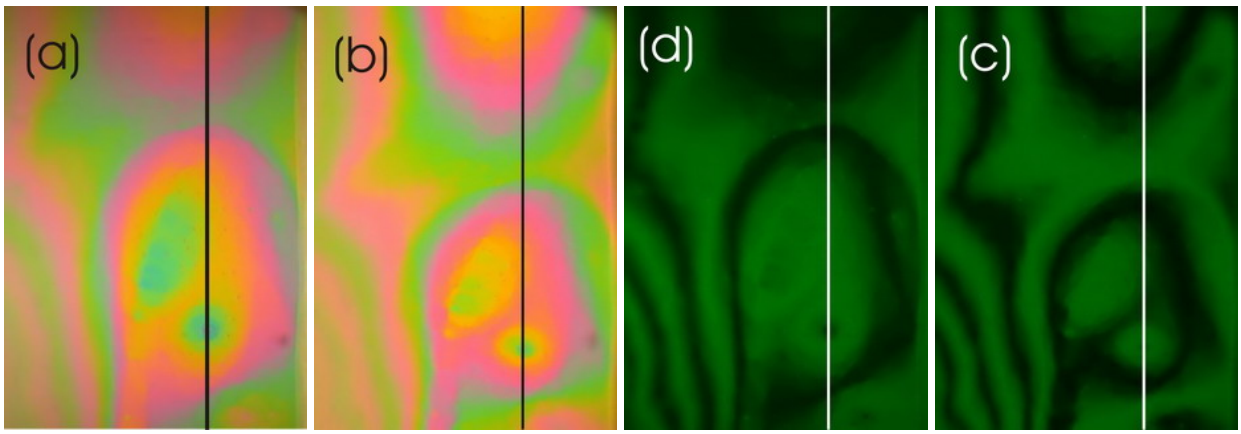

Figure 4.3: Reflection images of the free-standing LCP film (a, d) and elastomer film obtained after the crosslinking (b, c). Reflection images (a, b) are made in white, unpolarized light and (d, c) in monochromatic green light with the wave length λ = 547nm.

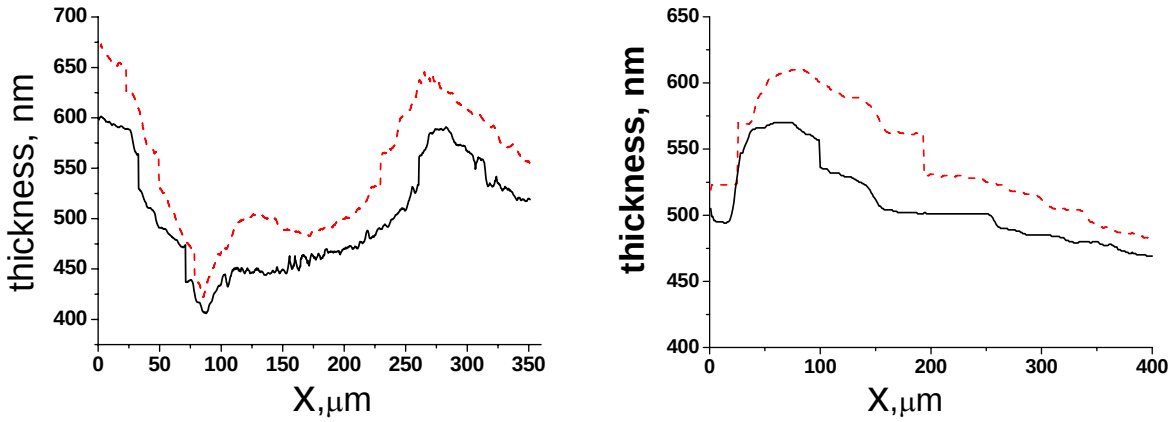

Figure 4.4: Film thickness profile calculated from the date of optical reflectometry. (a) The thickness of the homopolymer BR153B film crosslinked in smectic A phase Fig 4.3. (b) The thickness of the copolymer BR162A film cross-linked in SmC* phase. The solid line represents the film thickness profile before crosslinking and dashed-line after the crosslinking.

In Fig. 4.4a the film thickness profiles of a homopolymer film before and after crosslinking in the SmA phase are shown. The film thickness after crosslinking is slightly larger than before it. For different film regions the changes of the film thickness are in the range between 4 and 10 percent. The same tendency has been found for all studied LC polymers, crosslinking increases the film thickness if crosslinking is done in SmA, SmC* and SmX phase. For the crosslinking in the isotropic phase no measurements have been done. One would expect that the ratio of the film thickness before and after crosslinking have to be the same for the different film regions, but the thickness changes are not homogeneous, in the thick film regions thickness increases stronger than in the thin regions.

Another interesting phenomenon caused by a crosslinking process can be observed with crossed polarizers, after the crosslinking birefringence observed in the SmC* and SmX phases disappears. Two different explanations can be proposed for this phenomenon: first one is that crosslinking decreases mesogens tilt and as a consequence birefringence diminishes. Another possibility is that crosslinking process destroys tilt correlation in the neighbouring layers and material becomes optically uniaxial.

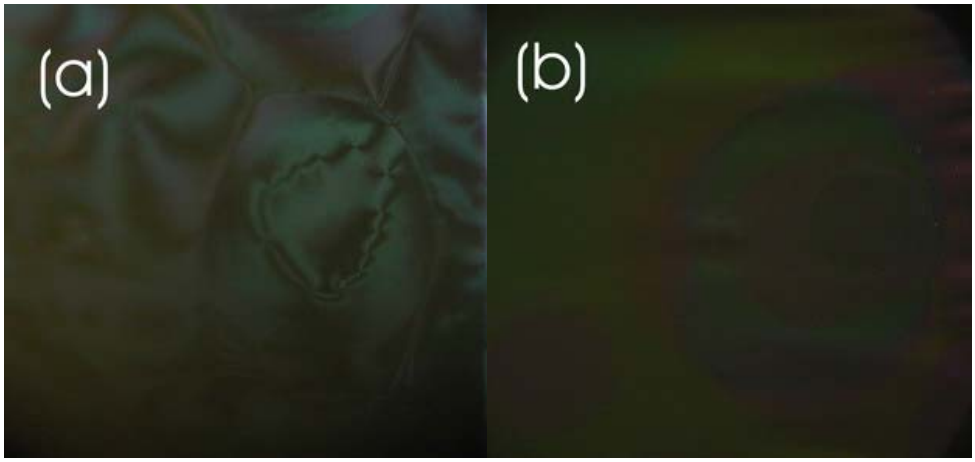

Figure 4.5: Smectic LC polymer film in the SmC* phase observed with crossed polarizers (a) before and (b) after the crosslinking.

Only on the basis of optical observations no conclusion can be made concerning the mechanism responsible for the disappearance of a birefringence. Other experimental techniques such as X-ray diffraction or FTIR – polarized measurements can help to understand the mechanism of the film thickness changes and disappearance of birefringence in SmC* and SmX phases.

4.2 Strain-induced compression of free-standing elastomer films

Using an optical reflectometry and optical microscopy the deformational behaviour of free-standing smectic elastomer films prepared from the smectic LC copolymers and homopolymer have been studied. All elastomer films have been prepared by crosslinking of precursor polymer films in the SmA phase.

The strain values perpendicular to the film surface λ_z and in the film plane λ_y have been measured at different values of the applied strain in x direction λ_x (Fig. 4.7a). The change of the film thickness was measured by the optical reflectometry and the values of strain in the layer plane λ_x and λ_y have been measured from optical microscopy images by the measurement of the distance between two chosen points on the film surface. Fig. 4.6 shows the thickness of the elastomer CT86 film in the SmA phase measured at different values of applied strain $\varepsilon_x = \lambda_x - 1 = l/l_0 - 1$, where l and l_0 are the length of deformed film and initial film length respectively (Fig. 4.7a). The changes of the thicknesses of three regions with different initial thicknesses have been measured. Fig. 4.6b shows the dependence of the strain perpendicular to the film surface $\lambda_z = d/d_0$ on the value of applied strain, where d is the film thickness and d_0 is the film thickness at zero deformation.

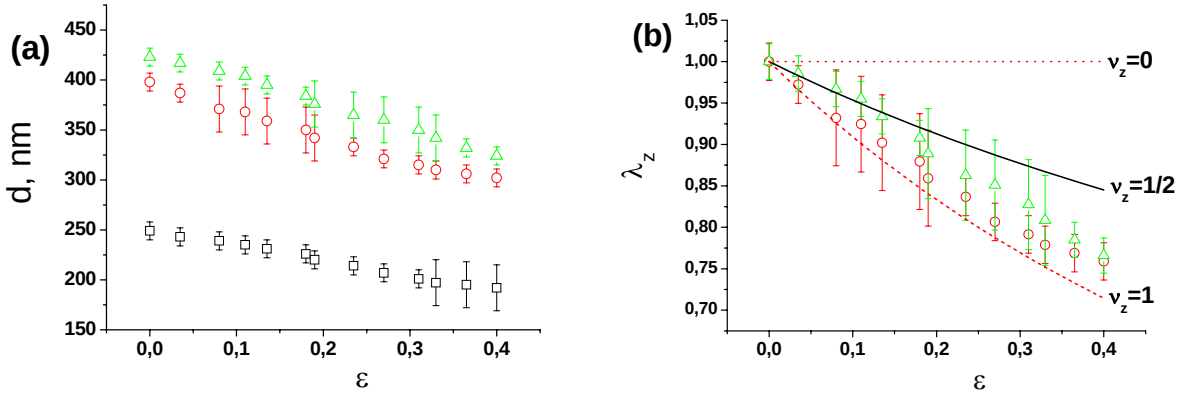

Figure 4.6: Deformation of the CT86 elastomer film crosslinked in SmA phase at T = 115°C, the time of crosslinking is 400 minutes, the measurement was made in the SmA phase T = 120°C. (a) Dependence of the film thickness d on deformation for three regions with different initial thicknesses. (b) The strain perpendicular to film surface $\lambda_z = d/d_0$ at different values of stretching deformations.

Three lines on the Fig. 4.6b represent deformation of the material with Poisson's ratio $\nu_z = 0$ (dotted line), $\nu_z = 1/2$ (solid line) and $\nu_z = 1$ (dashed line), $\nu_z = -(\varepsilon_z/\varepsilon_x)$ Deformation

with the Poisson's ratio $\nu_z = 0$ would mean that the film thickness is constant at all values of deformation, such behaviour is observed for the deformation of certain types of smectic elastomers , stretched parallel to the smectic layer plane [12-14]. The volume of the film has to be constant during deformation and stretching deformation is compensated by a shrinking in the layer plane perpendicular to the stretching direction. The experimentally obtained dependence at small values of deformation is close to the solid line with Poisson's ratio $\nu_z = 1/2$ (Fig. 4.6 b), this means that stretching deformation induces equal contractive deformations in the layer plane and perpendicular to the film surface. Such deformational behaviour is normal for isotropic materials. At large values of deformation the experimental curve is close to the dashed-line with Poisson's ratio $\nu_z = 1$, this indicates that the stretching strain is mainly compensated by the compression of the film perpendicular to the smectic layer and shrinking in the layer plane is smaller than perpendicular to it. Compression perpendicular to the layer that is larger than in the layer plane indicates that the elastic modulus perpendicular to the layer is smaller than in the layer plane. But for a smectic elastomer that is highly improbable, because the smectic layer structure can only increase the elastic moduli perpendicular to the layers, therefore, the elastic modulus perpendicular to the smectic layers has to be at least not smaller than the modulus in the layer plane.

More detailed consideration of the structure of elastomer films studied here can help to give a more plausible explanation of this strange behaviour. All free-standing films studied here are prepared by crosslinking of free-standing LCP films, see section 2.5 for details. During the cross-linking of a free-standing LCP film, two sides of the film are covered by a copper mask in order to prevent cross-linking and only area in the middle is crosslinked. The area covered with the mask remains liquid and can be easily removed. But some amount of material from the uncrosslinked area gathers on the edge of the film (Fig 4.7 and 4.8).

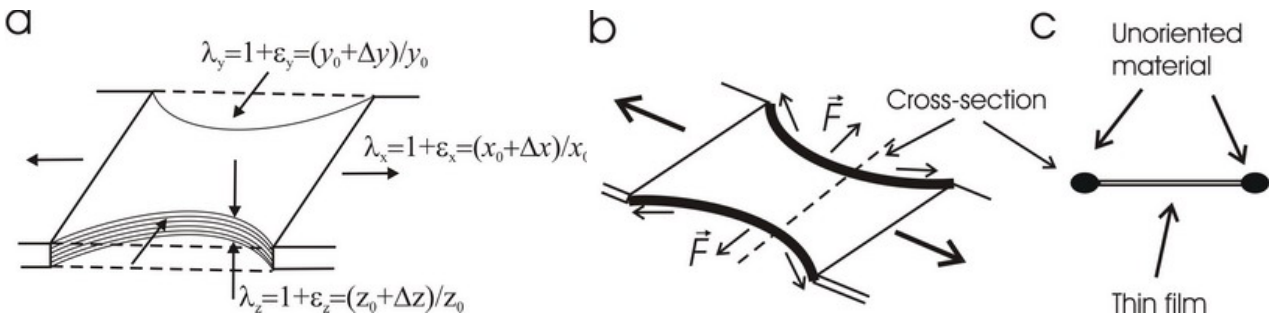

Figure 4.7: Schematic representation of (a) the deformation of free-standing elastomer film, (b) the structure of the film with the rand consisting of unoriented material and (c) cross-section of the film perpendicular to the stretching direction.

After that the film is usually crosslinked for the second time. The shape of this border is usually curved and stretching of the film tends to extend this border and that produce an additional stretching force perpendicular to the stretching direction (Fig. 4.7b). The cross-section area of the border consisting of an unoriented material can be comparable with the cross-section area of the film. If the anisotropy of the elastic moduli is low and the elastic modulus perpendicular to the smectic layers is not much larger than in the layer plane an additional stretching force acting in the layer plane can increase the compression of the film. The thinner the film region is, the stronger the influence of the stretching force on it will be; and therefore the stronger the compression of the film in this region will be (Fig. 4.6).

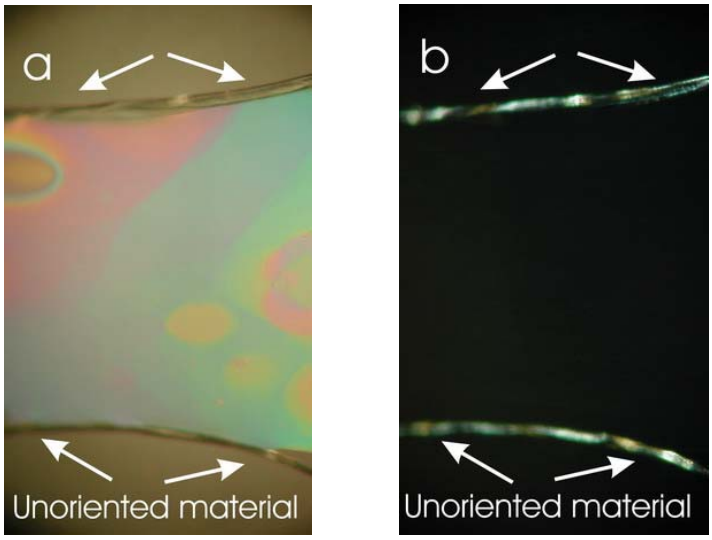

Figure 4.8: Reflection images of the free-standing elastomer film in SmA phase. Images made in a white light (a) unpolarized light and (b) with crossed polarizers.

Volume conservation of the film can be used for the calculation of the film compression λ_z from the values of strain in the layer plane λ_x and λ_y (stretching axis is parallel to the x-axis and the z-axis is perpendicular to the film surface, see Fig. 4.7a). Because any chosen volume is the same in deformed and undeformed film, the ratio of the volume of stretched film and film at zero strain is equal to one at any deformation, hence $V/V_0=\lambda_z\lambda_y\lambda_x=1$, using this relation, compression of the film perpendicular to the layer can be calculated as follows $\lambda_z = 1/\lambda_y\lambda_x$. Or simply knowing the values of strain in all three directions λ_z, λ_y and λ_x, the ratio of the deformed volume and volume at zero deformation can be calculated $V/V_0= \lambda_z\lambda_y\lambda_x$ and it has to be equal to one. This can be used as a verification of the reflectometry measurement results. Fig. 4.9a shows the measurement of the deformation in the layer plane λ_y, deformation perpendicular to the smectic layer plane calculated from the volume conservation $\lambda_z = 1/\lambda_y\lambda_x$ and λ_z obtained from the reflectometry measurements at

different values of the stretching strain. The values of the film compression obtained by two methods are in a good agreement with each other. The volume ratio calculated for different values of deformation is close to one (Fig. 4.9b), this confirms that the results of the reflectometry measurements are precise. Reflectometry measurement of the film thickness changes induced by stretching deformation in the Isotropic and SmC* phases are shown in Fig. 4.10. Qualitatively deformational behaviour in the SmC* phase and isotropic phase is similar to the deformation in the SmA phase (Fig. 4.6).

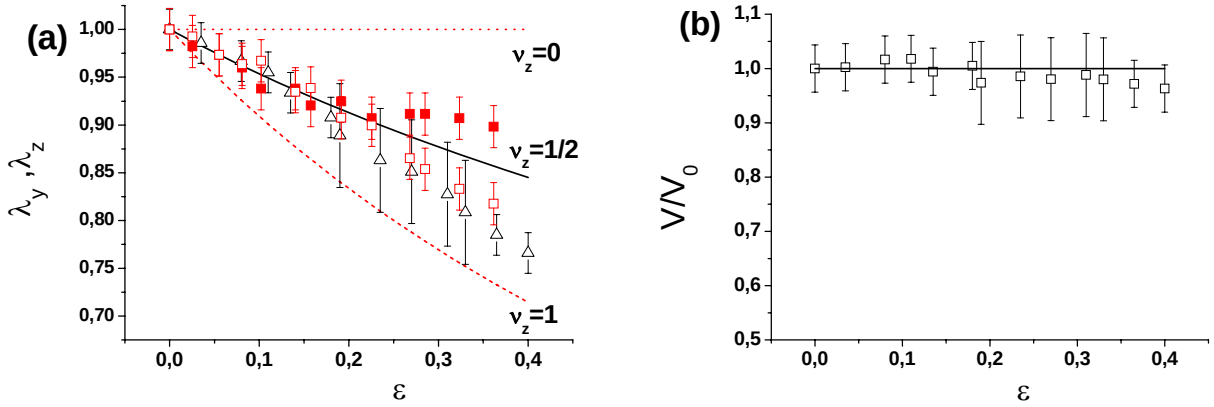

Figure 4.9: Deformation of a CT86 elastomer film cross-linked in SmA phase T = 115°C, the time of crosslinking is 400 minutes, stretching is in SmA phase T = 120°C. (a) Δ-d/d$_0$ obtained from the optical reflectometry measurements, ■ - $\lambda_y = \Delta y/\Delta y_0$, □- thickness calculated from the volume conservation $d/d_0 = \lambda_z = 1/(\lambda_y \lambda_x)$. (b) The ratio of the volume of the deformed film to the volume at zero strain calculated for a chosen area.

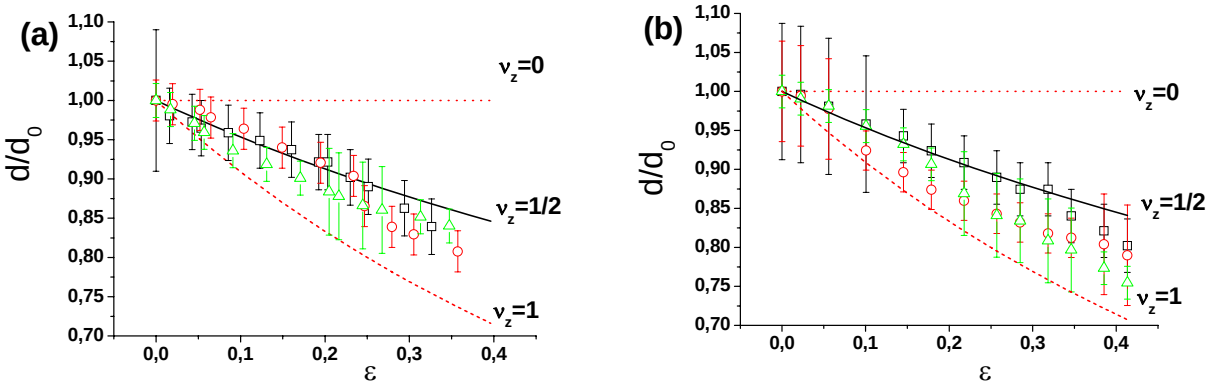

Figure 4.10: Compression of the CT86 elastomer film cross-linked in SmA phase T = 115°C, the time of crosslinking is 400 minutes. (a) Stretching is in the isotropic phase T = 140°C, (b) stretching is in the SmC* phase T = 80°C.

From these measurements a conclusion can be made that the smectic layer structure scarcely influences the deformational behaviour of the elastomer. This implies that elastic moduli perpendicular to the film surface and in the layer plane have close values.

The compression of the free-standing film of the elastomer BR162 is shown in Fig. 4.11. This elastomer has the similar structure with elastomer CT86 described above, only the crosslinker density is 10%, while for the elastomer CT86 it is 5%. There are two sets of experimental values which represent the compression of two regions of the film with slightly different initial thicknesses (◊ -d_0 = 547nm and ○- d_0 = 427nm). For both measurements experimental values lie under the theoretical curve for the material with Poisson's ratio $\nu_z = 1$ (dashed line). If the volume of the film is preserved this would mean that the width of the film would have to increase at large value of stretching deformation. This unusual behaviour will be discussed in more details below.

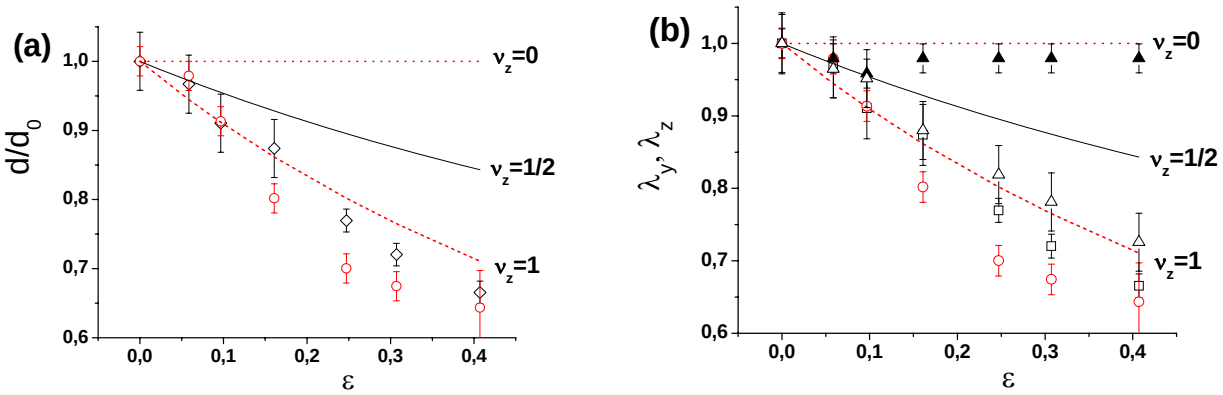

Figure 4.11: Compression of a BR162H elastomer film cross-linked in the SmA phase T = 110°C, the time of crosslinking is 240 minutes, stretching is in SmA phase T = 110°C. (a) Dependence of the film compression $\mathbf{d/d_0}$ on deformation for tow different film regions with different initial thicknesses (◊ -d_0 = 547nm and ○- d_0 = 427nm). (b) Compression of the film obtained from reflectometry measurements (Fig. 4.11a) and calculated from the volume conservation □ - $d/d_0 = 1/(\lambda_y \lambda_x)$, ■ - $\lambda_y = \Delta y/\Delta y_0$ – strain in the layer plane .

Fig. 4.12 and 4.13 show the deformational behaviour of two free-standing elastomer films prepared from the homopolymer BR153B. Both films have been prepared under identical preparation conditions, the same temperature of crosslinking T=180°C and irradiation time t = 240 minutes. But deformational behaviour of two films is completely different. For the first film (Fig. 4.12) only for small values of strain (ε < 10%) experimental values approximately coincide with theoretical curve for the deformation with Poisson's ratio $\nu_z = 1/2$ (solid line). Above this deformation experimental

values strongly deviate from this curve and experimental points lie under the theoretical curve with Poisson's ratio $\nu_z = 1$ (dashed line).

Shrinking of the film in the layer plane λ_y and compression of the film calculated from the volume conservation $d/d_0 = \lambda_z = 1/(\lambda_y \lambda_x)$ are presented in Fig. 4.12 b. Calculated compression of the film smaller than measured by optical reflectometry (Fig. 4.12a), calculated values of the film compression of the lie slightly above the curve with Poisson's ratio $\nu_z = 1$ (Fig. 4.12b). Discrepancy of the reflectometry date and calculated compression of the film occurs because the deformation in the film plane λ_y is measured for a large region and therefore film compression calculated from the volume conservation $d/d_0 = \lambda_z = 1/(\lambda_y \lambda_x)$ represents the average compression of the film while reflectometry data give the local film compression for the chosen regions.

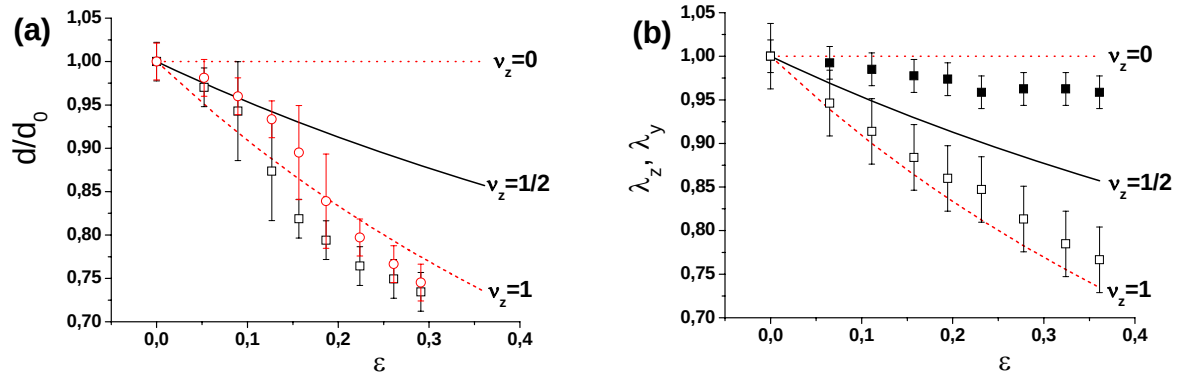

Figure 4.12: Compression of the BR153B film cross-linked in the SmA phase T = 180°C, the time of crosslinking is 180 minutes, stretching is in smectic A phase, T = 180°C. The length of the film is 0.75 mm and its width is 1.25 mm (see Fig. 4.14a). (a) Dependence of the film compression $\mathbf{d/d_0}$ on deformation for two different film regions with different initial thicknesses (○ -d_0 = 424 nm and □- d_0 = 403nm). (b) Compression of the film calculated from the volume conservation □ - $d/d_0 = \lambda_z = 1/(\lambda_y \lambda_x)$, ■ - $\lambda_y = \Delta y/\Delta y_0$ – strain in the layer plane .

Second film demonstrates quite a different deformational behaviour. Compression of the film perpendicular to surface for all value of deformation coincides with theoretical curve for isotropic material with Poisson's ratio $\nu = 1/2$ (Fig 4.13a). The compression of the film calculated from the values of shrinking deformation in the film plane λ_y is in a good agreement with reflectometry results (compare Fig 4.13 a and b).

The preparation conditions for these two films are identical, therefore the preparation conditions can not be responsible for the differences in the behaviour of two films. The only difference between two films is their geometrical parameters. Fig. 4.14 shows these two films, the widths of the films are approximately the same but the length of the fist one which corresponds to

measurements in Fig. 4. 12 is shorter than the length of the second film which corresponds to measurements in Fig 4.13. It can be supposed that for the short film the stretching force induced by the thick border of the film is stronger and this increases compression of the short film in comparison with the long one. The same behaviour was observed for the short film of elastomer BR162H (confer Fig. 4.11 and 4.12)

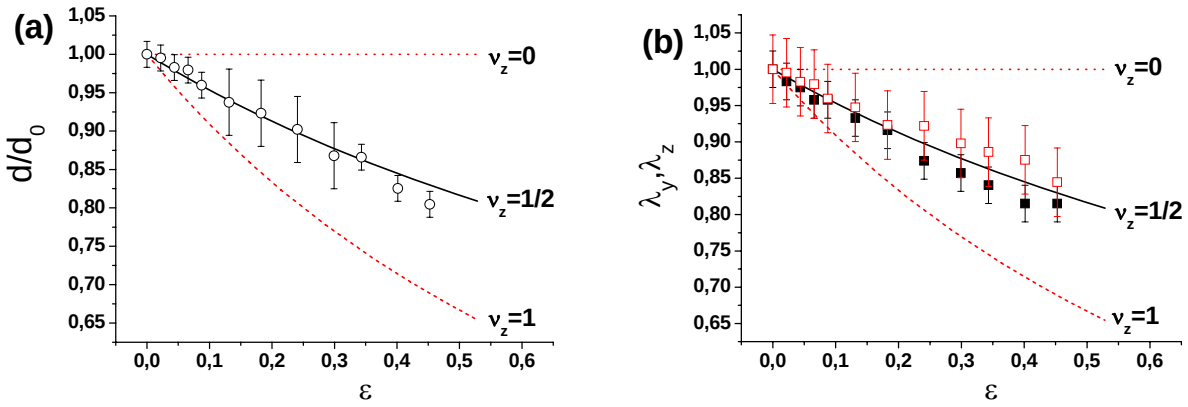

Figure 4.13: Compression of the BR153B film cross-linked in the SmA phase T = 180°C, the time of crosslinking is 180 minutes, stretching is in smectic A phase, T = 180°C. The length of the film is 1.13 mm and its width is 1 mm (See Fig. 4.14b). (a) The dependence of the film compression $\mathbf{d/d_0}$ on deformation obtained from the optical reflectometry data. (b) Compression of the film calculated from the volume conservation □ - $d/d_0 = \lambda_z = 1/(\lambda_y \lambda_x)$ and ■ - $\lambda_y = \Delta y/\Delta y_0$ – strain in the layer plane .

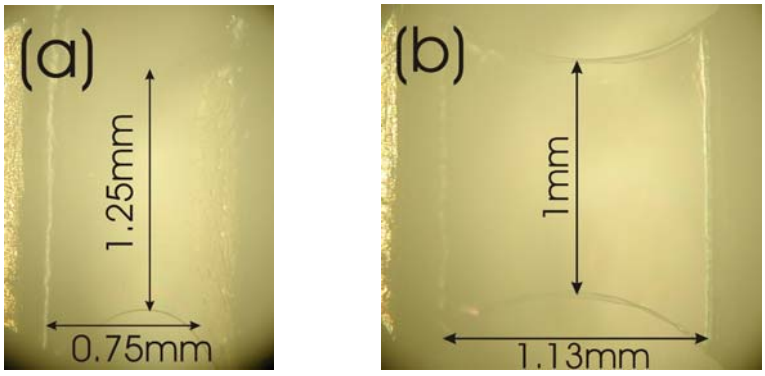

Figure 4.14: Two elastomer films of homopolymer BR153B crosslinked in the SmA phase at T = 180°C (a) corresponds to measurements on Fig 4.12 and (b) corresponds to measurements on Fig. 4.13.

4.3 Influence of crosslinking time on deformational behaviour of free-standing elastomer films

From the comparison of the behaviour of the two elastomer films with identical preparation conditions described above, it becomes clear that the geometrical parameters and influence of the border of the film, which induces a force stitching the film in the layer plane perpendicular to the stretching direction, has a strong effect on the deformational behaviour of thin free-standing elastomer films.

In order to prove this, films with the length much larger than the width of the film have been prepared. Precautions have been taken in order to prepare films with as small amount of unoriented material on the edges of a film as possible. Additionally, the crosslinking time was varied in order to check the influence of the crosslinker density on the deformational behaviour of smectic elastomer films.

At first, a film was crosslinked for a shorter time than usually; also the intensity of irradiation was diminished. After the cross-linking, stretching measurements have been performed, then the film was cross-linked one more time and stretching experiments have been repeated.

Fig. 4.15 shows the dependence of a free-standing film thickness on strain, measured by the reflectometry method. The film was prepared by crosslinking of the polymer BR162A in the SmA phase, irradiation time was 30 minutes. The initial length of the film is l_0=1.79mm and the width of the film in the middle w_0=1.24mm. The thickness of the film was calculated for three film regions with different initial thicknesses. Fig. 4.15b shows the strain perpendicular to the film surface $\lambda_z=d/d_0$ as a function of strain. From these measurements it is obvious that this film demonstrates a kind of behaviour that is qualitatively different from all previous experimental observation for the of LC elastomers studied in this thesis. The values of the strain, perpendicular to the smectic layer, lie above the solid curve which describes the deformation of an isotropic rubber with Poisson's ratio $\nu = 1/2$. This means that deformation perpendicular to the smectic layer is smaller than the shrinking in the layer plane. For the region with the largest initial thickness the film thickness is almost constant up to 20% and compression of the film reaches approximately 5% when applied strain value is 40%. This is a so-called in plane fluidity which is often observed for the smectic elastomers deformed parallel to the smectic layer [12-14]. In this case the thickness of a film perpendicular to the smectic layers does not change and stretching deformation is compensated by contraction strain in the smectic layer plane, with Poisson's ratio $\nu_y = 1$.

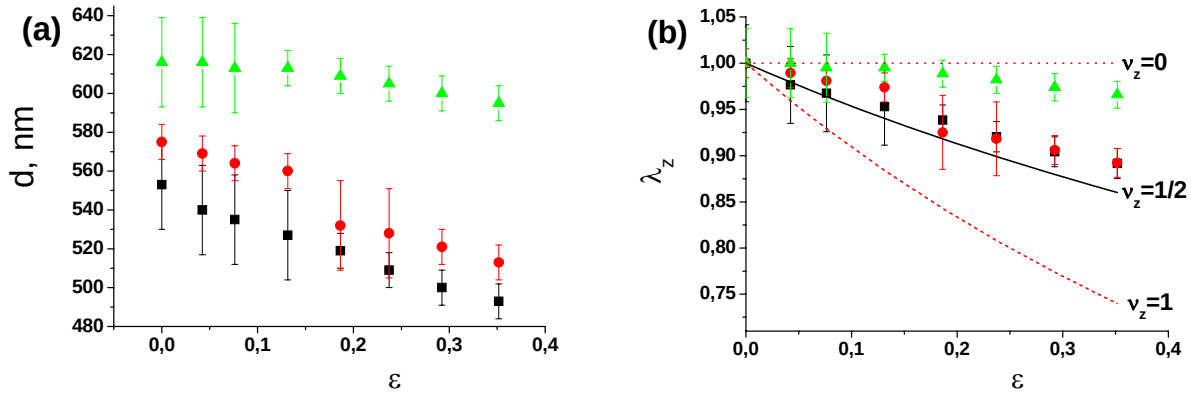

Figure 4.15: Compression of the BR162A elastomer film cross-linked in SmA phase, T = 115°C, irradiation time 30 minutes. Stretching is in SmA phase T = 115°C. The initial length of the film is l_0=1.79mm and the width of the film in the middle w_0=1.24mm. a) Reflectometry measurements of the film thickness, for three regions with different thicknesses, at different values of stretching . b) Deformation perpendicular to the film surface $\lambda_z = d/d_0$ as a function of applied deformation $\varepsilon_x = \lambda_x - 1 = l/l_0 - 1$, different symbols corresponds to the regions with different initial thicknesses (Fig. 4.15a) .

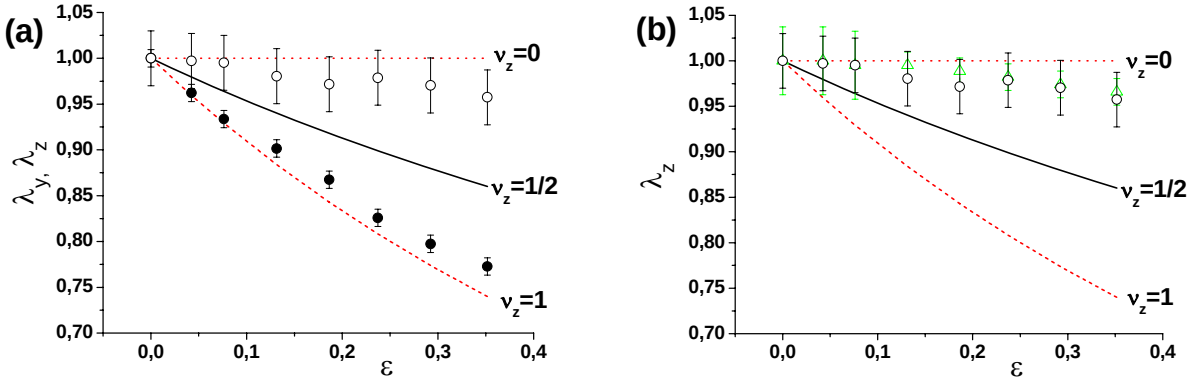

Figure 4.16: Compression of the BR162A elastomer film cross-linked in SmA phase T = 115°C, irradiation time 30 minutes, stretching is in SmA phase T = 115°C. The initial length of the film is l_0=1.79mm and the width of the film in the middle w_0=1.24mm. (a) The deformation of the film in the layer plane ● - λ_y and compression of the film calculated from the volume conservation ○- $\lambda_z = 1/(\lambda_y \lambda_x)$ (b) Comparison of the optical reflectometry results (Δ) and compression of the film calculated from the volume conservation (○).

Measurement of the deformation in the film plane can be used as additional prove for the in-plane fluidity behaviour. Fig. 4.16a shows the measurements of the contraction in the layer plane (filled symbols) and the values of the strain in z-direction calculated from the volume conservation. As expected, deformation in the layer plane coincides with the curve for the deformation with

Poisson's ratio $\nu = 1$. Fig. 4.16b shows both experimental value of the film compression measured by optical reflectometry and the values calculated from the deformation in the layer plane, under the condition of the volume conservation, both curves are almost equivalent. This confirms that the dependence of the film compression obtained by optical reflectometry measurements is correct.

After these measurements the film was one more time irradiated by UV light for 170 minutes, so the total crosslinking time was 200 minutes. After the second crosslinking the deformation curve shifts and compression of the film increases in comparison with the film with a short crosslinking time (Fig. 4.17). And only for the thick film region deformation is slightly smaller than for isotropic material, but only at small deformation (Fig. 7.14a). Compression of the thin film region is below the curve with the Poisson's ratio $\nu = 1/2$ (Fig. 7.14b)

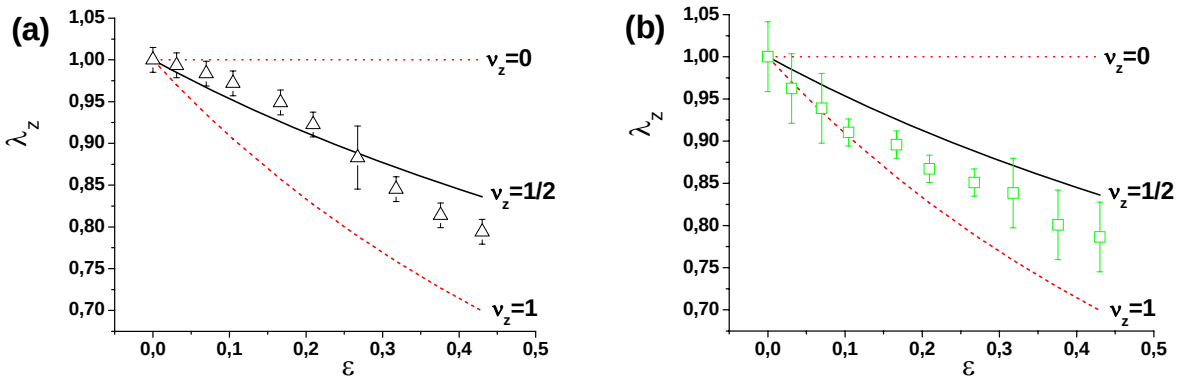

Figure 4.17: Compression of the elastomer BR162A film cross-linked in SmA phase T = 115°C, irradiation time 200 minutes, stretching is in the SmA phase T = 115°C. The initial length of the film is l_0=1.79mm and the width of the film in the middle w_0=1.24mm. Compression of the (a) thick film region with initial thickness d_0=620 nm and (b) thin film region with initial thickness d_0=560nm.

Deformation in the SmC* phase demonstrate a similar behaviour, at small deformations the contraction of the film perpendicular to the smectic layer is smaller than for the isotropic material for the thick film region and larger for the thin film region.

The results of the measurement of the film compression in the isotropic phase are shown in Fig. 4.19. The changes of the film thickness have been calculated for two regions with different initial thicknesses. As expected, the compression of the film is similar to the deformation of a isotropic rubber, experimental values for a thick film region coincide with the curve with Poisson's ratio $\nu = 1/2$ and for a thin region lie slightly under this curve.

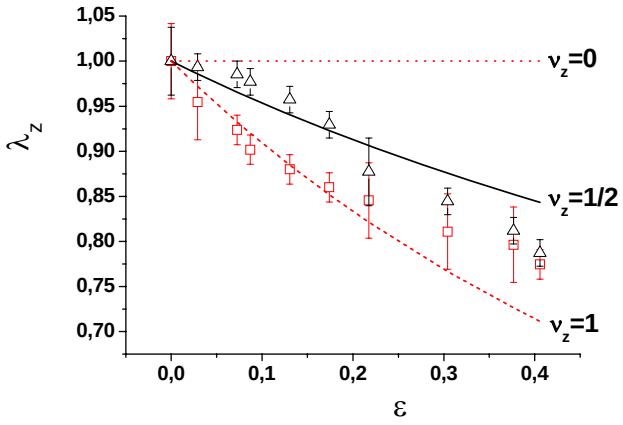

Figure 4.18: Compression of the elastomer BR162A film cross-linked in SmA phase T = 115°C, irradiation time 200 minutes, stretching in SmC* phase T = 80°C. The initial length of the film is l_0=1.79mm and the width of the film in the middle w_0=1.24mm. Compression of the (Δ) thick film region with initial thickness d_0=611 nm and (□) thin film region with initial thickness d_0=565nm.

Such behaviour is quite expectable, in the isotropic phase smectic layers are melting and there is no additional structure in the elastomer which can increase elastic modulus and prevent compression of the film.

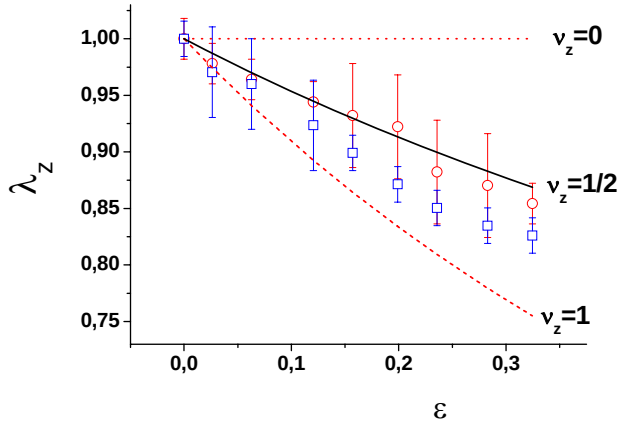

Figure 4.19: Reflectometry measurement of the compression of the elastomer BR162A film in the isotropic phase T = 180°C. The film was cross-linked in SmA phase T = 115°C, irradiation time was 200 minutes. The initial length of the film is l_0=1.79mm and the width of the film in the middle w_0=1.24mm. The compression of the (□) thick film region with initial thickness d_0=575 nm and the compression of the (○) thin film region with initial thickness d_0=501nm are shown.

Experimental investigations with the elastomer BR162H with 10 percent of crosslinker groups demonstrate the same tendencies. For the films with a short crosslinking time, compression of the

film is smaller than the compression of an isotropic rubber (Fig. 4.20) The initial length of the film is l_0=2.04mm and the width of the film in the middle w_0=1.45mm.

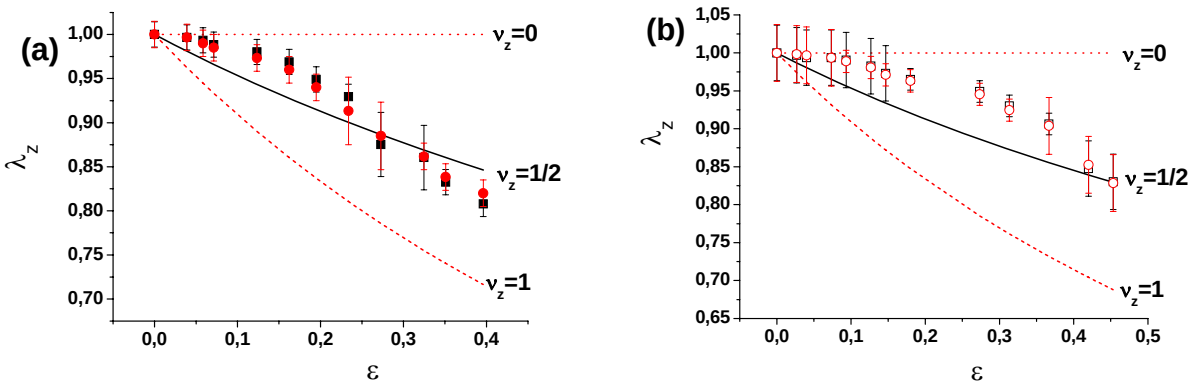

Figure 4.20: Compression of the elastomer BR162H film cross-linked in SmA phase, T = 115°C, irradiation time 70 minutes. Stretching is in the SmA phase T = 115°C (a) (● - d_0=606nm and ■- d_0=600nm) and in the SmC* phase T = 75°C (b) (○- d_0=624nm and □- d_0=630nm). The initial length of the film is l_0=2.04mm and the width of the film in the middle w_0=1.45mm.

Increasing of the total crosslinking time up to 320 minutes eliminates the anisotropy of elastic moduli and the deformational behaviour becomes similar to the deformational behaviour of an isotropic rubber (Fig. 4.21).

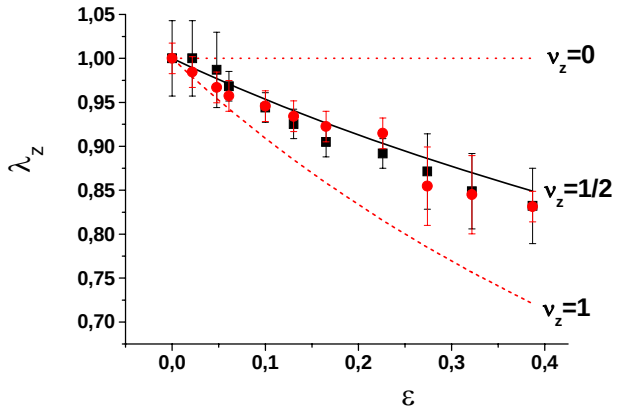

Figure 4.21: Reflectometry measurement of the compression of the elastomer BR162H film in the in the SmA phase T = 115°C. The film was cross-linked in SmA phase T = 115°C, irradiation time 320 minutes. The initial length of the film is l_0=2.04mm and the width of the film in the middle w_0=1.45mm.

Optical reflectometry measurements with the homopolymer BR153B with 7% of crosslinker groups again demonstrate that in the film crosslinked only for a short time, the smectic layer structure increases elastic modulus perpendicular to the smectic layers and stretching of the film does not induces compression perpendicular to the smectic layer (Fig. 4.22). But, this is only true for the thick film regions. In the thin regions the compression of the film is the same as in the case of an isotropic material. This proves one more time that for the thin free-standing film with inhomogeneous thickness the compression of the film is non-uniform and deformation without the compression of the film is only possible for the thick film regions.

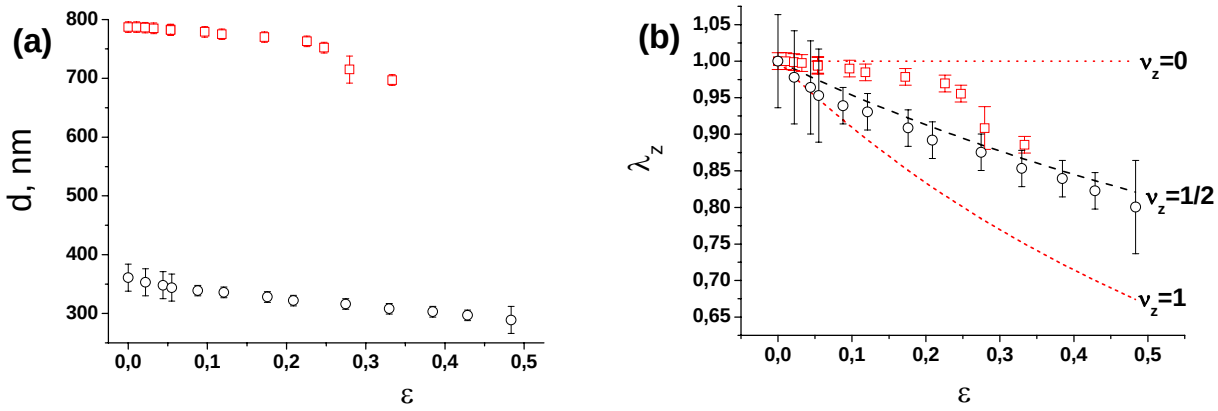

Figure 4.22: Compression of the homopolymer film cross-linked in the SmA phase, T = 175°C, irradiation time is 40 minutes. Stretching is in SmA phase T = 175°C. The initial length of the film is l_0=1.64mm and the width of the film in the middle w_0=1.18mm. (a) Reflectometry measurements of the film thickness at different values of stretching for two regions with different initial thicknesses. (b) Strain perpendicular to the film surface $\lambda_z = d/d_0$ as a function of applied deformation $\varepsilon_x = \lambda_x - 1 = l/l_0 - 1$.

In thin film regions the influence of the stretching force from the rand and surrounding thick regions diminishes constriction of the film in the smectic layer plane and as consequence the compression in these regions is stronger than in thick regions.

4.4 Conclusions

Based on the optical reflectometry measurements we come to a conclusion that, deformational behaviour of the films depends on the crosslinking time, geometrical parameters of films and in films with inhomogeneous film thickness on the thickness of a film.

The main factor that defines the elastic properties of the elastomer films, studied in this thesis is the density of crosslinkers, which depends on the time of crosslinking. The elastomers with a short crosslinking time are highly anisotropic. All free-standing films with a short crosslinking time, prepared from elastomers with different density of crosslinking groups (for the details of chemical structure of precursor LC polymers see chapter 2), demonstrate in-plane fluidity behaviour. These films can be stretched parallel to the smectic layers without the compression perpendicular to the smectic layer. Stretching deformation is compensated only by the contraction in the smectic layer plane. That indicates that in elastomers with a short crosslinking time the elastic moduli perpendicular to the smectic layers are much higher than the moduli parallel to the smectic layers. This is a usual behaviour for the smectic elastomers studied by the group of Prof. Finkelmann [12-14, 40], but has not been observed for the elastomers investigated in this work before [42-44, 47].

Increasing of the crosslinking time and therefore the crosslinking density diminishes the anisotropic of elastic moduli. The increasing of the crosslinker density, caused by the increasing of a crosslinking time, "softens" smectic layers and decreases the elastic modulus perpendicular to the layers. If a crosslinking time is long enough then, the elastic properties of the elastomer becomes anisotropic. The modulus perpendicular to the smectic layers and modulus in the layer plane have close values. Therefore, compression of such film is the same as compression of the isotropic rubber with Poisson's ratio $\nu_z=1/2$.

Another factor that defines observed deformational behaviour of smectic elastomer films is geometrical parameters of the film. An additional stretching force in the film plane, perpendicular to the stretching direction, caused by the edges of a film, induce stronger compression of the film perpendicular to the smectic layers. The smaller is the ration of the film to its length, the stronger is the influence of the film edge. This means that for the films with the same width but with different lengths, deformational behaviour of the long films is mainly defined by their elastic moduli parallel and perpendicular to the smectic layers. While in the case of short films the compression of the film is stronger in comparison with long film because of the stronger influence of additional stretching force. Hence, only the film with the length large in comparison with the film width shows the behaviour mainly defended by the elastic properties of the material. Therefore, the behaviour of the film with length large in comparison to its width is close to the behaviour of ideal film without any influence of the edges. In short film the influence of the additional stretching for is so strong, that compression of the film is stronger than for isotropic material with Poisson's ratio $\nu_z=1/2$. In some short films the influence of this stretching force is so strong that compression of the film is the same as for a material with Poisson ratio $\nu_z=1$ (see for instance Fig. 4.11a).

In the case of films with inhomogeneous thickness, one more factor influences the deformational behaviour. It is the thickness of the film, in the thin film region the compression of the film is stronger than in the thick film regions. The difference in compression of the regions with different thicknesses is caused by an addition stretching force from the film edges. The force, of course, is the same for different regions, but its influence is stronger for the thin regions. Therefore, the deviation of the measured compression of the film, from the ideal behaviour of a film with a homogeneous film thickness and without influence of the stretching force caused by the material gathering on the film edges (see Fig. 4.7), is smaller for thick film regions than for thin film regions.

Chapter 5 X-ray measurements

This chapter represents the results of the X-ray measurements of the smectic layer thickness at different temperatures and the X-ray measurements of the compression of free-standing elastomer films during stretching parallel to the smectic layers. In the first part the temperature-dependent X-ray diffraction measurements of the smectic layers thickness of unoriented bulk liquid crystalline polymers and elastomers are described. Second part deals with the compression of the smectic elastomer films perpendicular to the smectic layers. The thickness of the smectic layers at different values of deformation has been measured using the X-ray diffraction.

The temperature dependence of the smectic layer thickness has been measured for the copolymer (CT86) before and after crosslinking and for the homopolymer (BR153) in the crosslinked state. The X-ray measurements of the smectic layer thickness for the uncrosslinked homopolymer can be found elsewhere [48]. Comparison of the smectic layer thickness in different phases of the "diluted-" and homo-elastomer can help better understand the structure of the phases of these two different types of elastomers. In order to define the influence of the crosslinking on the smectic layers thickness and phase transitions, the X-ray measurements on the copolymer in uncrosslinked and crosslinked states have been performed.

The measurements on free-standing LCE films have to show whether the compression of free-standing smectic elastomer films, which was revealed by optical reflectometry measurements [47], leads to the compression of the smectic layers or some other mechanism is responsible for the film compression. For this purpose the thickness of the smectic layer as a function of deformation has been measured in the SmA and SmC* phases.

5.1 X-ray measurements of the temperature dependence of the smectic layer thickness

The crosslinking of liquid crystalline polymers into elastomers can influence the orientational order parameter S and also the smectic order parameter Σ in the case of smectic liquid crystalline polymers [27, 102]. The instability of the long-range translational order in one- and two-dimensional systems has been predicted by Landau and Peierls. In the one- and two-dimensional systems fluctuations destroy the long-range translational order [33, 49]. Therefore, in the smectic

phases which possess a translational order only in one-dimension, only the quasi-long-range translational order can be observed [103]. The crosslinking of the smectic liquid crystalline polymer can suppress fluctuations and stabilize the smectic structure [104, 105]. On the other hand cross-lining groups can induce defects in the smectic layers and at large concentration can decrease or destroy the smectic order [102, 104].

The main question which the X-ray measurements on unoriented samples have to answer is what is the influence of the crosslinking process on the phase transitions, the structure of the phases and the thickness of smectic layers.

The temperature dependence of the smectic layer thickness of the diluted liquid crystalline polymer (CT86) and homopolymer (BR153B) have been studied in an unoriented state. The structure of these two polymers is described in the section 2.1. The X-ray set-up and the details of the X-ray measurements on unoriented LC polymers and elastomers are described in the section 2.6.

For the diluted LC polymer, the X-ray measurements have been performed before and after crosslinking. At first X-ray measurements have been done for the capillary filled with the liquid crystalline polymer at different temperatures in order to study the temperature dependence of the smectic layers thickness. Then the same capillary was irradiated by UV-light in the smectic phase at the temperature 10°C above the SmC*-SmA phase transition. After the crosslinking, the X-ray measurements have been repeated at different temperatures. For the homopolymer the X-ray measurements have been done only in the crosslinked state.

Fig. 5.1a shows a typical 2D-diffractogram of the polymer CT86 before crosslinking at temperature T = 60°C. There are two peaks in the small-angle region which correspond to the diffraction on the smectic layers structure. The intensity of the second peak is very low in comparison with the first one and it hardly can be seen. But, it becomes clearly visible after the integration over an azimuthal angle (Fig. 5.1b). Usually, in a wide-angle region a peak which corresponds to the lateral distance between the mesogens can be observed; but it can not be seen in these measurements, because at the chosen distance between the sample and the detector, the diffraction angle of this peak is larger than the range of measured angles. Fig. 5.1b represents the integral intensity as a function of the scattering angle 2θ, but for the analysis of the smectic layer thickness it is more convenient to recalculate the intensity function into the function of the scattering vector $q = (4\pi / \lambda)\sin(\theta)$ (Fig. 5.2). Fitting peaks with Gauss function we get most important parameters: the position of the peak q_0 and the peak width at half-maximum ω.

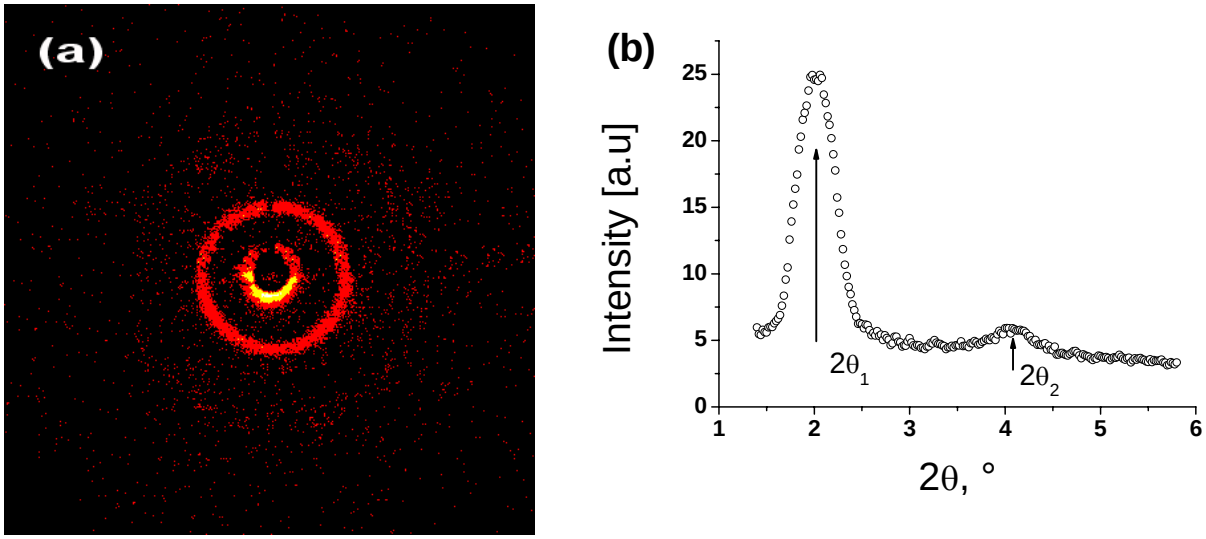

Figure 5.1: (a) X-ray diffraction pattern of the copolymer before cross-linking measured at the temperature T = 60°C. The X-ray wave length is λ = 1.79Å (Co Kα). (b) The X-ray diagram of the integral intensity after the integration by azimuthal angle. The positions of the first and the second peaks are $2\theta_1 = 2.02°$ and $2\theta_2 = 4.08°$ and the corresponding thicknesses of the smectic layer are $d_1 = 5.13$ nm and $d_2 = 2.57$ nm respectively.

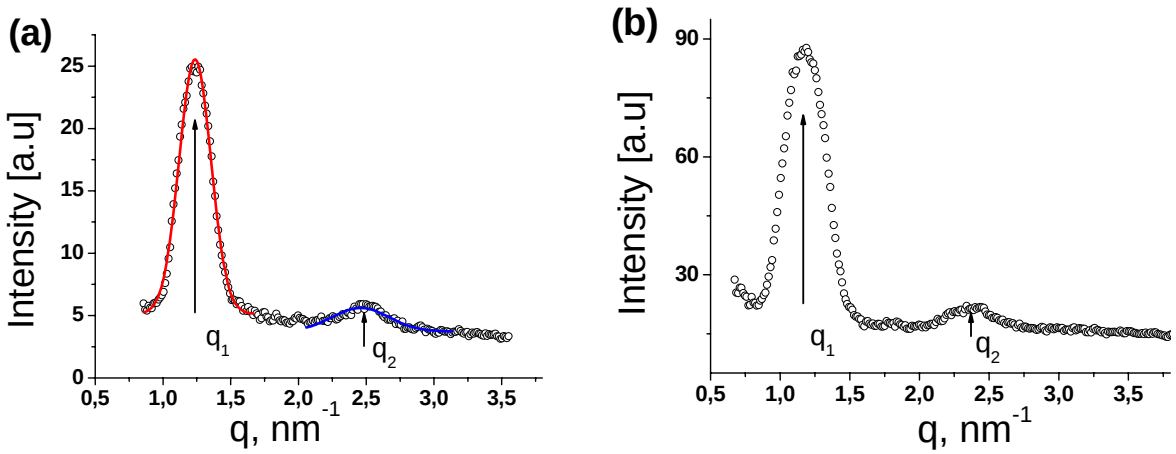

Figure 5.2: The integral intensity of the X-ray diffraction of the polymer CT86 as a function of the scattering vector q (a) before crosslinking measured at T = 60°C and (b) after crosslinking in the SmA phase measured at T = 65°C. In the case of the polymer, the positions of the first and the second peaks are $q_1 = 1.23$ nm^{-1} and $q_2 = 2.50$ nm^{-1} and the corresponding thicknesses of the smectic layer are $d_1 = 5.13$ nm and $d_2 = 2.57$ nm respectively. In the case of the elastomer, the positions of the first and the second peaks are $q_1 = 1.18$ nm^{-1} and $q_2 = 2.40$ nm^{-1} and the corresponding thicknesses of the smectic layer are $d_1 = 5.30$ nm and $d_2 = 2.63$ nm respectively.

From these parameters of the peak the smectic layers thickness d and the correlation length of the layers ξ can be found as follows:

$$d = \frac{2\pi}{q_0} \text{ and } \xi = \frac{4\pi}{\omega} \tag{5.1}$$

X-ray measurements on unoriented substance do not give complete information about its the structure of LC phases, but still, such important parameters as a layers thickness and correlation length can be defined.

The temperature dependence of the smectic layers thickness for the copolymer (Fig. 5.3) has been defined from the position of the first peak at different temperatures (Fig. 5.2). The maximal value of the smectic layers thickness is at the temperature close to the SmC*-SmA phase transition. The thickness of the layers in the SmC* phase is decreasing with decreasing temperature, that is quite expectable, while the tilt angle of the mesogens in the SmC* phase is increasing with decreasing of temperature.

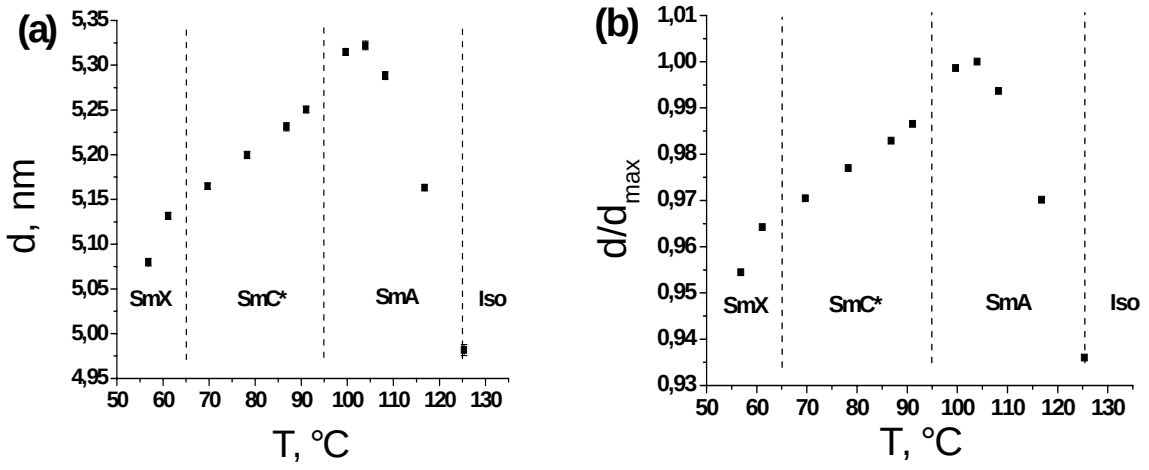

Figure 5.3: (a) The temperature dependence of the smectic layer thickness of the diluted polymer CT86 before cross-linking. (b) The ratio of the smectic layers thickness d to maximal value of the smectic layer thickness d_{max}.

The material under investigation shows a bit smaller layer shrinkage than typical 5-10% for a SmC*-SmA phase transition. Considering the value of the smectic layer distance d at the temperature of the SmX-SmC* phase transition as the minimal value we get the layers shrinkage about 3%. But, the smectic layer shrinkage at the minimal measured temperature 55°C is about 4,

5%, this value is quite close to the typical value (5-10%). The smectic layer thickness in the SmA phase is decreasing with increasing of temperature. That can be explained by the diminishing of the orientational order parameter S. Hence the orientational distribution function becomes brighter and the average inclination of the molecules increases. That in turn decreases the average projection of the molecules on the layer normal direction and the thickness of the smectic layers becomes smaller. The temperature dependence of the smectic layer thickness of the copolymer after crosslinking (Fig. 5.4) is similar to the temperature dependence before crosslinking (Fig. 5.3). The smectic layers thickness is maximal at the SmC*-SmA phase transition (Fig. 5.4).

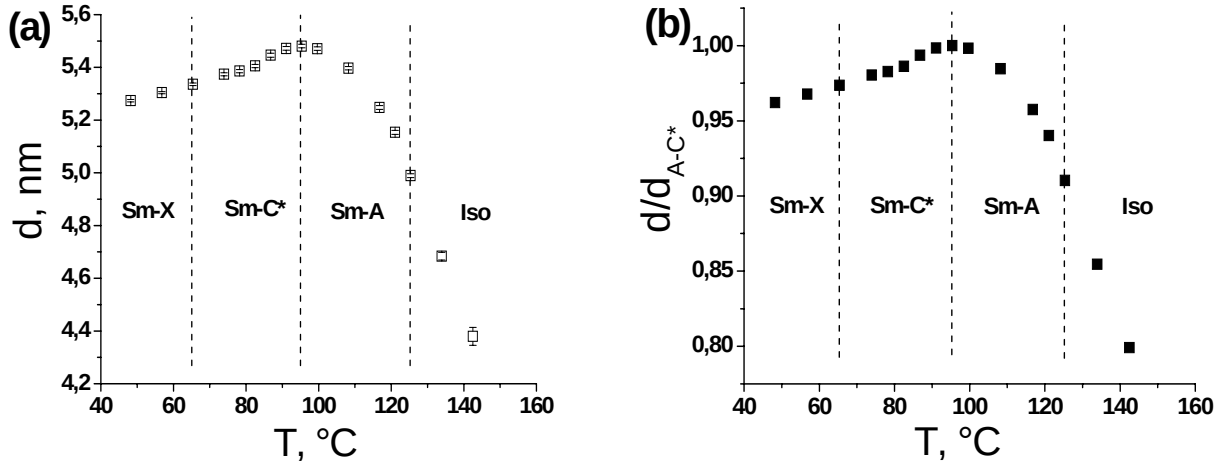

Figure 5.4: (a) The temperature dependence of the smectic layer thickness of the copolymer after crosslinking in the SmA phase. (b) The ratio of the smectic layers thickness *d* to maximal value of the smectic layer thickness d_{max}.

The thickness of the smectic layer at the temperature of the SmC*-SmX phase transition is 2.5% smaller then at the SmA-SmC* phase transition. Comparing the smectic layer thicken at the temperature of the SmC*-SmA phase transition with the value at the lowest measured temperature we get the smectic layer shrinkage close to 4%. So, the smectic layer shrinkage slightly decreases in the crosslinked material in comparison with the uncrosslinked.

In case of the crosslinked material the diffraction peak from the smectic structure can be observed above the SmA-Isotropic phase transition of the non-crosslinked polymer. From that observation we can make a conclusion that crosslinking stabilizes smectic structure and due to this, the smectic layer reflexes remain at the temperatures higher than the SmA-Isotropic phase transition

temperature of the uncrosslinked material. However, the intensity of the peak rapidly decreases above the SmA – Isotropic transition (Fig. 5.5a).

The width of the peak gets broader, which means that the correlation length becomes smaller (Fig. 5.5b). The tendency of decreasing smectic layers thickness with increasing temperature preserves in the isotropic phase.

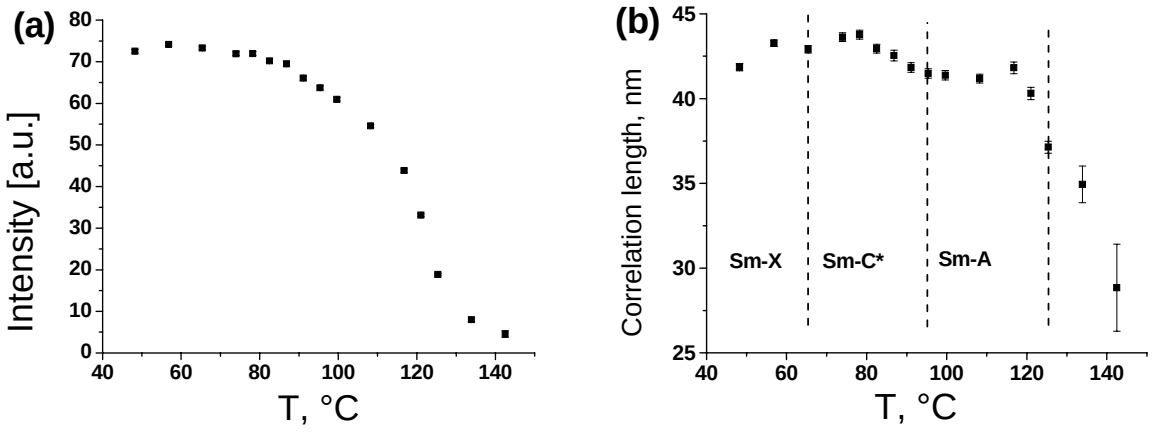

Figure 5.5: (a) Temperature dependence of the intensity of the first peak for the diluted elastomer. (b) The correlation length of the smectic layers of the diluted elastomer calculated from the width of the first peak.

As in the case of the uncrosslinked material, diminishing of the smectic layer thickness of the elastomer at high temperatures can be explained by decreasing of the orientational order parameter S. Decreasing intensity of the peak and rapidly decreasing correlation length indicate that the smectic order parameter Σ becomes smaller at high temperatures.

Comparing the smectic layer thickness of the diluted polymer before and after cross-linking (Fig. 5.6) we can see that the maximal smectic layer thickness after crosslinking is approximately 3% lager than before crosslinking.

The increasing of the smectic layer thickness can be explained by increasing of the orientational order parameter. This means that after crosslinking the orientation distribution function becomes narrower and orientational order parameter increases and the average tilt angle with respect to the director becomes smaller.

The temperature dependence of the smectic layer thickness of the elastomer prepared by crosslinking of the homopolymer is shown in Fig. 5.7. This elastomer shows behaviour different from the behaviour of the diluted elastomer (Fig 5.4 and Fig. 5.7).

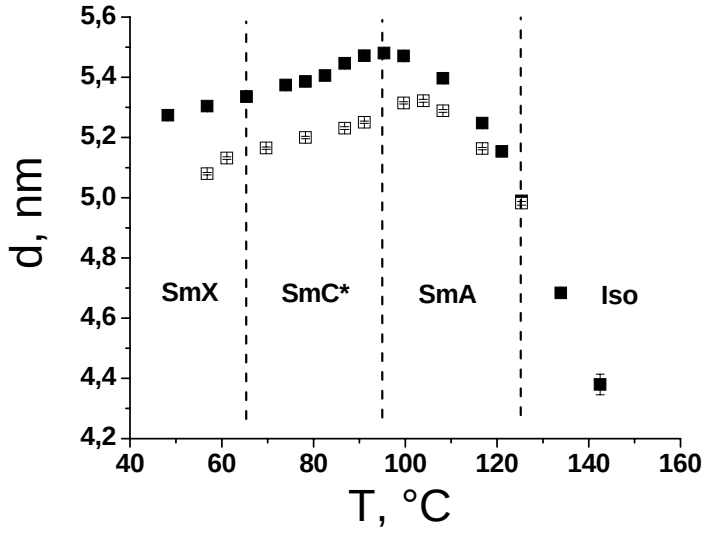

Figure 5.6: The temperature dependence of the smectic layer thickness of the copolymer before crosslinking □ and after crosslinking ■ in the SmA phase.

The maximal layer thickness is not at the SmC*-SmA phase transition temperature but in the SmA phase close to the SmA-isotropic phase transition. Upon cooling from the Sm-*A* phase, as usually, the decreasing of the smectic layer thickness is observed.

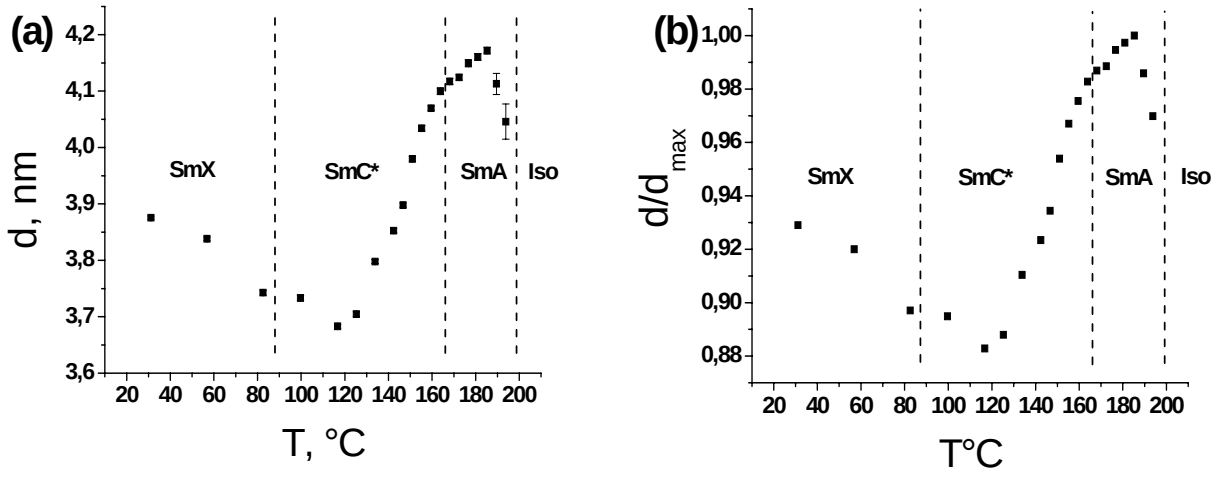

Figure 5.7: (a) Temperature dependence of the smectic layer thickness of the homopolymer crosslinked in the SmA phase. (b) The ratio of the smectic layers thickness *d* to maximal value of the smectic layer thickness d_{max}.

But at further cooling in the SmC* phase the smectic layer thickness starts to increase and continues to increase in the SmX phase. Contrary to the diluted elastomer, smectic layers shrinkage of the homoelastomer is about 10%.

The temperature dependence of the peak intensity (fig. 5.8a) and the correlation length (fig. 5.8b) of the homopolymer are different from those of the diluted elastomer (fig. 5.5). In the case of the diluted elastomer the intensity of the peak is continuously decreasing with increasing of temperature (fig 5.5a). In the case of the elastomer obtained by crosslinking of the homopolymer the intensity of the peak is slightly decreasing with increasing of temperature up to 140°C. After that it starts to grow and reaches its maximum near the SmC*-SmA phase transition and only after that the intensity starts to decrease rapidly.

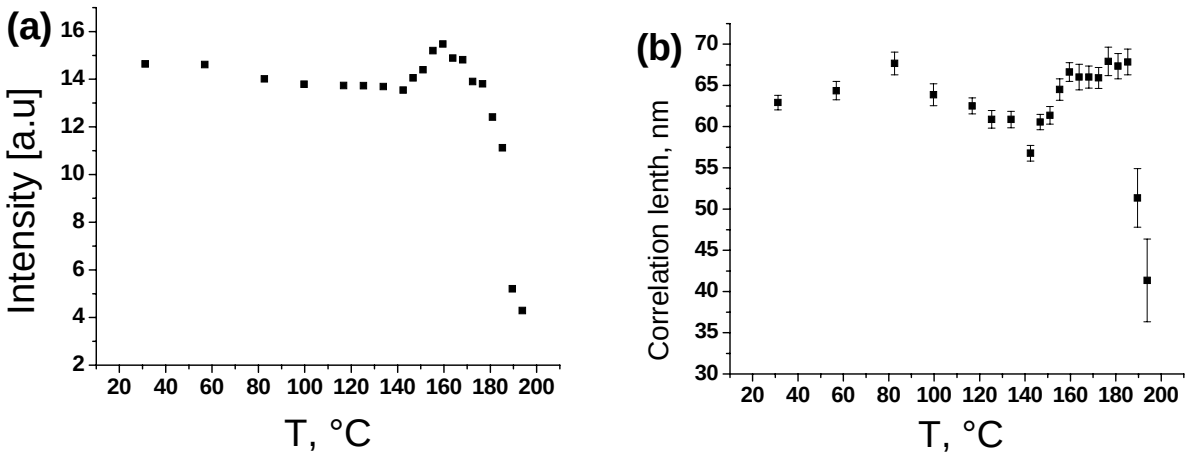

Figure 5.8: (a) The temperature dependence of the intensity of the first peak for the homoelastomer. (b) The correlation length of the smectic layers of the homoelastomer calculated from the width of the first peak.

In order to understand the change of the smectic layer thickness in different phases more a detailed analysis of the diffraction patterns is required. The diffraction pattern of the crosslinked homopolymer has the similar structure as in the case of the diluted elastomer (Fig. 5.1 a), there are two peaks in the small-angle region. But more detailed consideration shows that these two diffraction patterns have a very important difference. The diffraction angle of the second peak θ_2 in the case of the diluted elastomer is approximately two times larger than the diffraction angle of the first peak θ_1, i.e. $\theta_2 \approx 2\theta_1$. In case of the homoelastomer it's not the case and $\theta_2 < 2\theta_1$. Therefore it's obvious that in the case of the crosslinked homopolymer the second peak is not the second order diffraction from the same structure as the first peak. Hence, a conclusion can be made that the

substance has the layer structure with two different periods d_1 and d_2 which correspond to the first and second peaks respectively. Fig. 5.9a shows the temperature dependence of the d_1 and d_2 calculated from the position of the first and second peaks. The changes of the smectic layer thicknesses d_1 and d_2 are not always correlated. The ratio of these two quantities changes with the temperature (Fig. 5.9b). In the SmX phase it's close to 1.55 and is almost constant. In the SmC* phase it's continuously growing along with the increase of the temperature. At the SmC*-SmA phase transition the ratio reaches the value 1.95 and it only slightly changes in the SmA phase.

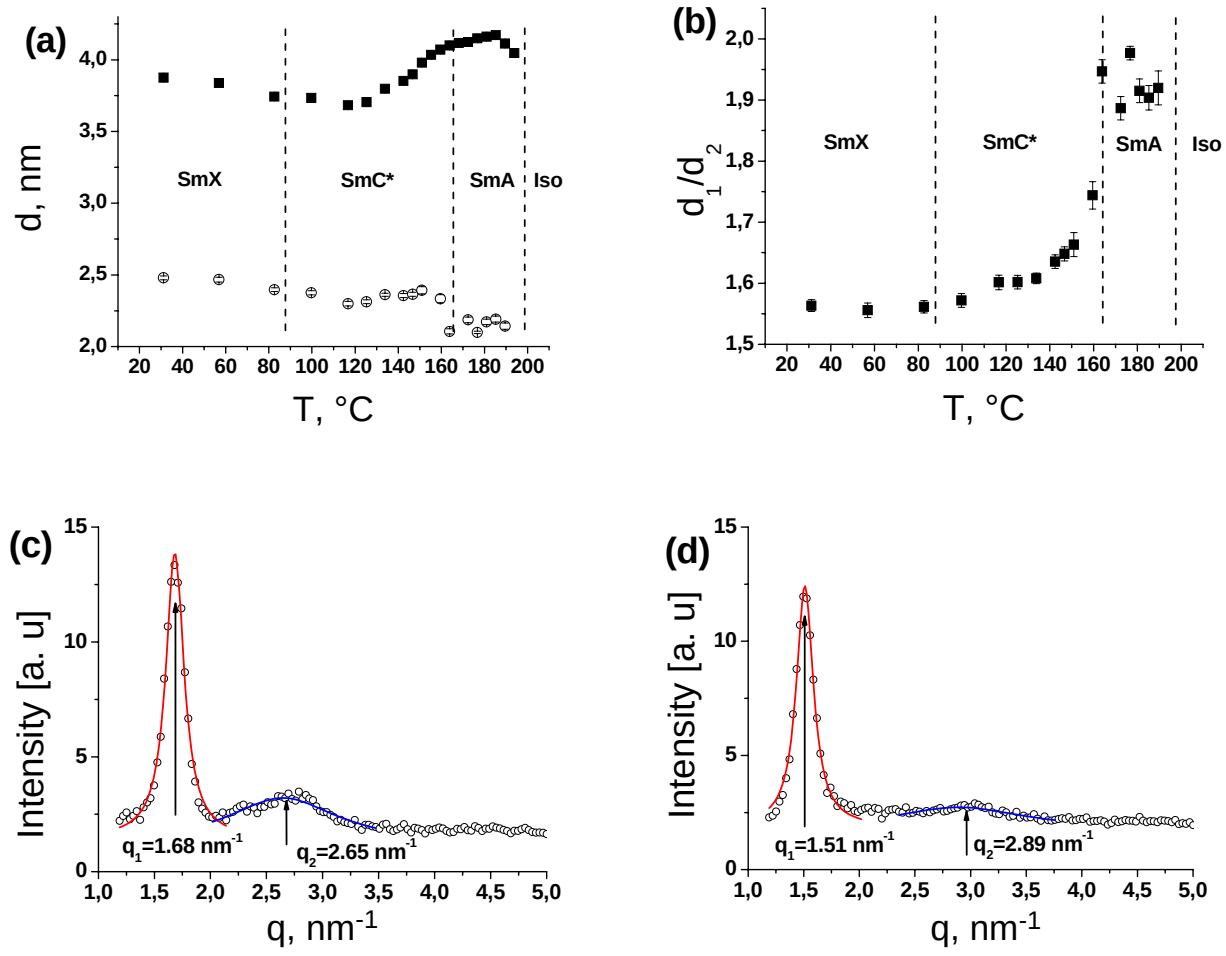

Figure 5.9: (a) Temperature dependence of the smectic layer thickness of the homopolymer after crosslinking in the SmA phase, calculated from the position of the first peak d_1 - ■, and second peak d_2 - ○. (b) The ratio of the smectic layers thicknesses d_1 to d_2. (c) The integral intensity of the X-ray diffraction of the homopolymer as a function of the scattering vector q measured at T = 100°C, the positions of the first and the second peaks are q_1 = 1.68 nm^{-1} and q_2 = 2.65 nm^{-1} and the corresponding thicknesses of the smectic layers are d_1 = 3.73 nm and d_2 = 2.37 nm; (b) measured at T = 181°C, the positions of the first and the second peaks are q_1 = 1.51 nm^{-1} and q_2 = 2.89 nm^{-1} and the corresponding thicknesses of the smectic layers are d_1 = 4.16 nm and d_2 = 2.17 nm.

Based on these data the following structure of the phases can be suggested. At low temperature a partially bilayer SmX_d phase with the constant degree of interdigitation is observed. At higher temperature a partially bilayer SmC_d* phase with the temperature dependant degree of interdigitation.

In the interval of the SmA phase the ratio of d_1 and d_2 is close to 1.9 so the phase is a partially bilayer SmA_d phase with only slightly interdigitating layers. Quite an interesting fact is that in this material the smectic layer thickness of one monolayer d_2, of which the bilayer structure is arranged, is smaller in the SmA phase than in the SmC* phase, this means that the average tilt angle in the SmA phase has to be larger than in SmC* phase.

The length of the mesogenic units have to be approximately equal to the thickness of the sublayer $d_2 \approx 2.5$nm. The mesogenic units in the case of the diluted LC polymer and homopolymer are the same, therefore the values of the smectic layer thickness obtained for the diluted elastomer d ≈ 5.2 nm can not correspond to simple SmA and SmC* phases and these phases have to be bilayer or partially bilayer phases.

Fig. 5.10a shows the smectic layer thicknesses calculated from the position of the first and second peaks and Fig. 5.10 b shows the ratio of these values for the diluted polymer. Figures 5.11a and 5.11b show the same values but for the crosslinked diluted polymer.

In the diluted polymer the ratio of the smectic layer thicknesses d_1 and d_2 is close to 2 and doesn't change almost in the whole interval of the measurement temperatures. Only at high temperature close to the SmA-Isotropic phase transition a very small interdigitation of the layers is observed $d_1/d_2 = 1.92$.

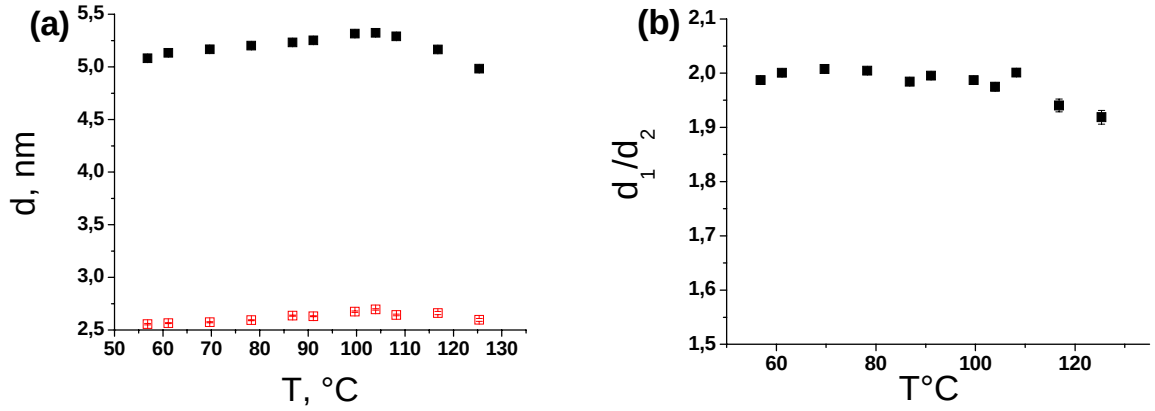

Figure 5.10: (a) Temperature dependence of the smectic layer thickness of the liquid crystalline copolymer, calculated from the position of the first peak d_1 - ■, and second peak d_2 - □. (b) The ratio of the smectic layers thicknesses d_1 to d_2.

In case of the elastomer the ratio of the values d_1 and d_2 is close to 2 and is constant at all temperatures. Apparently, crosslinking prevents the interdigitation of the neighbouring layers at high temperature which was observed for non crosslinked material.

So, in contrast to the homoelastomer, there is no layer interdigitation in diluted polymer and elastomer. All phases are bilayer phases, for example SmC_2* and SmA_2 phases. Fig. 5.13 shows the structure of the smectic phases of the diluted and homopolymer. Because of the complex structure of the smectic phases the thickness of the layers can change not only due to the variation of the molecules tilt, but also due to the interdigitation of the neighbouring layers. Therefore, in order to understand the orientation of molecules in different phases we have to calculate the tilt angle of the molecules as a function of temperature. It can be found from the thickness change of smectic sublayer d_2, since it changes only due to the tilt variation of molecules.

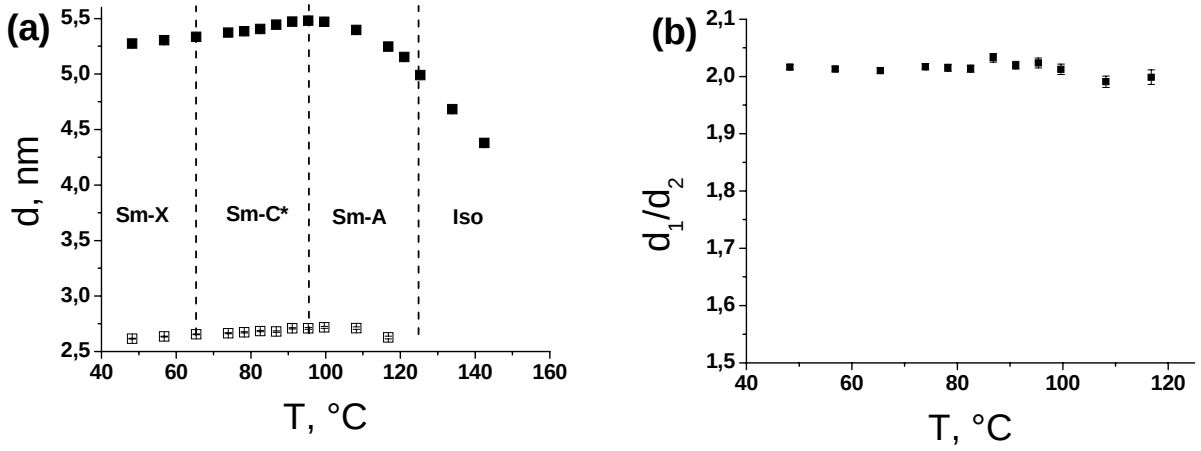

Figure 5.11: (a) Temperature dependence of the smectic layer thickness of the diluted LC polymer CT86 crosslinked in the SmA phase calculated from the position of the first peak d_1 - ■, and second peak d_2 - □. b) The ratio of the smectic layers thicknesses d_1 to d_2.

From the obtained X-ray data we can calculate the average tilt angle of the molecules as a function of the temperature. In case of diluted polymer and elastomer the largest film thickness has been found for the temperature of the SmA-SmC* phase transition. If we assume that at that temperature the average tilt angle is zero, this will mean that the layer thickness d_{max} is equal to the length of the molecules l, then the ratio $d(T)/d_{\max} = \cos\theta$, where θ is the average tilt angle.

The temperature dependences of the average tilt angle for the copolymer before and after crosslinking are shown in Fig 5.11a and b respectively. The tilt angles calculated from the temperature dependence of bilayer thickness d_1 and sublayer thickness d_2 are in a good agreement.

Comparison of Fig. 5.11a and Fig. 5.11b makes it clear that the tilt angle after crosslinking is a little bit smaller than before it. But, in both cases the average tilt angle of molecules in SmC* phase is about 15°-18°, this value is much smaller than in the case of conventional SmC phase, for which the tilt angle is usually about 30°. It's well known that the real structure of a SmA phase is different from the ideal model with zero tilt angle. X-ray measurements revealed that the smectic layer thickness in SmA phase is smaller than the length of the molecules. That difference can be explained by the de Vries model of smectic phase, a so-called defuse cone model, in that model the molecules are not perfectly aligned parallel to the director. The molecules are tilted, but the tilt direction of different molecules is not correlated, one can imagine that as molecules are distributed on the surface of a cone. Also, the tilt angle is not the same for all molecules, but has to be described by some distribution function.

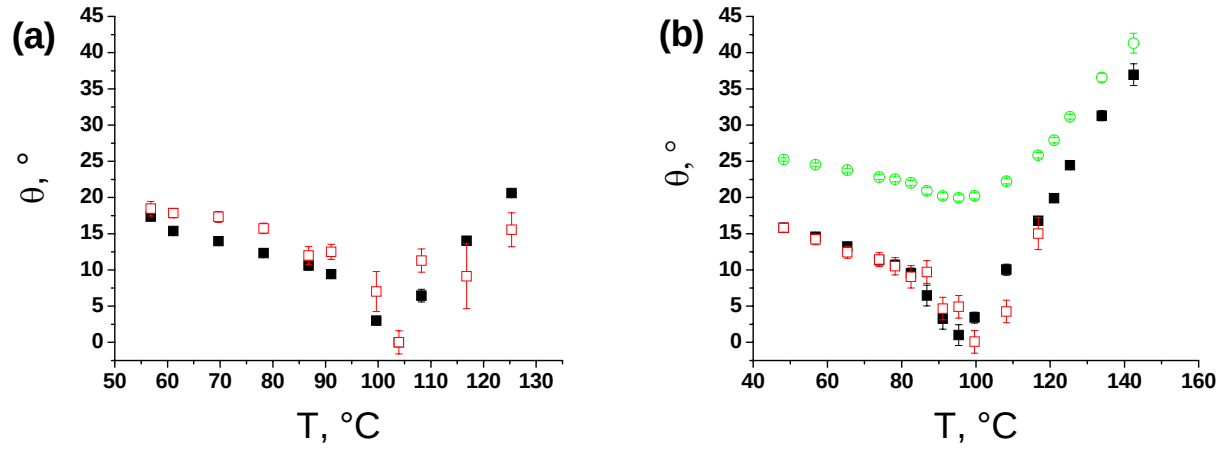

Figure 5.12: Temperature dependence of the tilt angle for the copolymer (a) before cross-linking ■ - calculated from the position of the first and □ - second peaks. (b) After crosslinking ■ - calculated from the position of the first and □ - second peaks. Tilt angle calculated from the position of the first peak for a non-zero average tilt at the SmA-SmC* phase transition ○ - $\theta_0 = 20°$.

Usually the orientational order parameter is about 0.8 and average tilt angle in SmA phase is approximately 20°. Assuming that the maximal thickness d_{max} corresponding to the temperature of SmA-SmC* phase corresponds to the average tilt angle $\theta_0 = 20°$ we can find the tilt angles for different temperatures Fig. 5.11b. The thickness of the layer is defined by the length of the molecules l and the tilt angle θ, $d = l\cos\theta$. The values of the tilt angle in SmC* phase calculated for a non-zero tilt in the SmA phase are higher than for the model with ideal alignment, but the change of the tilt angle at SmA-SmC* phase transition is much smaller than the one calculated for the model with molecules perpendicular to the smectic layers.

We also can calculate the tilt angle for the homopolymer after cross-linking, because the smectic layer thickness d_1 represents the smectic layer thickness of bilayer structure and the degree of the interdigitation of neighbouring layers is different at different temperatures we have to calculate the tilt angle from the thickness of the sublayer d_2 (Fig. 5.9a). In the case of homoelastomer maximal thickness of smectic sublayer d_2 was found not in SmA phase but in SmX phase. Assuming that the maximal value of the layer thickness corresponds to orientation of mesogens with zero tilt, tilt angle can be calculated from the thickness of the sublayer d_2 (Fig. 5.9a) at different temperature (Fig. 5.12).

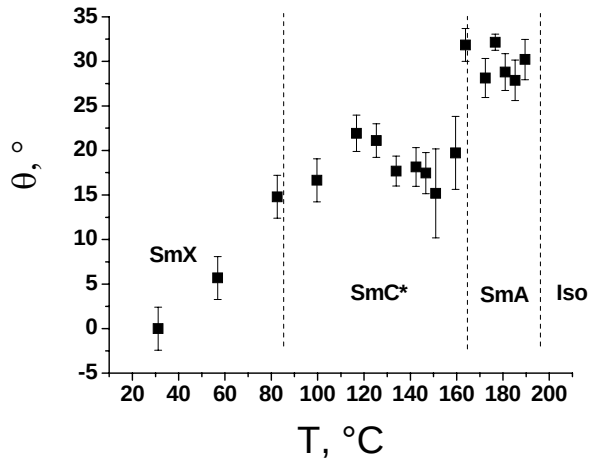

Figure 5.13: Temperature dependence of the tilt angle for the homopolymer in the crosslinked state calculated from the temperature dependence of the sublayer thickness d_2 (Fig. 5.9a).

.

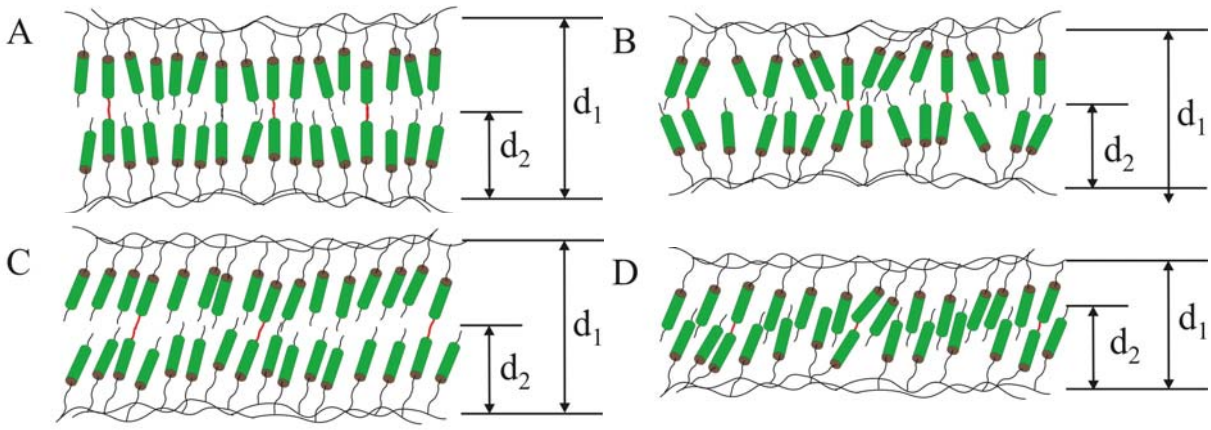

Figure 5.14: Schematic representation of the structure of the phases of the diluted polymer and elastomer and homopolymer, (a, b) show the structure of high temperature SmA_2 phase of diluted polymer and elastomer (a) and SmA_d phase with small interdigitation for the homoelastomer (b). (c, d) show the structure of low temperature tilted phases, SmC^*_2 in case of the copolymer and SmC^*_d partially bilayer for the homoelastomer.

Previous X-ray measurements of these two types of liquid crystalline polymers and elastomers; diluted- and homopolymer revealed quite a different behaviour at the SmA-SmC* transition [48]. Small layer shrinkage for the diluted elastomer and layer shrinkage about 10% typical for a SmA-SmC* transition for the elastomer obtained from the homopolymer, because in these measurements only the overall smectic layer thickness of bilayer phases was considered

From the results of the X-ray measurements shown above, it becomes clear that layer shrinkage in the homoelastomer is mainly due to the layer interdigitation in SmC* phase and the shrinkage of the layer is not directly correlated with the tilt of the molecules.

Unexpectedly, the maximal thickness of the sublayer for the homoelastomer is not in the SmA phase or at the temperature of the phase transition from the SmA phase into the SmC* phase how it was in the case of the diluted polymer and elastomer, but at low temperature in the SmX phase. What is even more astonishing, is the fact that the smectic tilt angle in the SmA is larger than in the SmC* phase. There is no explanation for this strange behaviour. It is possible that the mesophases of the studied elastomer have more complicated structure. X-ray measurements on oriented material can help better understand the structures of the mesophases in studied LC polymers and elastomers.

The results of the X-ray measurements show that in liquid crystalline mesogens with exactly the same structure of the mesogens and crosslinkers addition of unsubstituted siloxane groups into the backbone can change the structure of the mesophases.

5.2 Smectic layer compression in free-standing LCE films stretched parallel to the smectic layer plane

The mechanical properties of LCEs are in general different from those of conventional isotropic rubbers. Due to high smectic layer compression moduli, the elastic moduli parallel to the director are much higher than perpendicular to it. High anisotropy of the elastic moduli is responsible for so-called in-plane fluidity behaviour of the smectic LC elastomers. If such elastomer is stretched parallel to the smectic layers the dimension of the sample perpendicular to the layers does not change and stretching deformation is compensated only by a contraction in the layer plane [12-14].

Elastomers studied in this work demonstrate quite a different behaviour, during the stretching of a free standing film with smectic layers parallel to the film surface, the optical

thickness of the sample changes and the measured Poisson ratio is close to ½ like in an isotropic rubber [47].

Using X-ray spectroscopy and optical reflectometry the deformation of free-standing elastomer films has been studied. The idea is to ensure that the optical and X-ray data are obtained from the same elastomer film under identical preparation conditions. Simultaneous measurement by these two methods can help to find the relation between the optically observed thickness changes of the film (macroscopic effect) and the smectic layer compression (as its possible microscopic origin). The question we are trying to answer is: do the observed optical thickness changes correspond to actual film thickness changes, and particularly to changes of the individual smectic layer spacing? X-ray measurements allow to determine the smectic layers thickness under the influences of lateral strain and to clarify this question.

The material used to prepare free standing films is a random side-chain copolymer CT86 (see chapter 2 Fig. 2.4). The phase sequence in the non-crosslinked material is SmX 65°C SmC* 95-96°C SmA 125°C Iso. Samples for the X-ray measurement have been prepared by irradiation of free-standing films of the photo-crosslinkable polymer (in the SmA phase) as described in chapter 2. The time of UV irradiation was 2 hours.

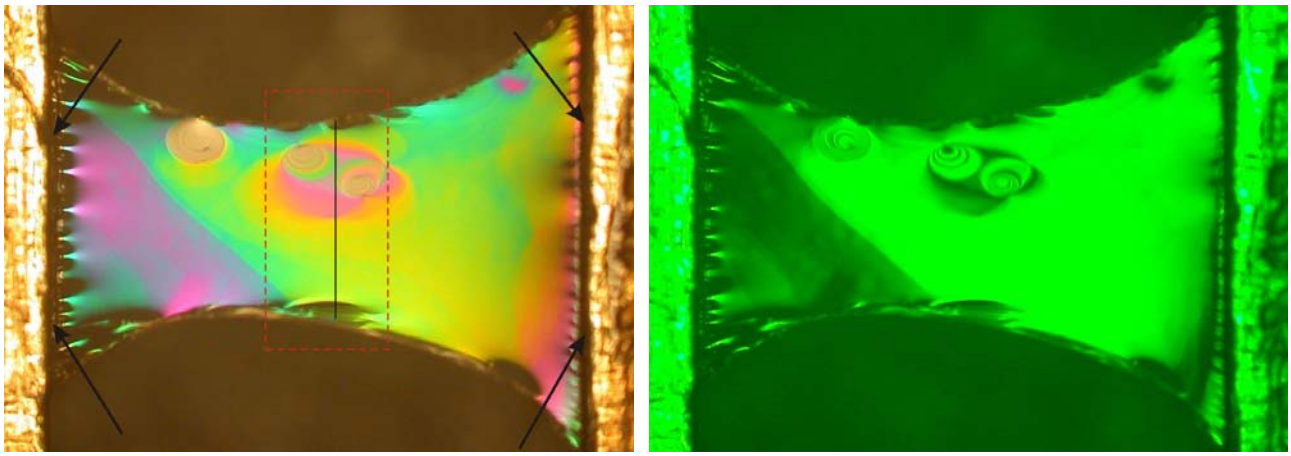

Figure 5:15 (a) Reflection image of the free standing film of smectic LCE in a white light (a) and in a monochromatic light with the wave length $\lambda = 547$ nm (b). The film was cross linked at $T = 120$°C in the smectic A phase, $\varepsilon_x = 34\%$. The arrows point at the meniscus with non-oriented material.

After UV irradiation, the sample consists of a well oriented free standing film with an area of approximately 5 mm^2 and a thickness of approximately 0.5μm. Most of the smectic material, however, is contained in the lateral meniscus of the film (see both sides of Fig 5.15a) which extends over a region of a few dozen micrometers from the edges of the support, and in bulk material on the support itself. The thickness of the meniscus can be much larger than the film thickness, and in

contrast to the film, the smectic layers may be randomly oriented in the meniscus and in the bulk phase.

Using optical reflectometry data, thickness profiles of the film at different values of strain have been calculated. White light and monochromatic (λ = 547 nm) reflection images were used for the determination of the film thickness. The colour images allow to define the correct order of interference and the monochromatic images allow a quantitative calculation of the optical phase difference $\Delta\varphi$. For the details see the section 2.5.

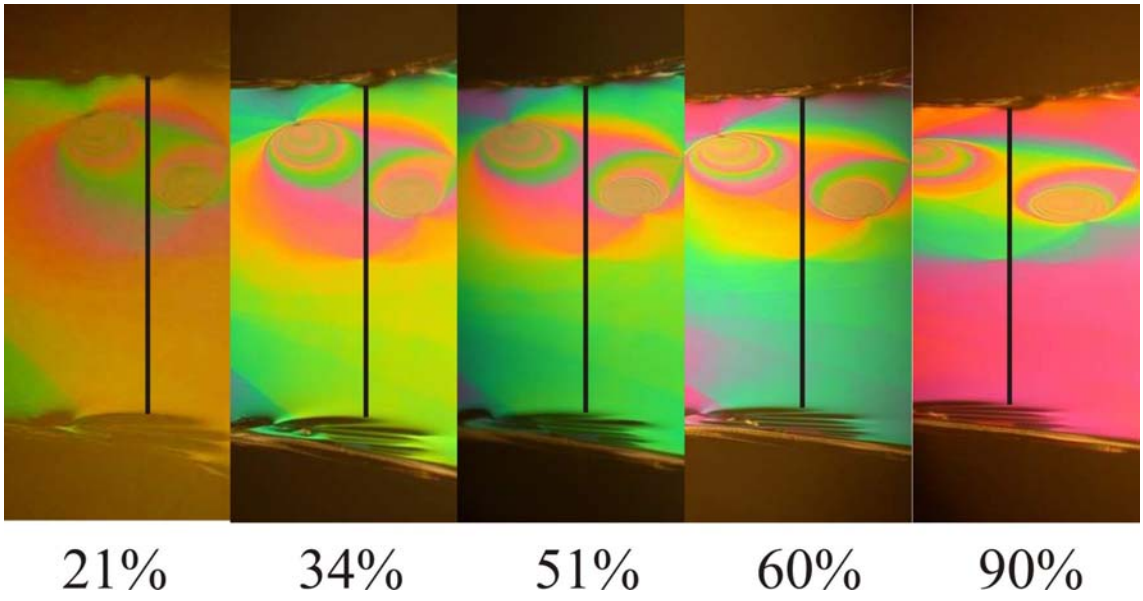

Figure 5:16 Reflection image of the part of the film (Fig. 5.15 a) at different strains, ε_x in % is given below the images.

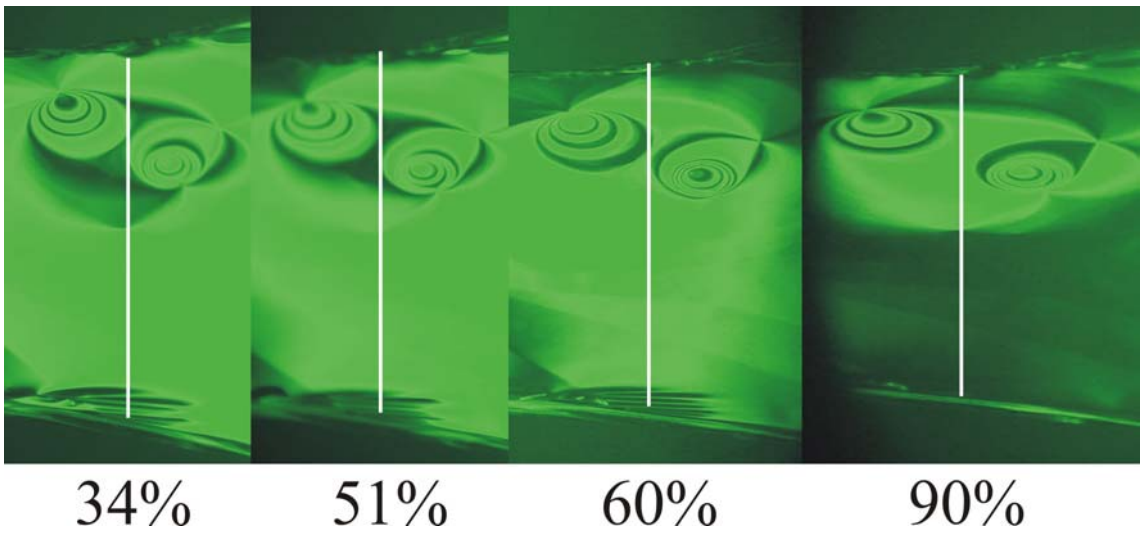

Figure 5.17: Reflection image of the part of the film (Fig. 5.15 b) at different strains, ε_x in % is given below the images.

Knowing this phase difference, one can determine the optical path $2\pi \cdot d_{(opt)} / \lambda = \Delta\varphi$ and the film thickness $d_{film} = d_{(opt)} / n_0$.

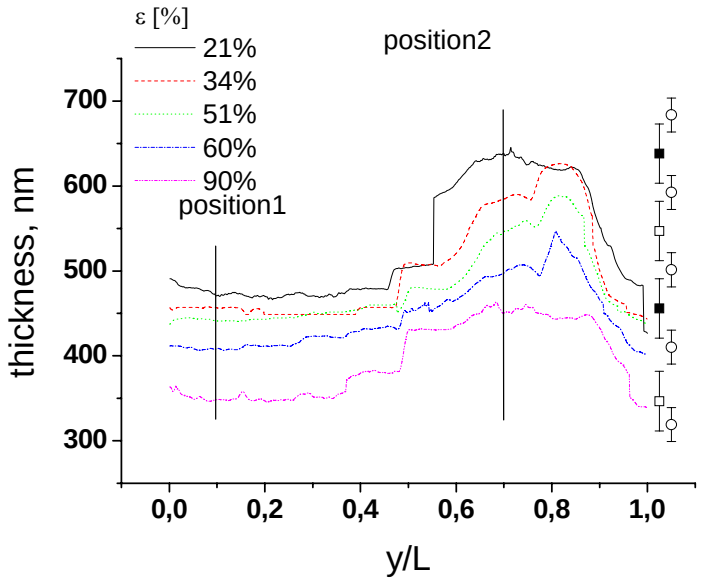

Figure 5.18: Thickness profiles of the film calculated for the given cross-section from the optical reflectivity at wave length λ = 547 nm. The width of the film depends on strain; it has been rescaled in the graph. *L* is the width of the film at a given deformation. Symbols ■ mark thicknesses for maximal reflectivity, □ mark reflectivity minima and ○ mark thicknesses for intermediate reflectivity, the corresponding error bars reflect the respective experimental uncertainty.

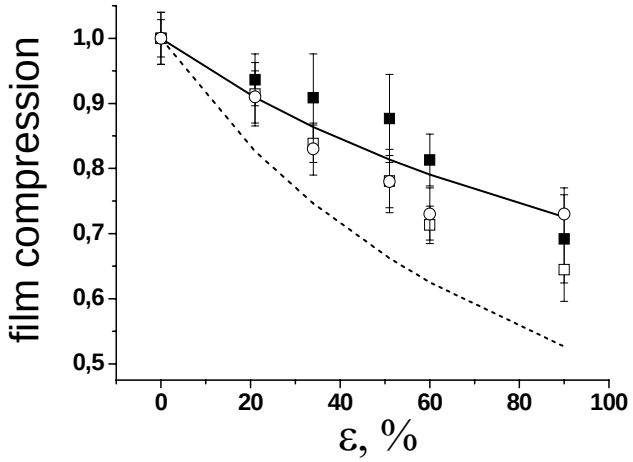

Figure 5.19: Exemplary normalised film thickness d/d_0 for two given points of the cross-sections, ■- position 1 and □- position 2 (Fig. 5.18) as a function of deformation, d_0 is the thickness of the non-deformed film, the solid line represents the film thickness change expected for an isotropic material (Poisson ratio ½) and the dashed line gives the lateral shrinkage in the film plane for a material with Poisson ratio $\nu_y = 1$ (no layer compression). The reduced width of the film cross-section $(y_0+\Delta y)/y_0$ is given by open circles.

For the calculation of the real film thickness it has been assumed that the changes of refractive index during stretching are negligible and it can be treated as a constant. This assumption has to be verified in independent experiments.

Fig. 5.19 shows exemplarily the dependence of the film thickness upon strain (open and solid squares) at two given points on the film, which we have labelled as positions 1 and 2 in the film thickness profiles in Fig. 5.18.

The x axis is parallel to the stretching direction and the z axis is taken perpendicular to the film surface. The solid line in Fig. 5.19 represents this theoretical thickness change of an isotropic incompressible material with Poisson's ratio ½ (see chapter 4). Since the lateral contraction of the film must compensate the product of strains in x and z, we have included in Fig. 5.19 the normalization factors $\lambda_y = y'/y_0$ for the length of the film profiles, i.e. for the lateral in-plane extensions of the film near the middle between the drawing edges (dark bars in Fig. 5.16). In an isotropically deformed material, these points should coincide with the $z'/z_0 = d/d_0$ data. From the graph, one acknowledges that the optical thickness change indeed reflects the change of the film thickness, and the assumption of a constant n_0 is justified. The dashed line shows, for comparison, the lateral shrinkage in the film plane for a material with Poisson ratio $\nu_y = 1$ (no layer compression). Experimental observation shows that compression of the film is close to that of an isotropic rubber, and the Poisson ratio is close to ½.

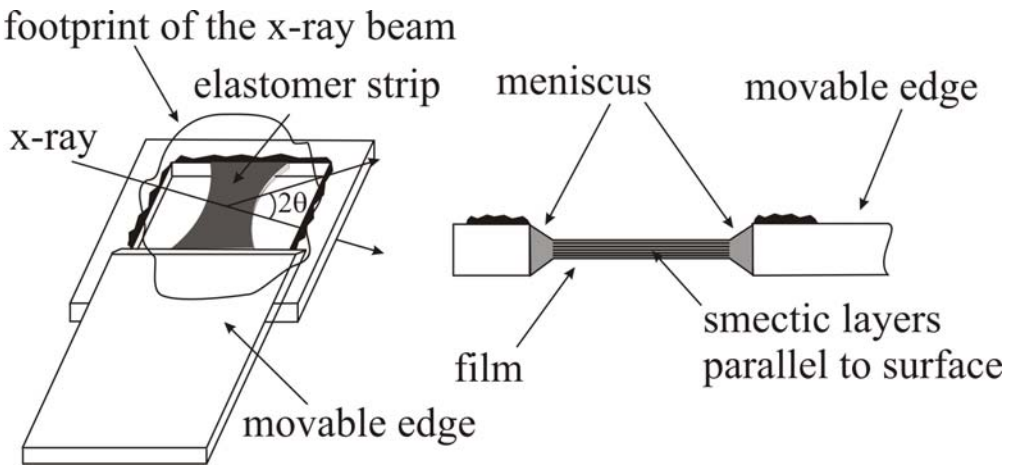

Figure 5.20: The geometry of the small angle X-ray scattering (SAXS) measurement of the free standing smectic elastomer films.

X-ray measurements of the smectic layer spacing give the answer to the question whether the film thickness change corresponds to an actual compression of individual smectic layers. A

certain problem is the sensitivity of the available X-ray setup, when a very small signal from the film is recorded. Fig. 5.20 sketches the experimental geometry for the small-angle X-ray diffraction measurements.

Measurements were performed in the SmC* and SmA phases at T = 90°C and T = 120°C respectively. The values of the smectic layer spacing obtained for the relaxed film at zero deformation at given temperatures are in a good agreement with the smectic layer spacing measured in the elastomer balloons [45] and on unoriented bulk elastomers (section 5.1). Fig. 5.21 shows small angle X-ray scattering (SAXS) data of the smectic elastomer film at zero deformation in the SmA phase. The intensity distribution for the non-stretched film has three peaks.

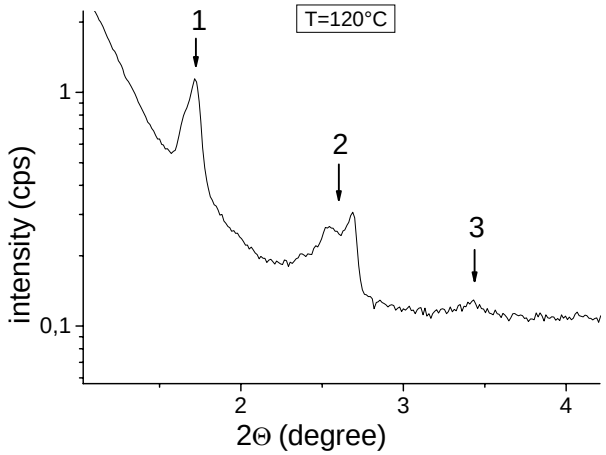

Figure 5.21: Small angle X-ray scattering (SAXS) measurement of the free standing smectic elastomer film at zero deformation in the SmA phase at T = 120°C.

Peaks labelled 1 and 3 correspond to the first and second order diffraction peaks of the bulk material, mainly located in the meniscus and on the metal frame (Fig. 5.20), and only in small part from the signal of the free standing film. The second peak may correspond to some internal structure of the smectic layers with a characteristic length less than the smectic layer thickness. It is not relevant for this experiment and will not be discussed further.

Films were stretched under the microscope, and the optical thickness profile as well as strains in x and y directions were determined. Then, samples were placed in the SAXS setup and the X-ray spectrum was recorded for the SmC* and SmA phase. After that, the same procedure was repeated for the next stretching step. In this way the set of optical reflectometry and X-ray measurements for different values of strain has been obtained. After the set of experiments, the drawing edges were approached again to the original positions, in order to verify the reversibility of

the deformations. The strain was not completely reversible, a small residual deformation of a few percent remained when the samples had been stretched by more than 50 %.

X-ray measurements on the stretched film reveal the appearance of a new scattering peak (1') between the first and second peaks (Fig. 5.22), this peak corresponds to the diffraction from the smectic layers in the thin film, at zero stretching this peak coincides with the peak from the bulk material.

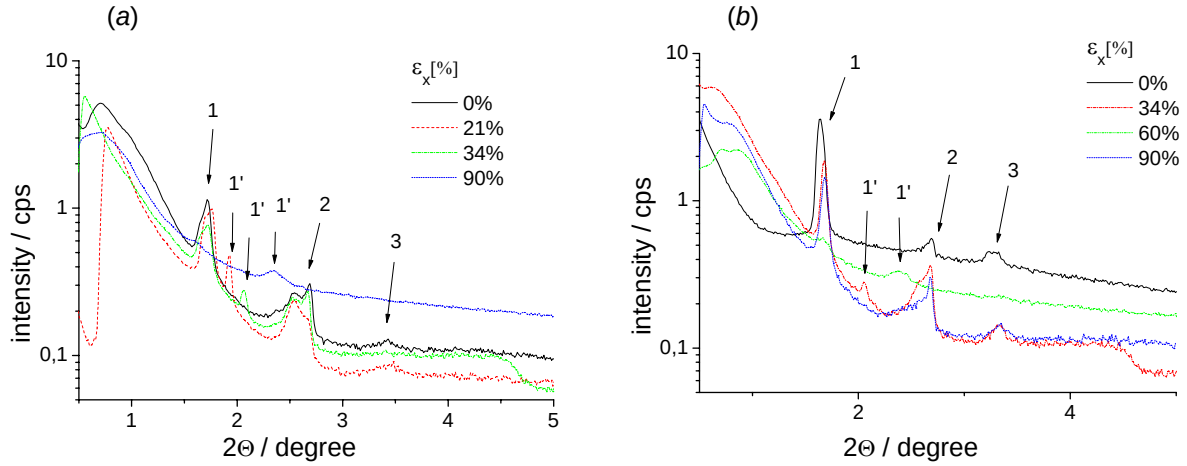

Figure 5.22: Small angle X-ray scattering (SAXS) measurement of the free standing smectic elastomer film at different values of deformation a) SmA phase at $T = 120°C$ and b) SmC* phase $T = 90°C$.

The positions of the peaks corresponding to the bulk material in the meniscus and on the frame (see fig. 5.20) do not change with the film deformation. In spite of random orientation of the material in the meniscus Bragg condition is fulfilled for some part of the material, and due to the large amount of bulk material, the intensity of the peak from undeformed material is even higher than from the oriented thin film. The position of the additional peak depends on the value of stretching strain ε_x. With increasing of the strain the position of this additional peak shifts to larger diffraction angles. This indicates that stretching of the film induces compression of the smectic layers. On one hand, it is better to measure the signal only from the oriented thin film without the scattering background from the unoriented material in the meniscus. But covering the meniscus with the mask we cover the part of the film and decrease already a very weak scattering signal from the film. It turned out to be more convenient to measure the X-ray scattering signal with a larger beam aperture and to ignore the bulk signal in the evaluation. Most experiments have been made without covering the meniscus and edges. Finally, it is convenient to have the original, constant layer peak as a reference at fixed position. In order to demonstrate that the small peak 1' is indeed the film peak, a couple of X-ray

reference measurements have been performed where the meniscus has been covered with a copper mask. The diffraction signal originates in that case only from the oriented material in the free standing film, and the bulk peaks disappear. This proves that the peaks labelled 1 and 3 in Fig. 5.22 correspond to diffraction from the meniscus or bulk material or from non-deformed strain free parts of the film close to the meniscus. In Fig. 5.22, one can also see that the intensities of peaks 1 and 3 reduce drastically with increasing elongation of the film, when the edges are moved more and more sidewards, out of the X-ray footprint.

From the position of the addition X-ray peak the thickness of the smectic layers in the thin film can be evaluated using Bragg's equation. Fig. 5.23 represents the smectic layer spacing *d* extracted from Bragg's equation as a function of deformation. Filled squares give the experimental results, and the solid line represents the calculated thickness change if we consider the film as incompressible isotropic material.

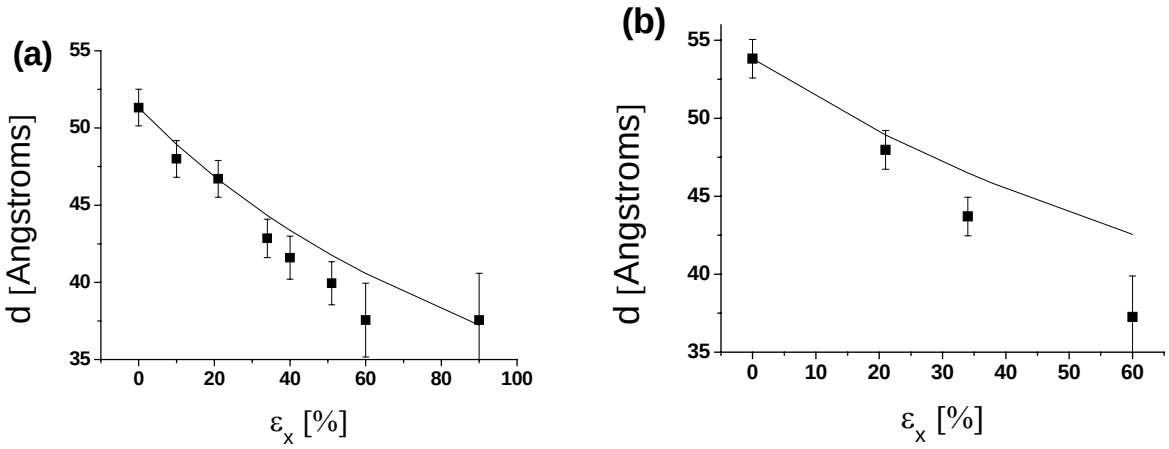

Figure 5.23: Dependence of the smectic layer spacing on strain, squares represent experimental values obtained from the small angle X-ray scattering measurements of the free standing smectic elastomer films (a) in the SmA phase at $T = 120°C$, (b) in the SmC* phase at $T = 90°C$; the solid line represents the relative thickness as a function of strain calculated for an isotropic material (Poisson ratio $\nu = 1/2$).

From the comparison of the optical reflectometry and X-ray measurements, it is obvious that the contraction of the film normal to the layer plane is indeed strongly correlated with the compression of the smectic layers by a lateral strain, and the film thickness change is proportional, in good approximation, to the molecular layer thickness change. This confirms one more time that the results of optical reflectometry measurements are precise and prove that the assumption concerning the constant refractive index is correct. Compression of the smectic layer one more time indicate that in the studied elastomer the anisotropy of elastic moduli parallel and perpendicular to the director is very low. The width of the 1' peak from the film increases with the increase of the strain,

while the integral intensity of this peak is conserved. This can be due to non-uniform compression of the film regions with different thickness or due to decreasing orientational order of the mesogens.

X-ray measurements unambiguously prove the compression of the smectic layers during the stretching of the free-standing elastomer film. They demonstrate that the smectic layers can be compressed reversibly by up to 30% by stretching the samples.

But on the molecular level this compression can be realized by different mechanisms. The compression of the film can be due to a strain induced tilt in the SmA phase and increasing of the tilt angle in the SmC* phase. But if the mesogenic tilt is induced by a lateral strain, then it can be expected that the tilt direction will be mainly oriented along the stretching direction and this will have to produce a strong birefringence of the film. This has not been found in optical observation with crossed polarizers. Because of the weak dependence of the smectic layer on tilt angle this mechanism is not effective at small angles and in this case threshold behaviour can be expected. But the X-ray measurements revealed almost a linear dependence of the layer thickness on deformation for small strain values. Both arguments are not valid if we deal not with conventional SmA phase but with a so-called de Vries smectic A phase (Fig. 5.24). In this case the tilt angle is already not zero in the undeformed film, but the direction of the tilt is random within the layers or between the neighbouring layers. Due to the random orientation the symmetry of the phase is uniaxial like in a conventional SmA phase. In smectic elastomers formed by such material, the tilt angle of the mesogenic units can easily adapt to the deformation of the LCE film.

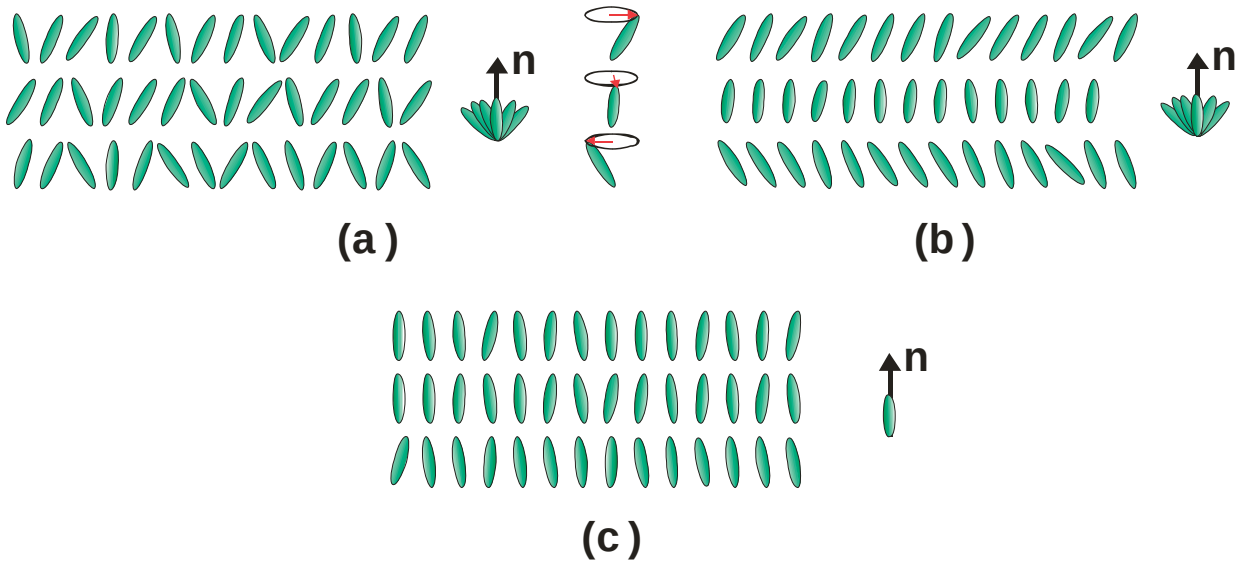

Figure 5.24: Different models for the molecular arrangement in the SmA phase. (a) The original de Vries model: molecules are randomly tilted in every layer. (b) Inside one layer molecules are tilted in one direction. But, there is no correlation of the tilt azimuth between the layers. (c) Ordinary SmA phase with non-tilted molecules.

The next possible mechanism is the decreasing of the orientational order of the mesogens. The thickness of the smectic layer is proportional to the average projection of the molecules long axis on the layer normal. If the deformation decreases the orientation order and the distribution function becomes broader in the stretched film, this will decrease smectic layer spacing. Broadening of the X-ray peak at large values of deformation can indicate that the orientational order decreases in the stretched film at least to some degree.

Alternatively, it is possible that during compression of the elastomers studied here, normal to the smectic layers, neighbouring layers interpenetrate mutually. Since the mesogen layers are separated by non-mesogenic, structureless siloxane layers, this may require much lower energy than in conventional low molecular mass smectics, and the layer compression modulus may therefore be comparably small.

On the basis of the X-ray measurements it cannot be distinguished which of these explanations is correct. Additional information concerning the changes of the mesogens orientation in the stretched film is required. One of the possible methods for the measurement of mesogens orientation is polarized Fourier transform infrared (FTIR) spectroscopy. The measurements of the influence of stretching of the film on the orientation of the mesogens by polarized FTIR spectroscopy are presented in the next chapter.

Chapter 6 Polarized FTIR spectroscopy measurements

The elastic properties of monodomain smectic elastomers are usually highly anisotropic [1, 12-14, 40, 83] and deformation of a smectic elastomer parallel to the smectic layer plane does not change the thickness of smectic layers and the dimension of the sample perpendicular to the smectic layers [1, 12-14, 40, 83].

As was all ready described in previous chapters, for the material studied in this work it has been found that the stretching of the free-standing films in the SmA phase parallel to smectic layers induces a compression of the film thickness [47], the measured Poisson's ratio ν is isotropic and close to ½ [42, 47]. The principal question about the molecular interpretation of this behaviour is unsolved so far.

Simultaneous optical reflectometry and small angle X-ray scattering measurements described in the section 5.2 have shown that during the stretching of thin films with layers parallel to the surface, the changes of the optical film thickness are consistent with the measured changes of the molecular layer spacing. The film thickness changes are in a good agreement with the smectic layer compression derived from the X-ray measurements, and with a Poisson ratio close to ½ [42]. Maximal value of the layer compression induced by a mechanical deformation is about 30% [42]. Such huge changes of the molecular lattice parameter have been observed for the first time.

Neither optical reflectometry nor small angle X-ray scattering gives information about molecular mechanisms of the layer compression. There are at least three possible scenarios of the smectic layers compression: the first one is the induction of the mesogens tilt, the second mechanism is the interpenetration of the neighbouring layers, and the third one is the reduction of the orientational order of the mesogens.

Polarized Fourier transform infrared (FTIR) spectroscopy is one of the most suitable methods for the measurement of the orientation of molecules. Using polarise FTIR spectroscopy the influence of external forces such as electromagnetic field [106-109] and mechanical strain [2, 110] on the orientation of the molecules in soft materials can be studied. The results of the FTIR measurement of the orientation of the mesogenic molecules in free-standing smectic elastomer films stretched parallel to the smectic layers are presented below.

6.1 Polarized FTIR spectroscopy measurements of the mesogens orientation in deformed elastomer film

Using FTIR spectroscopy (Section 2.4) deformation of the elastomer films with the same structure as the film described in the section 5.2 was studied. The preparation conditions are exactly the same as for the film used in the X-ray measurements. For the details of the free-standing smectic elastomer films preparation see section 2.5.

The obtained elastomer films are well oriented free-standing elastomer films attached to the support edges at two opposite sides (see for instance Fig. 5.15) [47]. As in free standing film of low molecular mass smectics [111-113], the smectic layers in smectic elastomer films are parallel to the film surface [42, 45]. The films have the dimensions of about 2 mm (width) and 3-4 mm (length), and the thickness of the films is approximately 1 μm. The film thickness is not uniform, and the number of layers varies in the film plane.

The films are uniaxially stretched in discrete steps and FTIR measurements were repeated after each step. The average in-plane strain is determined from the distance of the two fixed edges of the film. A typical FTIR spectrum of the studied elastomer is represented in Fig. 6.1. The assignment of the particular absorption lines to individual bond types in the molecule has been achieved using standard methods [99].

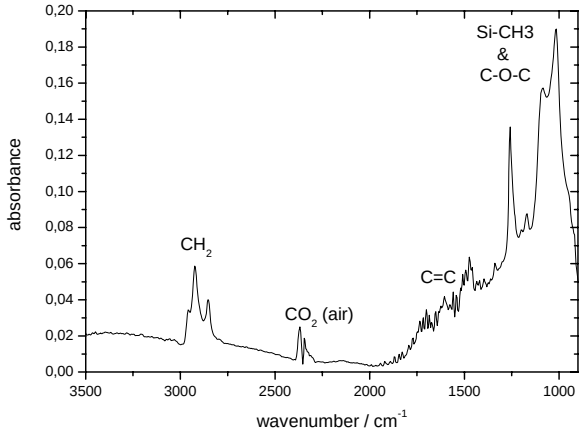

Figure 6.1: The infrared absorbance spectrum of a thin free-standing LCE film. The combinations of individual bond absorption peaks are indicated. The large background in the low wave number part is essentially contributed by water vapour in the path of the IR beam.

The dependence of the absorbance A_ν of the corresponding band ν upon the orientation of the polarizer Ω contains detailed information on the average orientation of the bond and the orientational order of molecular segments in the sample [99]. The absorbance A_ν is proportional to the scalar product $<(\boldsymbol{\varepsilon}\boldsymbol{\mu})^2>$ where **ε** is the polarisation vector of the IR beam, **μ** is the molecular transition dipole moment [2, 99, 106, 107, 114], and the brackets indicate averaging over all molecules in the measured region. The dependence of the absorption on the polarizer angle is given by Eq. 2.11 see section 2.7.

Parameters $A(\Omega_0)$ and $A(\Omega_0+90°)$ define the main axes of the (time-averaged) projection of the absorbance ellipsoid in the layer plane, Ω_0 describes the mean bond orientation in the film plane and Ω is the orientation of the polarizer [115, 116]. In order to obtain these parameters from the orientational dependence of absorbance, it has to be fitted by the Eq. 2.12 (section 2.7).

The absorption bands of the CC and CH_2 groups are well separated, so the heights of the absorption peaks corresponding to these bands can be precisely determined for the different values of the film deformation. The absorbances of the $SiCH_3$ and C-O-C bands overlap, for this reason they can not be used for the determination of the molecules orientation. Fig. 6.2 shows a polar plot of the measured orientational absorbance dependence for the CC and CH_2 bands for the different values of deformation.

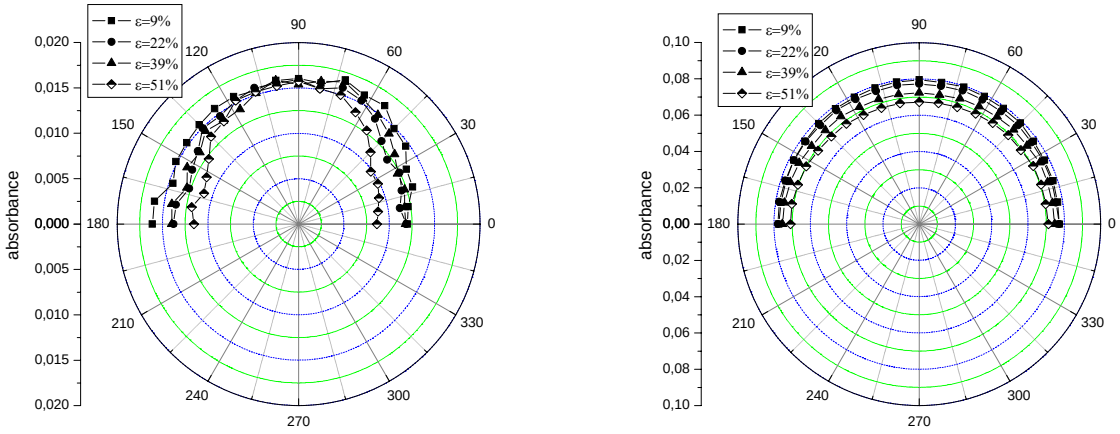

Figure 6.2: Polar plot of CC (a) and CH_2 (b) bonds absorption for the different values of deformation in SmC* phase, uncorrected raw data.

During the stretching of the film its thickness decreases and the volume of material in the measured spot becomes smaller, as well as the number of molecules giving contribution into the absorbance diminishes. This was taken into account and the absorbances were corrected with a

scaling factor proportional to the film thickness. However, this correction affects only the absolute absorption data, all absorbance values for the different polarizer orientation are multiplied by the same factor. This does not change their angular dependence containing the most important information for our measurements.

From the previous experimental result it is known that deformation behaviour of the elastomer under investigation is similar to the deformation of the isotropic rubber with Poisson's ratio $\nu = 1/2$ (see section 6.2). This means that strain values in y and z directions are equal $\lambda_y = \lambda_z$. From the volume conservation $(V/V_0 = 1 = \lambda_x \lambda_y \lambda_z)$ we get $\lambda_y = \lambda_z = 1/\sqrt{\lambda_x}$. The film thickness L_z of deformed film is related to the initial film thickness L_{z0} as follows $L_z = L_{z0}\lambda_z = L_{z0}\lambda_x^{-1/2}$. We multiply the measured absorbances of stretched films with the factor $\lambda_x^{-1/2}$, and refer to them in the following text as "corrected absorbances". Fig. 6.3 represents the corrected data for different deformations in SmA and SmC* phases.

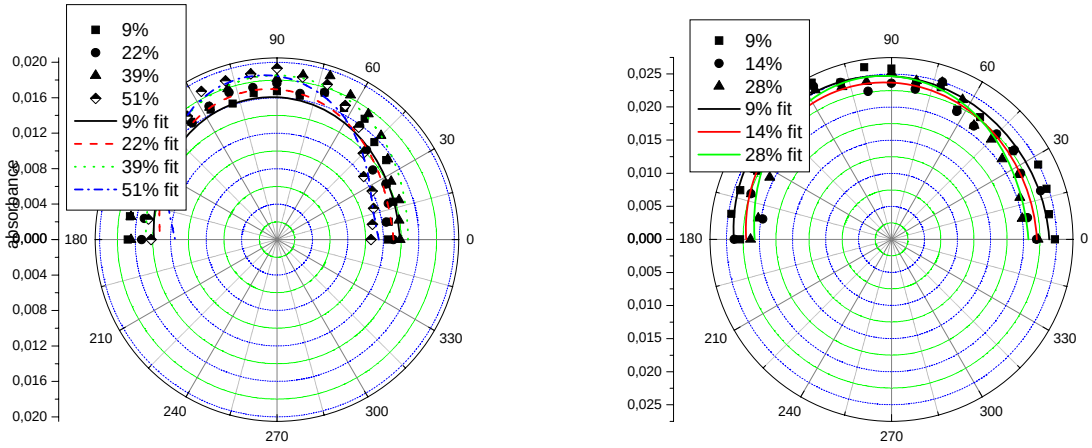

Figure 6.3: Polar plot of normalized absorbance for the CC bond in SmC* (a) and SmA (b) phases at different values of deformation, corrected with the film thickness changes in stretched films (see text). One fit curve (9% strain) is shown exemplarily.

Fitting the angular dependence of the absorbance with Eq. 2.12, we obtain the projections $A(\Omega_0)$ and $A(\Omega_0+90°)$ of the main axes of the absorbance ellipsoid. The direction of the IR beam propagation is perpendicular to the smectic layers, and the polarization vector lies in the smectic layer plane. In order to extract the orientation of the mesogens from the angular dependence of the absorbance, it is necessary to consider the orientation of the bonds in the mesogens. The maximum and minimum absorptions, $A_{\|}$ when the electric field of the IR beam is along the

maximum transition moment, and $A_\perp$ when the electric field is perpendicular to it, have been measured in earlier studies [99]. It is known from experimental observations that the absorption ellipsoid of the CC bond has its maximal value parallel to the long axis of the mesogenic units and its minimal value perpendicular to it; and its quantitative values are also available [99]. Because the average orientation of the mesogens in the smectic phase is perpendicular to the smectic layers, it is reasonable to suppose that the minimal value of absorption measured in the smectic plane, $A(\Omega_0+90°)$, approximately corresponds to the minimal value of the CC absorption ellipsoid $A_\perp$ .The value $A(\Omega_0)$, in accordance with Eq. 2.11, is a combination of the absorptions parallel and perpendicular to the mesogen long axis, with coefficients depending on the angle between the electric field of the IR beam and the average orientation of the long axes of the mesogen units. For the normal incidence, we obtain [99, 115, 116]

$$A(\Omega_0) = A_{\parallel} \sin^2(\phi_0) + A_\perp \cos^2(\phi_0) \tag{6.1}$$

with the unknown angle ϕ_0 between the layer normal and the time-averaged bond direction, the geometry is sketched in Fig. 6.4.

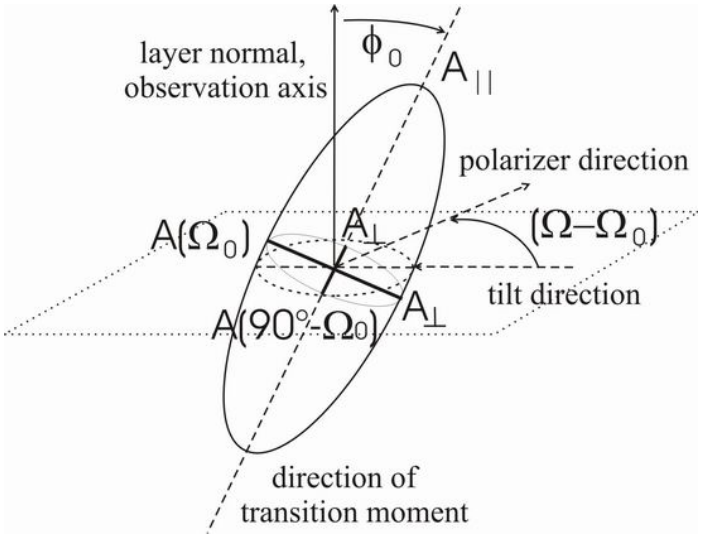

Figure 6.4: Absorbance ellipsoid and geometry in the polarized FTIR spectroscopy measurements on free standing films. The film plane is sketched by the dashed parallelogram.

The absolute values of both $A_{\parallel}$ and $A_\perp$ depend upon the amount of material in the measured spot, which can not be exactly determined in these measurements because of the inhomogeneity of the film thickness. But, their ratio $R = A_{\parallel} / A_\perp$ is known and can be used for the

calculation of the bond orientation. Because of the geometry of the measurement only the value of the absorption ellipsoid perpendicular to the long axis of molecule $A_\perp$ can be obtained from the experimental data.

At zero deformation average orientation of the mesogens in the SmA phase is normal to the layer, $\phi_0 = 0$. In order to estimate the value of the absorption ellipsoid parallel to the long axis of the mesogens, we employ the dichroic ratio $R_{CC} = A_\parallel / A_\perp = 5.4$ measured for CC bonds in similar materials [99]. From $A_\perp = A(\Omega_0+90°)$ and known R_{CC} it is possible to determine $A_\parallel$ for a given film, to substitute $A(\Omega_0)$, $A_\perp$ and $A_\parallel$ into Eq. 6.1 and to determine the angle ϕ_0 between the average long axis of the mesogen units and the smectic layer normal. This procedure is useful only for the CC bond absorption line. Since the dichroic ratio for the CH_2 bonds is close to one, we do not consider the CH_2 absorption line for the further analysis.

FTIR measurements have been performed in the SmA and SmC* phases. Fig. 6.3 shows the polar plots of the polarized FTIR spectroscopy data of the CC bond for different film deformations in the SmC* (Fig. 6.3a) and SmA (Fig. 6.3b) phases. The film is stepwise stretched in the FTIR set-up, and after every step of deformation angular dependence of the absorbance is recorded. The strain value was determined from the change of the distance between two edges of the frame to which the film is attached. This distance was measured optically from the photos of the film made after every stretching step. The stretching direction is close to the angle $\Omega = 90°$ on the polar diagrams in Fig. 6. The quantitative values of the absorbance in the SmC* and SmA phases (Fig 6a, b) can not be compared directly because this measurements were done on two films with different thicknesses.

It is obvious that the absorbance of the CC bond is almost independent of the polarizer orientation in both phases (modulations for different Ω is less than 20 %, $A(\Omega_0)/A(\Omega_0+90°) = 1.2$ but if the film compression is due to the induced tilt, then for $\varepsilon_x = 28$ % the ratio $A(\Omega_0)/A(\Omega_0+90°)$ has to be 1.96). In the SmC* phase, the absorbance in the film plane is only slightly anisotropic. But for the SmC* a much higher anisotropy is expected due to the strong tilt of the mesogens in the SmC* phase, approximately 30°, the ratio of the maximal and minimal absorbance values should be close to 2. The possible explanation is that the elastomer has a polydomain structure and the measurement area includes domains with different orientation of the **c** director. This would diminish the anisotropy to some average value which is much smaller than in the case of a monodomain. Alternatively, we can suppose that the elastomer crosslinked in the SmA phase reaches a smaller tilt angle when cooled into the SmC* phase.

In SmA, the almost circular graphs show that the stretching of the film up to almost 30 % does not change the absorbance spectra qualitatively. The shape of the angular dependence of the absorbance does not change, this means that the deformation does not induce tilt in the stretching direction. If the tilt angle of the mesogens would increase but with random orientation in the layer plane this would increase the absolute value of absorbance for all orientations of the polarizer. However, the experimental data indicate that the absolute value of the absorbance hardly changes.

In order to estimate the change of the tilt angle in the SmA and SmC* phases quantitatively, we fit the experimental data of Fig. 6.3 with Eq. 2.12 with the average absorption *a*, the modulation *b*, and the angle Ω_0 of the absorbance maximum chosen as fit parameters (see chapter 2).

From these parameters, we obtain the values $A(\Omega_0)$, $A(\Omega_0+90°)$ and Ω_0, which define the direction of the CC bond projected onto the smectic layer plane, and the mean mesogenic tilt θ. Fig. 6.5 exemplarily shows the fit for the SmC* phase at strain ε = 39%.

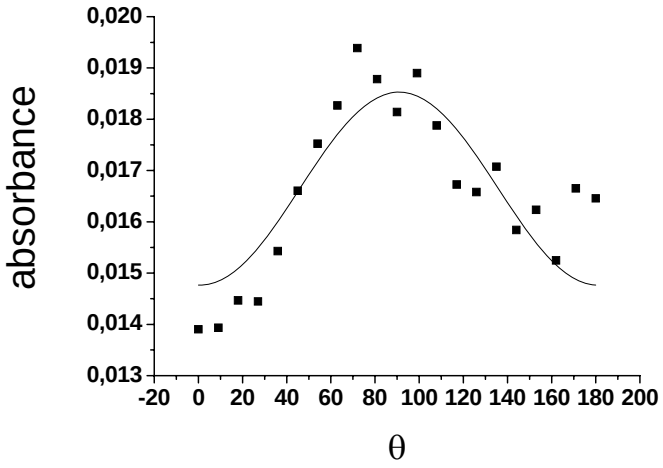

Figure 6.5: Fit of the experimental IR absorbance spectrum in the SmC* phase at a strain ε = 39 % with the function from equation (2), parameters a = 0.01665, b = 0.00188, Ω = 91°.

The ratio $A(\Omega_0)/A(\Omega_0+90°)$, characterising the anisotropy of the absorbance spectra and indicating changes of the mesogenic tilt, slightly increases with the increasing of deformation in both SmC* and SmA phases.

In order to obtain the tilt angle of the mesogens as a function of film strain we have to consider the geometry of the absorbance ellipse in the tilt plane (Fig. 6.4). The absorbance in this plane can be described by Eq. 6.1, using the experimentally obtained parameters $A(\Omega_0)$ and

A(Ω_0+90°) and the dichroic ratio for the CC bond given above [99] the angle ϕ_0 between layer normal and the long axis of the absorbance ellipsoid of the CC bond can be calculated. As was already pointed out above, the transition moment of the CC bond is along the mesogen long axis [99], therefore ϕ_0 is equivalent to the tilt angle θ of the mesogens. Fig. 6.6 shows the tilt angles as a function of deformation obtained from the FTIR spectra for the SmC* (■) and SmA (□) phases.

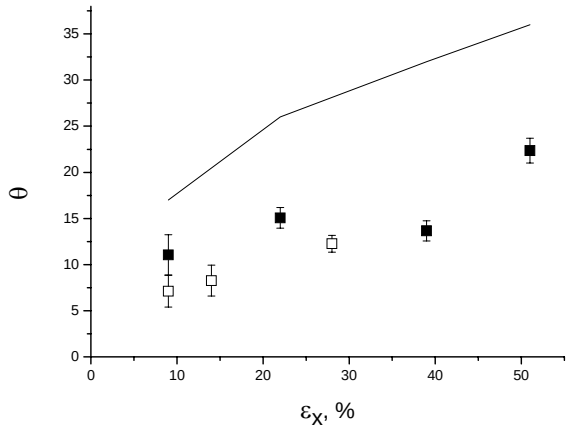

Figure 6.6: Tilt angle of the mesogens at different values of deformation in the SmC*(■) and SmA (□) phases, obtained from the polarized FTIR spectra [Eq. 6.1]. The solid line represents the mesogens tilt angle θ calculated on the assumption that the induced tilt is the only mechanism responsible for the compression of the film and that the film deforms like an isotropic material with Poisson's ratio $\nu = 1/2$ ($\theta = \arccos(\lambda_z) = \arccos(1/\sqrt{1+\varepsilon_x})$).

The graphs in Fig. 6.6 confirm that the stretching deformation induces tilt of the mesogens in the stretching direction, but the values of the tilt in the SmA and SmC* phases are too small to be the only mechanism responsible for the compression of the film and smectic layers.

This becomes even more obvious if we compare the strain ε_x that could be achieved with the measured tilt angles with the actual applied strain measured from the change of the film length. With the relation $\cos^2\theta = \lambda_z^2 = \frac{1}{\lambda_x} = \frac{1}{1+\varepsilon_{x,tilt}}$ valid for small strain, we calculate the (hypothetical) purely tilt induced strain $\varepsilon_{x,tilt} = \tan^2\theta$ that is shown in Fig 6.7. The symbols (■) and (□) represent the strain that corresponds to an assumed compression of the layers with $\cos\theta$

in the SmC* and SmA phases respectively, for comparison the straight line marks the actual strain ε_x.

Fig. 6.8 represents a comparison of the smectic layer compression induced by lateral stretching, as it has been obtained from X-ray measurements [42] with the hypothetical layer shrinkage related to the molecule tilt angle obtained from polarized FTIR spectroscopy. This figure gives the unambiguous evidence that strain induced tilt is too small to give the main contribution to the smectic layer compression.

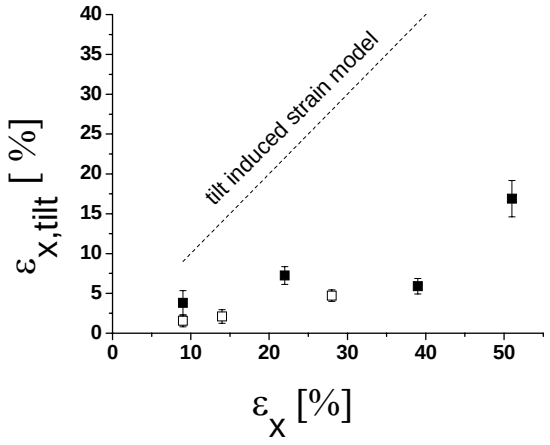

Figure 6.7: Comparison of the overall strain ε_x to the strain estimated from a pure tilt model for the SmC*(■) and SmA(□), $\varepsilon_{x,tilt} = \tan^2\theta$.

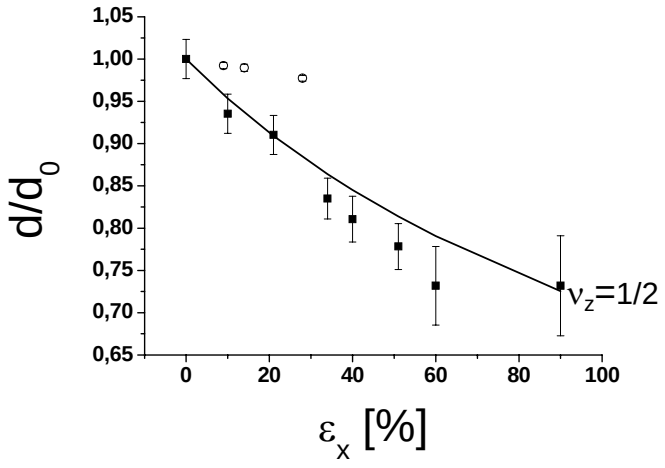

Figure 6.8: Comparison of the smectic layer compression d/d_0 obtained from X-ray (■) with data derived from the tilt angle measured by polarized FTIR spectroscopy (○) (d_0 – smectic layer thickness of the non-stretched film, d – smectic layers thickness after deformation). The solid line represents the layer thickness vs. strain characteristics calculated for an isotropic material (Poisson ratio $\nu = 1/2$).

It should be noted that this simplified model overestimates the effects of an induced mesogen tilt on the layer shrinkage, since of the total layer structure, only the mesogenic part shrinks with increasing θ, the mesogenic tilt will not directly influence the siloxane layer and the tilt of the spacer can also be different from the tilt angle of the mesogens. Thus, the actual effect of the measured tilt on the smectic layer thickness represents some upper estimate. The conclusion is that although there is a certain induced tilt towards the stretching axis, this tilt is by far not sufficient to explain the layer shrinkage found from the X-ray measurements and from the changes of the overall sample dimensions. Likewise, the rather uninfluenced absorption values indicate that the order parameter is not noticeably influenced by stretching the samples.

Several independent investigations have led to the conjecture that the material has already a tilt in the smectic A phase (de Vries type SmA) [117-119], with random azimuth. This assumption would be consistent with all FTIR data presented above, except that the minimum absorbance in SmA for normal incidence would not be equal to $A_{\perp,}$ but to an intermediate value $A = A_{\parallel} \sin^2(\theta) + A_{\perp} \cos^2(\theta)$.

Even if this assumption reflects the correct nature of the SmA structure in this class of elastomer materials, the conclusion remains valid that any additional strain induced tilt can only to a small part be responsible for the observed layer shrinkage. Otherwise the absorbance of the CC line would increase much more with increasing strain, in contrast to the data shown in Fig. 6.7 for the smectic A phase.

On a molecular level, we have to interpret this result in the following way: The main contribution to the sample deformation originates from shrinkage of the layers at almost unchanged molecular orientations. This implies that the mesogens in adjacent layers interpenetrate the intermediate spacer and siloxane layers.

Discussion and Conclusions

A smectic layer structure gives an additional contribution into the elastic energy of smectic elastomers and makes the elastic properties of the smectic elastomers highly anisotropic.

The deformation of a smectic elastomer parallel to the smectic layer plane is opposed by the elastic modulus of the same order as in a conventional isotropic rubber ($10^4 – 10^5$ N/m^2) [6, 12, 33]. The elastic modulus perpendicular to the smectic layers is expected to be of the same order as the smectic layer compression modulus (10^6 - 10^7 N/m^2) [6, 12, 33]. In this case the elastic modulus parallel to the layer normal (perpendicular to the smectic layers) $E_{\parallel}$ has to be much higher than the modulus $E_{\perp}$ perpendicular to the layer normal (parallel to the smectic layers). For such highly anisotropic smectic elastomers, it is expected that the deformation parallel to the smectic layers will not induce the compression of the elastomers perpendicular to the smectic layers. Indeed, such behaviour, a so-called in-plane fluidity, has been found for some smectic elastomers [1, 12-14, 40, 83]. While for other smectic elastomers optical observations have revealed the compression of the elastomers perpendicular to the smectic layers during the stretching parallel to the smectic layer plane [42-44, 47].

In this thesis the second type of smectic elastomers has been studied in more details by different experimental methods; such as optical reflectometry, X-ray diffraction and polarized FTIR spectroscopy. The results of these experimental investigations can help to understand what is the reason for the two different types of deformational behaviour, why the elastomers studied by Finkelmann and coworkers [1, 12-14, 40, 83] show the in-plane fluidity behaviour, but in the case of the free-standing elastomer films studied in this thesis the dimensions of the film perpendicular to the smectic layer decrease during the stretching parallel to the smectic layers [42-44, 47].

The main characteristic defining the deformational behaviour of smectic elastomers is the anisotropy of elastic properties parallel and perpendicular to the director [13]. Already for the elastomer with the low anisotropy of elastic moduli ($E_{\parallel} / E_{\perp} = 4$) [14, 20] deformation perpendicular to the smectic director does not cause compression of the film parallel to the director only at deformations smaller than 20%. Larger deformations induce a small compression of the sample perpendicular to the smectic layers [20].

Therefore, we can suppose that the anisotropy of the elastic moduli of the elastomers studied here is even smaller and it is not sufficient to prevent compression of the smectic layers.

And indeed, the values of elastic moduli parallel and perpendicular to the director measured in the experiment with free-standing elastomer balloons and free-standing elastomer film (see section 3) indicate that the elastic moduli perpendicular to the smectic layer and in the layer plane have close values. However, the results of these two methods are not precise enough to give the exact ratio between the elastic moduli parallel and perpendicular to the director. The main source of experimental errors in these measurements is the inhomogeneous thickness of the elastomer balloons and free-standing elastomer films. From the obtained experimental values of the elastic moduli we can suppose that the ratio of the moduli parallel and perpendicular to the director has to be smaller than two or even can be close to one. Because of the low anisotropic of elastic moduli, the compression of elastomer films perpendicular to the smectic layers no longer penalize by much higher elastic modulus than the deformation in the layer plane and it is energetically more favourable if a stretching deformation is compensated by the shrinking of the film perpendicular to the smectic layers as well as in the smectic layer plane.

In order to be sure that elastic moduli perpendicular to the film surface are defined by the smectic layer compression modulus we have to know whether compression of the film found by the optical reflectometry measurements is realized by compression of the smectic layers or not. Because some mechanisms of deformation can realize the compression of the film without the compression of the smectic layers.

Compression of the smectic LCEs during deformation parallel to the smectic layers can be explained by one of the following mechanisms. Some of these mechanisms include the compression of the smectic layers and some do not.

(a) Compression of the film can take place without compression of the smectic layers if some of the layers of the film break down and the number of the layers decreases during deformation. In this case it is highly probable that large deformation will be irreversible in this case, but optical reflectometry proves that even after quite a large deformation, up to 80-90%, the changes of the film length and thickness are reversible. If the film is shrunk back, its thickness takes its initial value and only a very small irreversible change of the film length takes place, not more than 2-4%. Moreover the stretching process can be repeated many times and the film does not break down if the strain value is smaller than some critical value. The X-ray measurements provide the direct evidence of the layers compression during deformation (see section 5.2), therefore this mechanism can be excluded as an explanation for the deformational behaviour of the smectic LCE films studied in our experiments.

(b) The thickness of the smectic layers is proportional to the average projection of the mesogens on layer normal, hence the change of the mesogen tilt can change the layers thickness,

and vice versa. Therefore, the induced tilt of the mesogen is one of the possible explanations for the compression of the smectic layers. In the first approximation the model of an ideal smectic A phase can be taken for the calculation of the induced mesogens tilt. In the ideal smectic A phase all mesogens are parallel to the director and the equilibrium smectic layer thickness d_0 is equal to the length of mesogens. In this case the thickness of the layer for the tilted mesogen is $d = d_0\cos\theta$ where θ is the tilt angle. In order to reach compression of the smectic layers on 1/3, measured in the X-ray measurements (see section 5.2), the tilt angle has to be almost 50°. The direction of the induced tilt has to be parallel to the stretching axis, therefore the projection of the long axes of the mesogens on the stretching direction has to be much larger than perpendicular to it. In this case the optical axis has to deviate from the layer normal and will be tilted with respect to the layer normal. However, the homogeneous tilt in one direction induces a macroscopic share deformation that will be incompatible with the border condition for the film fixed at two edges. In order to satisfy the border condition with zero macroscopic shear, a stripe domain structure can be accommodated, similar to the stripe domain structure in nematic elastomer [26, 31], but with alternating stripes parallel to the surface of the film. In both cases, stretching deformation has to induce a strong birefringence. The optical observation with crossed polarizers has revealed only a small birefringence in the stretched films. Large induced tilt angle was not found by the polarized FTIR measurement. Although these measurements have found the induced tilt but its value is too small to be responsible for the observed large compression of the smectic layers.

(c) In real smectic phases molecules are slightly tilted with respect to the director, but the projection of the long axis of the molecules on the smectic layer plane is random and the symmetry of the phase is uniaxial. In some smectic A material the tilt angle can reach almost the same value as in conventional smectic C phase, but the projections of the molecules on the smectic layer plane are distributed randomly and this phase remains uniaxial. De Vries was the first who propose the existence of such materials; therefore uniaxial smectic phase with the large tilt of mesogens has been called the de Vries smectic A phase. Some experimental observations are in favour of this model for the diluted elastomers studied here [48]. It is well known that parts of polymer molecules with different chemical structure can be non-mixable and that causes a microphase separation. Due to the microphase separation, smectic layers consisting of mesogenic units are separated by siloxane layer and the tilt between the adjacent smectic layers is not strongly correlated. The direction of the tilt may be randomly distributed for the different layers, macroscopically the average orientation of the mesogens is parallel to the layer normal and optically the phase has a uniaxial symmetry like in the case of a conventional smectic A phase. In such material the compression of the smectic layers just changes the tilt angle. Because

the tilt angle in initial state is not zero, the change of the tilt angle without threshold strain can be expected. However, due to the elongation of the film in the stretching direction and compression perpendicular to it, the preferential alignment of the tilt direction parallel to the stretching axis can be expected, therefore the optical properties in this case also have to change as in case of induced tilt in a conventional smectic phases. The film will become birefringent in the stretched state; however, this has not been found by the optical observation and the results of the polarized FTIR spectroscopy measurements (see section 6) provide evidence against this model [44].

(d) Another possibility for the layer compression is the decreasing of the orientation order parameter, in this case the average projection of the mesogen on the layer normal becomes smaller and as a consequence the thickness of the layer will decrease. Also, for some LCEs experimental investigation revealed that the stretching parallel to the director can induce the break down of smectic layers and drastic decreasing of the orientational order parameter [13, 40]. We suppose that it is not true for the elastomers that have been studied here. In case of a break down of the smectic layers, the X-ray measurements reveal a drastic decreasing of the intensity of small angle smectic reflections [14, 40]. Although the intensity of the smectic layer reflex decreases for the stretched free-standing smectic elastomer film it still can be observed at a very large deformation (see section 5.2). The decreasing of the orientation order parameter has to increase the average projection of the mesogens long axes on the smectic layer plane; and that can be observed by polarized FTIR spectrometry measurements, but that was not confirmed experimentally (section 6.1).

On the basis of the polarized FTIR spectrometry and X-ray measurements, the decreasing of the orientational order can not be considered as a main process responsible for the layer compression; also some decreasing of the orientational order at large deformation takes place.

(f) Finally, there is a possibility that the mesogenic units interpenetrate into the adjacent smectic layer. In ordinary smectic LCEs such process is energetically unfavourable because of the large layer compression moduli of the order 10^7 N/m^2. However, this model is the only one that explains all observations satisfactory.

So we come to the conclusion that the compression of the film corresponds to compression of the smectic layers. This makes the interpretation of the elastic moduli measurement unambiguous, elastic moduli perpendicular to the film surface, which have been measured in the experiments with elastomer balloons, have to include contribution from the smectic layer compression moduli. The elastic moduli perpendicular to the smectic layers measured in the SmA is approximately $E_{\parallel} \approx 2 \times 10^6$ N/m^2.

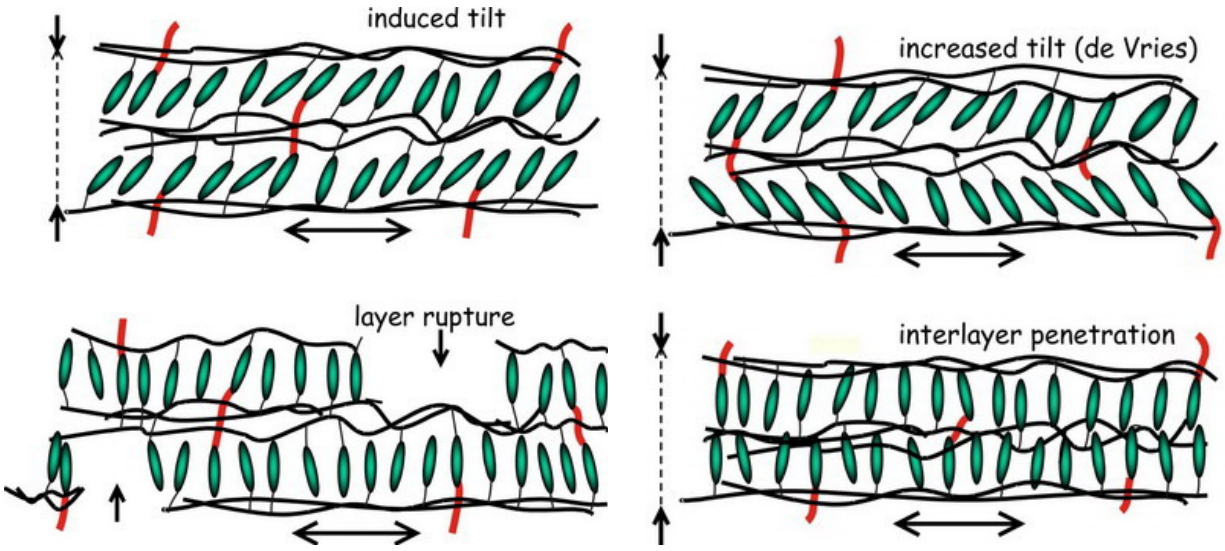

Figure 7.1: Schematic representation of molecular mechanism which can be responsible for the compression of the smectic film perpendicular to the smectic layer during the stretching deformation parallel to the layer plane [43].

This value is larger than the elastic moduli of an isotropic rubber, but smaller than the moduli usually measured for the smectic elastomers parallel to director (10^7 N/m^2). But for some highly anisotropic smectic elastomers, which show in-plane fluidity behaviour, elastic moduli parallel to the director close to this value have been measured (3.2×10^6 N/m^2) [83]. This indicates one more time that the reason for the compression of the film perpendicular to the smectic layers is not the low modulus parallel to the director, but the low anisotropy of elastic moduli. Elastic moduli measured parallel to the smectic layers in the SmA phase are approximately 2×10^6 N/m^2, but this value can be overestimated and the real value can be smaller (see for details section 3.2). This value is larger than the elastic moduli of an isotropic rubber (10^5 N/m^2), but that is not an unusual situation, as for some elastomers, the elastic moduli parallel to the smectic layers that are ten times larger than in isotropic phase of the same material have been measured [14]. The increasing of the modulus parallel to the smectic layer in this material has been attributed to in-plane defects [14]. If the smectic layers are distorted or contains defects, then the elastic modulus parallel to the director $E_{\parallel}$ will give some contribution in to the elastic modulus perpendicular to the director $E_{\perp}$ [13].

It is well know that the elastomer network obtained by a crosslinking in the smectic LC polymer suppress the layer-displacement fluctuations and stabilizes the smectic structure [104]. But at the same time, crosslinkers introduce defects into the smectic layer structure and at high

concentration the disorder caused by defects prevails over the stabilizing effect and correlation between smectic layers diminishes [102, 104, 120].

Summarizing all these facts we can make a conclusion that in the investigated elastomer crosslinking density is high enough to produce a high consternation of defects which diminishes the correlation of the smectic layers and "softens" smectic layers, decreasing the elastic moduli parallel to the director [13, 14]. The same defects can increase the elastic moduli parallel to the smectic layers. As a result, the elastomers studied here have a very low anisotropy of the elastic moduli and as a consequence, the free-standing smectic elastomer films compensate stretching deformation not only by a shrinking in the smectic layer plane but also by compression perpendicular to the smectic layers.

An additional prove that the low anisotropy of elastic moduli and the compression of the smectic layers is caused by the defects in the smectic layers induced by crosslinkers have been found during the study of the influence of the crosslinking time on the deformational behaviour of free-standing elastomer films. The compression of the films during the stretching parallel to the smectic layers, for the films with different crosslinking times, was studied by an optical reflectometry. These measurements have revealed that elastomer with a very short crosslinking time demonstrate a deformational behaviour similar to the deformational behaviour of the elastomers with a low anisotropy of elastic moduli ($E_{\parallel} / E_{\perp} = 4$) described by Komp et al.[14, 20]. During the stretching of the films with short crosslinking time parallel to the smectic layer, its dimension perpendicular to the smectic layers does not change at small deformations ($\varepsilon_x \le 15 \div 20\%$) Poisson's ratio ν_z is equal to zero or changes of the film thickness are smaller than for the isotropic material with Poisson's ratio $\nu_z = 1/2$. It seems that these films are the missing link between the two types of elastomer studied by Finkelmann et al. [1, 12-14, 40, 83] and Stannarius et al.[42-46]. It is not clear how densely these elastomers are crosslinked, but crosslinking density is high enough for the transformation of the polymer films into elastomers; deformations up to 40-50% are almost completely reversible.

It has to be mentioned that in the inhomogeneous elastomer films the deformation with Poisson's ratio $\nu_z = 1$ or close to one was found only for the thick regions of the film, while for the thin film regions compression is stronger and the thinner the film region the closer the deformation curve to the deformation curve of the isotropic material with Poisson's ratio $\nu = 1/2$. If the same film is crosslinked one more time the measured dependence of the film compression becomes close to the compression of isotropic material. If the total crosslinking

time is long enough, than the film demonstrate the deformational behaviour of the isotropic material with Poisson's ratio $\nu = 1/2$.

The density of crosslinker in the elastomers studied here is approximately the same as in the elastomer studied by Finkelmann et al. [1, 12-14, 40, 83], it is between 5 and 10%. But, in the elastomers studied by Finkelmann et al. [1, 12-14, 40, 83], crosslinking leads to highly anisotropic elastomers, while for the elastomer studied here only in the lightly crosslinked films mechanical properties are anisotropic. Complete crosslinking softens smectic layers and diminishes the anisotropy of elastic properties to such degree that elastomers become almost an isotropic rubber.

Even though a microscopic characterization of the network structure in the materials investigated is not available, we may speculate about the microscopic origin of the differences between the materials investigated in [12-14, 40] and those studied in this thesis [42-47].

It is a well-know fact that crosslinkers form a network which stabilizes the smectic structure against layer-displacement fluctuation, but they also induce defects into the smectic structure which diminish smectic order [104]. Theoretical models predict that introduction of defects into the smectic phase can soften smectic phase and drastically decrease smectic layer compression moduli [121, 122].

In the elastomers studied by Finkelmann and co-workers, the crosslinker distribution can be inhomogeneous because of the preparation technique [40, 80, 83]. An as a result some regions with the low concentration of crosslinkers and hence with the low concentration of defects have intact smectic layer structure with high layer compression moduli.

In the case of the materials studied here, the distribution of the crosslinkers is expected to be more uniform and in this case defects in the layer structure are more homogeneously distributed and suppress the smectic order in the whole volume of the material. This decreases the smectic layer compression moduli and probably increases elastic moduli parallel to the smectic layers. Because in smectic elastomers with the high concentration of in-plane defects the elastic modulus parallel to the layer normal $E_{\parallel}$ gives some contribution in to the elastic modulus parallel to the smectic layers plane $E_{\perp}$ [13, 14].

In order to prove these ideas the deliberate manipulation of the crosslinkers distribution is necessary, that is technically very difficult to realize and has not been achieved yet.

The experimental results of this thesis can be summarized as the follows:

- Elastic moduli of the smectic elastomer perpendicular to the smectic layers have been measured in experiments with free-standing elastomer balloons (chapter 3).

- Elastic moduli parallel to the smectic layer have been measured by uniaxial stretching of free-standing elastomer films. The elastic moduli parallel and perpendicular to the smectic layer have close values. The experimental values obtained by these two methods are not very precise because of inhomogeneity of the thickness of free-standing films and elastomer balloons (chapter 3).

- Using optical reflectometry the compression of the free-standing smectic elastomer films during the stretching parallel to the smectic layers have been studied (chapter 4). These measurements have been done for the elastomer films prepared from LC a homopolymer and copolymers with different densities of crosslinking groups (see chapter 2). Also the influents of the time of crosslinking on deformational behaviour have been studied. These experiments have revealed that, elastomers crosslinking for quite a long time, demonstrate behaviour similar to isotropic rubber with Poisson's ratio $\nu = 1/2$. While elastomers with a short crosslinking time demonstrate the in-plane fluidity behaviour (there is no compression of the film perpendicular to the smectic layers) with Poisson's ratio $\nu_z = 1$ for small deformations. These experimental observations indicate that, not only the chemical structure of the precursor LCP defines the properties of the obtained elastomer, but also preparation conditions play an important role.

- Simultaneous optical reflectometry and small angle X-ray scattering measurements described in the section 5.2 have shown that during stretching of free-standing smectic elastomer films with layers parallel to the surface, the changes of the optical thickness are consistent with the measured changes of the molecular layer spacing. The compression of the film thickness is in a good agreement with the smectic layer compression derived from X-ray measurements, and with a compression of isotropic material with Poisson ratio close to ½. The maximal value of the layer compression induced by a mechanical deformation is about 30% [42].

- The result of FRIR spectroscopy measurements have proved that the main mechanism of the smectic layer compression during the deformation parallel to the smectic layers is the interpenetration of the neighbouring layers (chapter 6) [44]. Experimental results show

that stretching also induces a small tilt of the mesogens, but the value of the tilt angle is too small to be the main mechanism responsible for the compression of the smectic layers.

Bibliography

1. I. Kundler, E. Nishikawa, and H. Finkelmann, Macromol. Symp., 1997. **117**: p. 11.
2. J. Li, M. Tammer, F. Kremer, A. Komp, and H. Finkelmann, Eur. Phys. J. E, 2005. **17**(423).
3. H. Finkelmann, A. Greve, and M. Warner, Eur. Phys. J. E, 2001. **5**: p. 281-293.
4. W. Gleim and H. Finkelmann, in *Side Chain Liquid Crystalline Polymers*, C.B. McArdle, Editor. 1989, Blackie and Son: Glasgow.
5. H. Finkelmann, in *Liquid Crystallinity in Polymers*, A. Ciferri, Editor. 1991, VCH: Weinheim.
6. E. Nishikawa, *Smektische Einkristall-Elastomere*. 1997, Albert-Ludwigs-Universität Freiburg in Breisgau: Freiburg. p. 113.
7. R. Köhler, R. Stannarius, C. Tolksdorf, and R. Zentel, Appl. Phys. A, 2005. **80**: p. 381.
8. W. Lehmann, H. Skupin, C. Tolksdorf, E. Gebhard, R. Zentel, P. Kruger, M. Losche, and F. Kremer, Nature, 2001. **410**: p. 447.
9. C. M. Spillmann, B. R. Ratna, and J. Naciri, Appl. Phys. Lett., 2007. **90**: p. 021911.
10. H. Finkelmann, E. Nishikawa, G. G. Pereira, and M. Warner, Phys. Rev. Lett., 2001. **87**: p. 015501.
11. P. M. Hogan, A. R. Tajbakhsh, and E.M. Terentjev, Phys. Rev. E, 2002. **65**: p. 041720.
12. E. Nishikawa, H. Finkelmann, and H.R. Brand, Macromol.Rapid Commun., 1997. **18**: p. 65.
13. D. Kramer and H. Finkelmann, Macromol. Rapid Commun., 2007. **28**: p. 2318-2324.
14. A. Komp and H. Finkelmann, Macromol. Rapid Commun., 2007. **28**: p. 55-62.
15. P. D. Olmsted, J. Phys. II France, 1994. **4**: p. 2215-2230.
16. M. Warner, P. Bladon, and E.M. Terentjev, J. Phys. II France, 1994. **4**: p. 93-102.
17. J. Küpfer and H. Finkelmann, Macromol. Chem. Phys., 1994. **195**: p. 1353-1367.
18. L. Golubovic and T.C. Lubensky, Phys. Rev. Lett., 1989. **63**(10): p. 1082-1085.
19. M. Warner, Journal of the Mechanics and Physics of Solids, 1999. **47**(6): p. 1355-1377.

20. A. Komp, *Smektische Elastomere mit perfluorierten Mesogenen*. 2006, Albert-Ludwigs-Universität: Freiburg. p. 147.
21. W. Meier and H. Finkelmann, Condensed Matter News, 1992. **1**(7): p. 15-19.
22. P. G. de Gennes, M. Hébert, and R. Kant, Macromol. Symp., 1997. **113**: p. 39.
23. M. Hébert, R. Kant, and P.G.d. Gennes, J. Phys. I, 1997. **7**: p. 909.
24. H. Wermter and H. Finkelmann, e-polymers, 2001. **13**.
25. J. Küpfer, E. Nishikawa, and H. Finkelmann, Polymers for Advanced Technologies, 1994. **5**: p. 110 115.
26. I. Kundler and H. Finkelmann, Macromol. Chem. Phys., 1998. **199**: p. 677-686.
27. S. Disch, C. Schmidt, and H. Finkelmann, Macromol. Rapid Commun., 1994. **15**: p. 303.
28. J. F. D'Allest, P. Maissa, A. ten Bosch, P. Sixou, A. Blumstein, R. Blumstein, J. Teixeira, and L. Noires, Phys. Rev. Lett., 1988. **61**: p. 2562.
29. W. Gleim and H. Finkelmann, Macromol. Chem., 1987. **188**: p. 1489-1500.
30. *Handbook of liquid crystals.*, ed. J.G. D. Demus, G. W. Gray, H.-W. Spieß and V. Vill. Vol. 3 High Molecular Weight Liquid Crystals. 1998, Weinheim: Wiley-VCH Verlag GmbH.
31. G. C. Verwey, M. Warner, and E.M. Terentjev, J. Phys. II, 1996. **6**: p. 1273.
32. Terentjev, E.M., J. Phys.: Cond. Mat., 1999. **11**: p. R239.
33. M. Warner and E.M. Terentjev, *Liquid crystal elastomers*. International series of monographs on physics. 2003, Oxford: Clarendon press.
34. E. M. Terentjev, M. Warner, and G.C. Verwey, J. Phys. II France, 1996. **6**: p. 1049-1060.
35. J. M. Adams and M. Warner, Phys. Rev. E, 2005. **72**: p. 011703.
36. J. M. Adams and M. Warner, Phys. Rev. E, 2005. **71**: p. 021708.
37. J. M. Adams, M. Warner, O. Stenull, and T.C. Lubensky, Phys. Rev. E, 2008. **78**: p. 011703.
38. O. Stenull, T. C. Lubensky, J. M. Adams, and M. Warner, Phys. Rev. E, 2008. **78**: p. 021705.

39. E. M. Terentjev and M. Warner, J. Phys. II France, 1994. **4**: p. 849-864.

40. E. Nishikawa and H. Finkelmann, Macromol. Chem. Phys., 1999. **200**: p. 312.

41. W. Ren, P. J. McMullan, and A.C. Griffin, Macromol. Chem. Phys., 2008. **209**: p. 1896-1899.

42. V. Aksenov, J. Bläsing, R. Stannarius, M. Rössle, and R. Zentel, Liq. Cryst., 2005. **32**(7): p. 805.

43. R. Stannarius, V. Aksenov, J. Bläsing, A. Krost, M. Rössle, and R. Zentel, Phys. Chem. Chem. Phys., 2006. **8**: p. 2293-2298.

44. V. Aksenov, R. Stannarius, M. Tammer, P. Kölsch, F. Kremer, M. Rössle, and R. Zentel, Liq. Cryst., 2007. **34**(1): p. 87-94.

45. R. Stannarius, R. Köhler, U. Dietrich, M. Lösche, C. Tolksdorf, and R. Zentel, Phys. Rev. E, 2002. **65**: p. 041707.

46. H. Schüring, R. Stannarius, C. Tolksdorf, and R. Zentel, Macromolecules, 2001. **34**: p. 3962.

47. R. Stannarius, R. Köhler, M. Rössle, and R. Zentel, Liq. Cryst., 2004. **31**: p. 895.

48. M. Rössle, L. Braun, D. Schollmeyer, R. Zentel, J.P.F. Lagerwall, F. Giesselmann, and R. Stannarius, Liq. Cryst., 2005. **32**: p. 533.

49. P. G. de Gennes and J. Prost, *The physics of liquid crystals*. 2nd ed. International series of monographs on physics. 1993, Oxford: Clarendon press.

50. S. Chandrasekhar, *Liquid Crystals*. 2nd ed. 1992, Cambridge: Cambridge University Press.

51. F. Reinitzer, Monatsheft der Chemie, 1888. **9**: p. 421.

52. Timothy J. Sluckin, David A. Dunmur, and H. Stegemeyer, *Crystals That Flow: Classic Papers from the History of Liquid Crystals.* 2004, London and New York: Taylor and Francis. 512.

53. O. Lehmann, Zeitschrift für Physikalische Chemie, 1889. **4**: p. 462-472.

54. D. Vorländer, Berichte der Deutschen Chemischen Gesellschaft, 1906. **39**: p. 803-810.

55. D. Vorländer, Berichte der Deutschen Chemischen Gesellschaft, 1907. **40**: p. 1970-1972.

56. A M. Figueiredo Neto and S.R.A. Salinas, *The physics of lyotropic liquid crystals. Phase transitions and structural properties.* 2005, New York: Oxford University Press.

57. P. M. Chaikin and T.C. Lubensky, *Principles of condensed matter physics*. 1995, Cambridge: Cmabridge University Press.

58. L. D. Landau and E.M. Lifshitz, *Statistical Physics, Part I*. 3 ed. Vol. 5. 1980, Oxford: Pergamon Press.

59. P. S. Pershan, *Structure of liquid crystal phases*. World Scientific Lecture Notes in Physics. Vol. 23. 1988, Singapore: World Scientific.

60. Jan P. F. Lagerwall and F. Giesselmann, ChemPhysChem, 2006. **7**(1): p. 20-45.

61. C. Robinson, Trans. Faraday. Soc., 1956. **52**: p. 571-592.

62. HR. Dicke and R. W. Lenz, Journal of Polymer Science: Polymer Chemistry Edition, 1983. **21**(8): p. 2581-2588.

63. W. J. Jackson, Jr. Kuhfuss, and H.F. Kuhfuss, Journal of Polymer Science: Polymer Chemistry Edition, 1976. **14**: p. 2043-2058.

64. D. Sek, Acta Polymerica, 1988. **39**(1988): p. 599.

65. V. P. Shibaev, Fibre Chemistry, 1988. **19**(3): p. 157-170.

66. N. A. Plate and V.P. Shibaev, Macromol. Chem., Suppl., 1984. **6**: p. 3-26.

67. A. Roviello and A. Sirigu, Journal of Polymer Science: Polymer Letters Edition, 1975. **13**: p. 455-463.

68. A. Blumstein, K. N. Sivaramakrishnan, S. B. Clough, and R.B. Blumstein, Mol. Cryst. Liq. Cryst., 1979. **49**: p. 255-258.

69. H. Finkelmann, H. Ringsdorf, and J.H. Wendorff, Makromol. Chem., 1978. **179**: p. 273-276.

70. H. Finkelmann, H. Ringsdorf, W. Siol, and J.H. Wendorff, Makromol. Chem., 1978. **179**: p. 829-832.

71. V. P. Shibaev, N. A. Plate, and Y.S. Freidzon, Journal of Polymer Science: Polymer Chemistry Edition, 1979. **17**: p. 1655-1670.

72. V. P. Shibaev, R. V. Talroze, F. I. Karakhanova, and N.A. Plate, Journal of Polymer Science: Polymer Chemistry Edition, 1979. **17**: p. 1671-1684.

73. B. Reck and H. Ringsdorf, Macromol. Chem., Rapid Commun., 1985. **6**: p. 291-299.

74. W. Kreuder and H. Ringsdorf, Makromol. Chem., Rapid Commun., 1983. **4**: p. 807 - 815.

75. *Liquid crystals*. Topics in physical chemistry, ed. H. Baumgärtel, E. U. Franck, and W. Grünbein. Vol. 3. 1994, Darmstadt: Steinkopff Verlag GmbH & Co. KG.

76. M. V. Piskunov, S. G. Kostromin, L. B. Stroganov, V. P. Shibaev, and N.A. Plate, Macromol. Chem. Rapid Commun., 1982. **3**: p. 443-447.

77. H. Finkelmann, D. Naegele, and H. Ringsdorf, Macromol. Chem., 1978. **180**: p. 803-806.

78. R. Zentel and G.R. Strobl, Macromol. Chem., 1984. **185**: p. 2669-2676.

79. R. Zentel and M. Benalia, Macromol. Chem., 1987. **188**: p. 665-674.

80. E. Nishikawa and H. Finkelmann, Macromol. Chem. Phys., 1997. **198**: p. 2531-2549.

81. H. Finkelmann, H. J. Kock, W. Gleim, and G. Rehage, Macromol. Chem., Rapid Commun., 1984. **5**: p. 287-293.

82. J. Küpfer and H. Finkelmann, Macromol. Chem., Rapid Commun., 1991. **12**: p. 717-726.

83. N. Aßfalg and H. Finkelmann, Macromol. Chem. Phys., 2001. **202**(6): p. 794-800.

84. K. Semmler and H. Finkelmann, Polymer for Advanced Technologies, 1994. **5**: p. 231-235.

85. K. Semmler and H. Finkelmann, Macromol.Chem.Phys., 1995. **196**: p. 3197.

86. K. Hiraoka and H. Finkelmann, Macromol. Rapid Commun., 2001. **22**: p. 456-460.

87. E. Nishikawa, J. Yamamoto, H. Yokoyama, and H. Finkelmann, Macromol. Rapid Commun., 2004. **25**: p. 611-617.

88. S. T. Kim and H. Finkelmann, Macromol. Rapid Commun., 2001. **22**: p. 429-433.

89. I. Kundler and H. Finkelmann, Macromol. Rapid Commun., 1995. **16**: p. 679.

90. R. Stannarius, H. Schüring, C. Tolksdorf, and R. Zentel, Mol. Cryst. Liq. Cryst., 2001. **364**: p. 305.

91. M. Brehmer, R. Zentel, G. Wagenblast, and K. Siemensmeyer, Macromol. Chem. Phys., 1994. **195**: p. 1891.

92. S. Diele, S. Oelsner, F. Kuschel, B. Hisgen, H. Ringsdorf, and R. Zentel, Macromol. Chem., 1987. **188**: p. 1993.

93. Xin-Jiu Wang and Q.-F. Zhou, *Liquid crystalline polymers*. 2004, Singapore: World Scientific Publishing Co. Pte. Ltd.

94. Dierking, I., *Textures of liquid crystals*. 2003: Wiley-VCH Verlag.

95. E. Hecht, *Optics*. 2002, San Francisco: Addison Wesley.

96. Wartewig, S., *IR and Raman spectroscopy. Fundamental processing.* 2003, Weinheim: Wiley-VCH Verlag.

97. Stuart, B., *Modern Infrared Spectroscopy*, ed. D.J. Ando. 1996, Chichester: John Wiley & Sons.

98. H. Günzler and H.-U. Gremlich, *IR-Spektroskopie*. 2003, Weinheim: Wiley-VCH. 352.

99. H. Skupin, *Zeitaufgelöste*
Fourier-Transform-Infrarotspektroskopie
an Ferroelektrischen Flüssigkristallinen
Polymeren und Elastomeren. 2002: Leipzig.

100. M. Mooney, Journal of Applied Physics, 1940. **11**: p. 582.

101. J. Reibel, M. Brehmer, R. Zentel, and G. Decher, Adv. Mater., 1995. **7**(10): p. 849.

102. E. Nishikawa and H. Finkelmann, Macromol. Rapid Commun., 1998. **19**: p. 181.

103. R. Holyst, Phys. Rev. A, 1991. **44**(6): p. 3692.

104. D. M. Lambreva, B. I. Ostrovskii, H. Finkelmann, and W.H.d. Jeu, Phys. Rev. Lett., 2004. **93**: p. 185702.

105. G. C. L. Wong, W. H. De Jeu, H. Shao, K. S. Liang, and R. Zentel, Nature, 1997. **389**: p. 576.

106. J. Prigann, Ch. Tolksdorf, H. Skupin, R. Zentel, and F. Kremer, Macromolecules, 2002. **35**: p. 4150-4154.

107. M. Tammer, J. Li, A. Komp, H. Finkelmann, and F. Kremer, Macromol. Chem. Phys., 2005. **206**: p. 714.

108. S. Shilov, E.G., H. Skupin, R.Zentel, F. Kremer, Macromolecules, 1999. **32**: p. 1570.

109. H. Skupin, F. Kremer, S. V. Shilov, P. Stein, and H.Finkelmann, Macromolecules, 1999. **32**: p. 3746.

110. H. Wang, D. G.Thompson, J. R. Schoonover, S. R. Aubuchon, and R. A. Palmer, Macromolecules, 2001. **34**: p. 7084.

111. C. Y. Young, R. Pindak, N. A. Clark, and R.B. Meyer, Phys. Rev. Lett., 1978. **40**(12): p. 773.

112. D. E. Moncton and R. Pindak, Phys. Rev. Lett., 1979. **43**(10): p. 701.

113. Ch. Bahr and D. Fliegner, Phys. Rev. Lett., 1993. **70**(12): p. 1842.

114. S. V. Shilov, H.S., F. Kremer, T. Wittig, and R. Zentel, Phys. Rev. Lett., 1997. **79**: p. 1686.

115. W. G. Jang, C. S. Park, J. E. Maclennan, K. H. Kim, and N.A. Clark, Ferroelectrics, 1996. **180**: p. 213.

116. B. K. P. Scaife and J.K. Vij, The Journal of Chemical Physics, 2005. **122**: p. 174901.

117. L. Naji, R. Stannarius, S. Grande, M. Rössle, and R. Zentel, Liq. Cryst., 2005. **32**: p. 1307.

118. M. Rössle, R. Zentel, J. P. F. Lagerwall, and F. Giesselmann, Liq. Cryst., 2004. **31**: p. 883.

119. C. C. Huang, S. T. Wang, X. F Han, A. Cady, R. Pindak, W. Caliebe, K. Ema, K. Takekoshi, and H. Yao, Phys. Rev. E, 2004. **69**: p. 041702.

120. E. P. Obraztsov, A. S. Muresan, B. I. Ostrovskii, and W.H.d. Jeu, Phys. Rev. E, 2008. **77**: p. 021706.

121. L. Radzihovski and J. Toner, Phys. Rev. Lett., 1997. **78**: p. 4414.

122. L. Radzihovski and J. Toner, Phys. Rev. B, 1999. **60**: p. 206.